Università degli studi di Camerino

School of Advanced Studies

DOCTORAL PHILOSOPHY IN

Physics, Earth and Materials Sciences

XXXVII cycle

Development of Hydrometallurgical Processes for the Recovery of Critical and Precious Metals from Industrial Waste

PhD candidate

Dr. Raffaele Emanuele Russo

Supervisors

Prof. Gabriele Giuli

Prof. Mario Berrettoni

UNIONE EUROPEA
Fondo Sociale Europeo
Ministero dell'Università e della Ricerca
PON RICERCA E INNOVAZIONE
REACT EU
UNICAM Università di Camerino 1336
UNIVERSITÀ DI CAMERINO

This page intentionally left blank

Table of Contents

This page intentionally left blank

Preface

The recovery and extraction of metals are important challenges for modern industries due to growing environmental challenges and sustainability requirements. The advancement of metallurgical techniques, along with the quest for cleaner and more effective technologies, has sparked a rising interest with incorporating alternative methods into manufacturing processes. This thesis is placed in this framework and seeks to contribute to the improvement of methods for metal recovery, with a particular emphasis on sustainable practices.

Chapter 1 provides a general introduction to the main metallurgical processes for metal recovery, covering pyrometallurgical and hydrometallurgical methods. It also examines the use of organic acids applied in hydrometallurgical processes.

Chapter 2 deals with the main analytical methods used for characterization, such as XRD, ICP-OES, XAS, but it primarily focuses on multivariate analysis, with a particular emphasis on experimental design. It is important to note that the first paper on experimental design was published by Fisher over 100 years ago. Yet, despite of such a long time, this approach has not become as widespread as it should. Most researchers persist in studying and "optimizing" their problems one variable at a time. This approach is evident in numerous papers, where subsection titles proudly highlight this method: “3.1. Effect of pH”, “3.2. Effect of temperature”, “3.3. Effect of flow”, and so on. Moreover, this paragraph on Design of Experiments is written by the experience I have gathered over three years of doctoral research. Although my expertise is still developing, I have focused on maintaining a clear narrative throughout, incorporating practical insights, recommendations, and flowcharts to support anyone interested in exploring DoE. The aim is also to help readers avoid common mistakes, navigate challenges more effectively, and reach complex concepts with greater facilitate.

Chapter 3 presents three case studies that illustrate the practical application: recovery of lithium from LiFePO4 batteries; the recovery of molybdenum from a spent catalyst used in organic synthesis; and

silver from photovoltaic panels. Each case integrates experimental design techniques to optimize process parameters. Moreover, section 3.2.1, which covers the initial study of my research period, addresses not only the potential recovery of molybdenum but also presents data obtained using a univariate OVAT approach, which were then reprocessed using a multivariate method to extract the maximum amount of information and to describe how the multivariate method can improve the research.

In **Chapter 4** the general conclusions are reported.

List of scientific contributions

- **Russo RE**, Ventura M, Fattobene M, et al. Hydrometallurgical Molybdenum Recovery from Spent Catalyst Using Tartaric Acid Derived from Agrifood Waste. ACS Sustain Chem Eng. 2023;11(43):15644-15650. doi:10.1021/acssuschemeng.3c04318
- **Russo RE**, Awais M, Fattobene M, et al. Silver recovery from silicon solar cells waste by hydrometallurgical and electrochemical technique. Environ Technol Innov. 2024;36. doi:10.1016/j.eti.2024.103803
- **Russo RE**, Giampaoli A, Fattobene M, et al. Closed-Loop Lithium Recovery from LiFePO 4 Batteries Using Tartaric Acid Leaching. ACS Sustainable Resource Management. Published online March 24, 2025. doi:10.1021/acssusresmgt.4c00499

Additional papers not included in the thesis

- Bravetti F, **Russo RE**, Bordignon S, et al. Zwitterionic or Not? Fast and Reliable Structure Determination by Combining Crystal Structure Prediction and Solid-State NMR. Molecules. 2023;28(4). doi:10.3390/molecules28041876
- **Russo RE**, Zamponi S, Conti P, et al. Dechlorination of iron artefacts: A novel approach. Mater Lett. 2023;338. doi:10.1016/j.matlet.2023.133968
- Fattobene M, Papa F, **Russo RE**, et al. ON-SITE monitoring OF BVOCS emission in Tremiti island, Italy. Heliyon. 2024;10(1). doi:10.1016/j.heliyon.2023.e23822
- Fattobene M, Liu F, Conti P, **Russo RE**, et al. Distribution of Elements in Durum Wheat Seed and Milling Products: Discrimination between Cultivation Methods through Multivariate Data Analysis. Foods. 2024;13(12):1924. doi:10.3390/foods13121924
- Fattobene M, Santoni E, **Russo RE**, et al. Analysis of Posidonia oceanica's Stress Factors in the Marine Environment of Tremiti Islands, Italy. Molecules. 2024;29(17):4197. doi:10.3390/molecules29174197

Poster and oral communications

- Poster session at **Interregional Meeting of the Italian Chemical Society** – Sections Toscana, Umbria, Marche and Abruzzo (TUMA 2022) held in Perugia
- Poster session at **Gilberto Vlaic XVI School on Synchrotron Radiation: Fundamentals, Methods and Applications** held in Trieste;
- Flash communication at "**Scuola di Chimica Industriale**" held in Turin;
- Poster session at **11th Colloquium Chemiometricum Mediterraneum** held in Padova;
- Oral communication at "**Workshop di chemiometria**" held in Ravenna;
- Poster session at "**Convegno Società italiana di luce di sincrotrone (Sils) 2024**" held in Rende;
- Poster session at University Burgos for PhD day.

List of Specialized Training Schools

- School of multivariate analysis held in the University of Genoa;
- School of multivariate analysis: experimental design held in the University of Genoa;
- School of industrial chemistry held by Politecnico di Torino e SCI;
- GRICU & AIDIC DAET school 2022 - process decarbonization and energy transition;
- XVI school on synchrotron radiation "gilberto vlaic": fundamentals, methods and applications.

List of Abbreviations

ANOVA	ANalysis Of VAriance
CRM	Critical Raw Material
DoE	Design of Experiment
ICP-OES	Inductively Coupled Plasma Optical Emission Spectroscopy
LoD	Limit of Detection
LoQ	Limit of Quantification
MLR	Multiple Linear Regression
OLS	Ordinary Least Squares
OVAT	One Variable At Time
PPS	Potassium PerSulphate
REE	Rare-Earth Elements
SEM-EDX	Scanning Electron Microscopy – Energy Dispersive X-ray spectroscopy
VIF	Variance Inflation Factor
XANES	X-ray Absorption Near Edge Structure
XAS	X-ray Absorption Spectroscopy
XRD	X-Ray Diffraction

This page intentionally left blank

1

Introduction

The rapid progress of technology and industrialization has led to a significant increase in the demand for critical and precious metals. These metals, which include elements such as palladium, gold, rare earth elements (REEs), lithium and other one, are indispensable in various high-tech applications, including electronics, renewable energy technologies, catalysis, and advanced materials. However, their supply is often limited and concentrated in specific geographical regions (Figure 1), leading to supply chain vulnerabilities, price volatility, and geopolitical tensions.

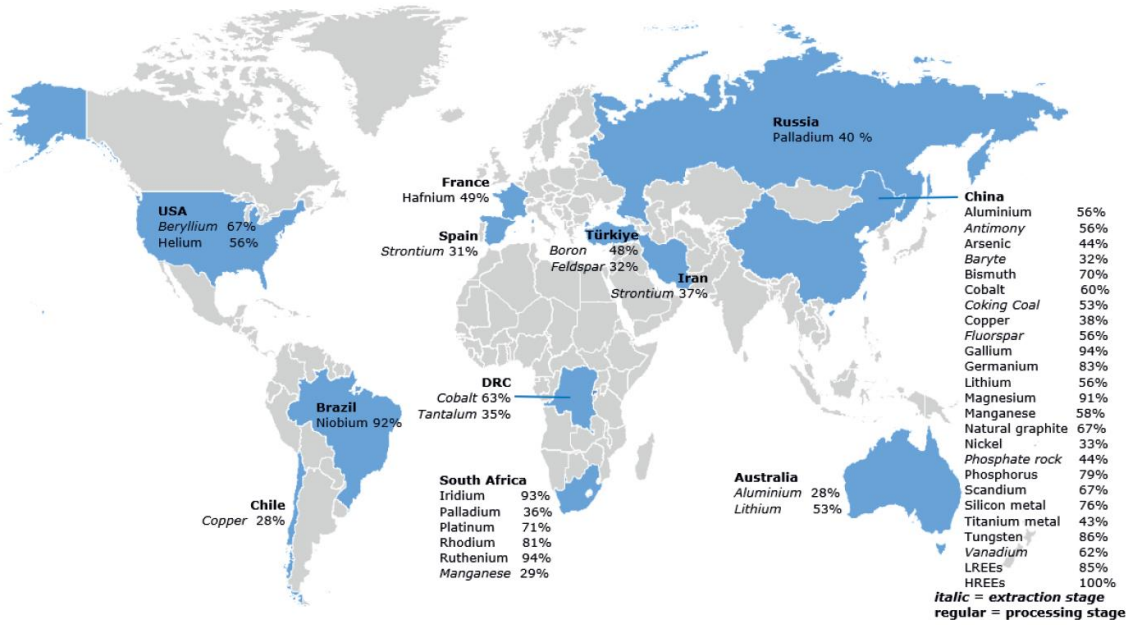

Figure 1. Countries accounting for largest share of global supply of CRMs from Study on the Critical Raw Materials for the EU 2023.

Figure 1 indicates China is the largest global supplier of many critical raw materials. In terms of the total number of critical raw materials (CRMs), China is the major supplier of 21 CRMs. This includes light and heavy REEs, refined cobalt, natural graphite, nickel and other CRMs: antimony, arsenic, baryte, bismuth, coking coal, refined copper, fluorspar, gallium, germanium, phosphate rock, phosphorus, scandium, silicon metal, titanium, tungsten and vanadium. In addition to China, several other countries are also important global suppliers of specific materials. For instance, South Africa and Russia are the largest global suppliers of platinum group metals, Democratic Republic of Congo of cobalt and tantalum, USA of beryllium and Brazil of niobium.[1]

The recovery of metals significantly influences the global demand for primary metal production by providing alternative sources of valuable materials, thereby reducing reliance on traditional mining. As the depletion of high-grade ores continues, the recycling and recovery of metals from waste streams and end-of-life products become increasingly necessary. This shift not only mitigates environmental impacts but also aligns with sustainable development goals. Recovering metals from waste materials offers significant environmental benefits, primarily by reducing the demand for virgin resources and minimizing ecological harm. This process not only conserves natural resources but also mitigates

pollution associated with traditional mining and metal extraction methods.[2] Moreover, utilizing secondary materials aligns with circular economy principles, promoting sustainability and resource efficiency. [3] In this view, metal recovery and recycling significantly reduce greenhouse gas emissions due to lower energy requirements compared to primary production. Economically, switching to recycled materials can lower feedstock costs for producers, enhancing sustainability while minimizing the environmental footprint of metal extraction. Secondary production from recycled materials can lead to a reduction of 4.5 to 12 Gt of GHG emissions globally by 2050, with maximum scenarios potentially exceeding 42 Gt.[4] In particular, metal recovery and recycling reduce CO_2-equivalent emissions and displace primary production, minimizing environmental impacts. Economically, increasing scrap supply can lower material prices, enhancing demand, while implementing best technologies can further decrease emissions, though still falling short of 2°C targets.[5] Another important aspect is the energy consumption. Primary metal production accounts for 6−10% of the global anthropogenic greenhouse gas (GHG) emissions and has an enormous energy demand of approximately 8% of the global energy demand. To mitigate environmental pollution and intensification of climate change by primary metal production, recycling is commonly included among the most viable options.[6] Thus, recycling metals can lower energy demands compared to primary production and it can mitigate the demand for primary metal production; however, due to permanently increasing metal demand and low concentrations in end-of-life products, primary metals will still be necessary even with high recycling rates. [4,6]

While the benefits of recycling are substantial, challenges remain, such as the need for advanced technologies. Thus, the challenge is to design a new, environmentally friendly and efficient method of recycling valuable metals. In fact, in recent years, the focus has shifted towards the development of green hydrometallurgical processes. Green chemistry principles aim to minimize the environmental impact of chemical processes by reducing the use of hazardous substances, enhancing energy efficiency. In the context of metal recovery, this involves the use of eco-friendly solvents, biodegradable chelating agents, and renewable energy sources. The goal is to develop processes that are

not only effective but also sustainable, reducing the overall environmental footprint of metal recovery operations.

This work aims to develop and optimize hydrometallurgical processes for the recovery of critical and precious metals from industrial waste and e-waste. The research focuses on the identification and characterization of waste streams, the selection of appropriate leaching agents, and the optimization of process parameters to maximize metal recovery. By advancing the understanding and application of green hydrometallurgical techniques, this work contributes to the broader goals of resource conservation, waste reduction, and environmental protection. The findings of this research have the potential to inform industrial practices and policy decisions, promoting a more sustainable and circular economy.

1.2 Pyrometallurgical Process

Pyrometallurgy is a metallurgical process involving elevated temperatures to facilitate metal recovery. The main steps in the process are:

Calcination

It is a thermal process that involves the decomposition of a material, facilitating the transformation of raw materials into more reactive forms. Calcining plays a crucial role in the pyrometallurgical process of extracting metals from ores by transforming raw materials into a more reactive form, enhancing their subsequent processing. This thermal treatment involves heating the ore to high temperatures, which facilitates the removal of volatile components and the alteration of mineral structures, making the metals more accessible for extraction.

Roasting

Roasting is a thermal process involving gas-solid reactions, which can include oxidation, reduction, chlorination, sulfation, and pyro-hydrolysis. A classic example of roasting is the oxidation of metal sulphide ores. The sulphide mineral is heated in the presence of air, allowing

oxygen to react with the sulphide to produce sulphur dioxide gas and metal oxide. The solid product resulting from this process is often referred to as "calcine." In sulfide roasting, if the temperature and gas conditions are such that the sulfide is fully oxidized, the process is known as "dead roasting." In some cases, such as when preparing feed for reverberatory or electric smelting furnaces, roasting is carried out with less oxygen, resulting in partial oxidation of the feed—this is called "partial roasting." When the roasting conditions lead to the formation of metal sulfates instead of oxides, the process is known as "sulfation roasting." Additionally, selective roasting can occur when a mixed sulfide feed (such as one containing both copper and iron sulfides) is processed under controlled conditions, resulting in the formation of metal sulfates for one metal and metal oxides for the other.

Smelting

Smelting involves thermal reactions in which at least one product is a molten phase. Metal oxides are commonly smelted by heating them with a carbon source, such as coke or charcoal, which serves as a reducing agent to release oxygen in the form of carbon dioxide, leaving behind the refined metal. Environmental concerns over carbon dioxide emissions have only recently emerged due to the recognition of the enhanced greenhouse effect. In the case of carbonate ores, these are often smelted with charcoal but may first need to undergo calcination. Additional materials, known as fluxes, may be added during smelting to help the melting process, facilitate the formation of slag, and assist in removing impurities, such as silicon compounds.

While traditionally associated with the extraction of metals from ores, pyrometallurgical techniques are also employed in the recovery of metals from industrial waste, such as electronic waste (e-waste), spent catalysts, metallurgical slags, and municipal solid waste incineration ash.[7–9] For example, copper and precious metals are commonly recovered from printed circuit boards (PCBs) via smelting in integrated copper smelters, where the waste is co-processed with copper concentrates.[9] Similarly, spent automotive

catalysts, which contain platinum group metals (PGMs), can be thermally treated to remove volatile contaminants and concentrate the PGMs for subsequent refining.[10]

1.3 Hydrometallurgical Process

Hydrometallurgical processes are a key component in the field of metal extraction and recovery, particularly advantageous for recycling metals from various sources, including industrial sludges and electronic waste. These processes involve the use of aqueous solutions to dissolve and extract metals from ores and waste materials through a series of chemical reactions. During leaching, waste is treated with acids, bases or salts to dissolve the metals. This step is critical, as the choice of leaching agent and conditions can significantly influence the efficiency and selectivity of metal recovery. Subsequently, the next step is the recovery and purification process, and various techniques can be employed:

1. **solvent extraction** is a common process for selectively concentrating metals. It is performed using an organic extractant that is dissolved in an organic phase. The organic phase is allowed to contact an aqueous phase containing the dissolved metal or metal ion complex, which are then stripped from the organic phase into an aqueous phase
2. **ion exchange** is a very common form of solution concentration and purification. In this case resins with functional groups are used to selectively adsorb metal ions from the solution, followed by elution to recover the metals in a concentrated form.
3. **precipitation** is a commonly used technique to recover metals from the solution. This involves adding reagents that react with the dissolved metals to form insoluble compounds. For instance, metals can be precipitated as hydroxides, sulphides, or other salts depending on the reagents used and the desired purity of the final product. Precipitation can also be accomplished using gasses and/or water.
4. **cementation** is another method where a more reactive metal, such as zinc or iron, is added to the solution to reduce and precipitate the desired metal. The basic principle of cementation is

contact reduction. In other words, the electrons from a less noble metal are given up to a more noble dissolved metal.

5. **electrowinning** consists of applying a potential or voltage and an associated current between a positive (anode) and negative (cathode) electrode pair. This technique is highly effective for metals such as copper, nickel, and cobalt, providing high-purity products. It is the most common method of recovering metal from solution in its metallic form.

Hydrometallurgical methods offer several advantages over traditional pyrometallurgical processes. These processes often operate at atmospheric pressure and moderate temperatures, significantly reducing energy consumption and associated greenhouse gas emission compared to high temperature pyrometallurgy. Additionally, these processes can achieve high selectivity and recovery rates for specific metals, making them particularly effective for processing complex and low-grade ores, as well as mixed metal waste streams. The environmental impact of hydrometallurgical operations is also generally lower, as they produce fewer emissions and can be designed to recycle reagents and minimize waste generation.

In conclusion, hydrometallurgical processes are indispensable for the recovery of critical and precious metals from industrial waste and electronic scrap. Their ability to operate under milder conditions, coupled with high selectivity and environmental benefits, makes them a preferred choice for modern metallurgical applications. Ongoing innovations and the integration of green chemistry principles are expected to further advance the efficiency and sustainability of hydrometallurgical techniques, ensuring their continued relevance in the circular economy.

1.3.1 Use of Organic Acids

Organic acids, such as citric acid, tartaric acid, and oxalic acid and etc, known for their biodegradability, provide several benefits, including reduced secondary pollution, enhanced selectivity for metals, and the potential for recyclability. This not only decreases operational costs but also aligns with sustainable practices by minimizing waste generation. These advantages make them particularly useful for

extracting metals from low-grade ores.[11–13] Moreover, the use of organic acids can reduce the environmental impact associated with traditional inorganic acids, which often lead to toxic waste and high salt loads. [14] Inorganic acids, such as sulfuric acid, hydrochloric acid, and nitric acid, have traditionally used in hydrometallurgical processes due to their strong acidic properties and ability to dissolve a wide range of metals. By definition they are highly corrosive, leading to severe damage to processing equipment, increasing maintenance costs and the need for specialized corrosion-resistant materials. Additionally, the use of inorganic acids often results in the generation of toxic and hazardous by-products.[15] For example, hydrochloric acid can release chlorine gas, while nitric acid can produce nitrogen oxides, both of which are harmful to human health and the environment.

For example, organic acids, such as citric and oxalic acid, have demonstrated superior leaching capabilities for metals like molybdenum, nickel, and vanadium, achieving over 93% recovery under optimal conditions.[16] In spent Ni-Cd batteries, a two-stage leaching process using citric and acetic acids successfully recovered 85% of cadmium and 50% of nickel, showcasing the effectiveness of organic acids in complex matrices. [17] Moreover, organic acids can facilitate leaching through mechanisms such as acidolysis and complexolysis, which enhance the dissolution of metals from ores and waste materials. [16,18] The combination of organic acids with oxidizing agents, like persulfate, can further intensify metal leaching, overcoming the limitations of organic acids alone.[19]

In conclusion, the use of organic acids in hydrometallurgical processes presents a promising way for the sustainable and efficient recovery of critical and precious metals. Their selective leaching capabilities, coupled with environmental and safety benefits, make them a compelling alternative to conventional mineral acids. Furthermore, the potential for recovering and reusing organic acids enhances the sustainability of these processes, contributing to the advancement of green chemistry and sustainable resource management. Future research and industrial applications are likely to further explore and optimize these processes, ensuring their scalability and economic viability.

2

Materials and methods

2.1 Design of experiments

The entire scientific community-chemists, biologists, physicists, engineers, and etc…-conducts experiments daily to discover valuable insights and drive innovation. For example, an engineer may seek to optimize an industrial process, aiming to improve efficiency, reduce costs, and minimize environmental impact. Through a careful design of experiment (**DoE**), researchers can systematically test variables, identify optimal conditions, and draw reliable conclusions, extracting the maximum amount of information from each study. This method contrasts with the classic approach used in the scientific community, where only one variable is changed at a time, a strategy known as the "One Variable at a Time" (**OVAT**) approach.

For example, let's consider the optimization of an organic synthesis by monitoring the effects of temperature and reaction time. This represents a basic bivariate study, simple to describe and visualize. Working in two dimensions is naturally more manageable, of course the approach can extend to cases involving more than two variables. In Figure 2a, OVAT approach is illustrated. Starting with a constant temperature of 25°C, the reaction time is progressively increased until the maximum yield is achieved in the experiments conducted. From this optimal time point, the reaction time is held constant while temperature increase until the maximum yield is reached. This point is considered an optimum. In this example, nine experiments were conducted, as only five values were tested for each variable. In the literature there are a lot of studies where are considered more than five points for factor, thus increasing the number of experiments. In the second approach (Figure 2b), a central composite design with face-centered points is employed. Remarkably, only nine experiments are needed to explore the entire experimental domain comprehensively, reaching the true optimal conditions. Another approach of DOE, different from what was previously described, involves conducting only four experiments (versus nine of the OVAT) corresponding to the corners of a cube. Once the direction of maximum yield is identified, an optimization design can then be applied to give a very precise estimate of the true optimum operating condition.

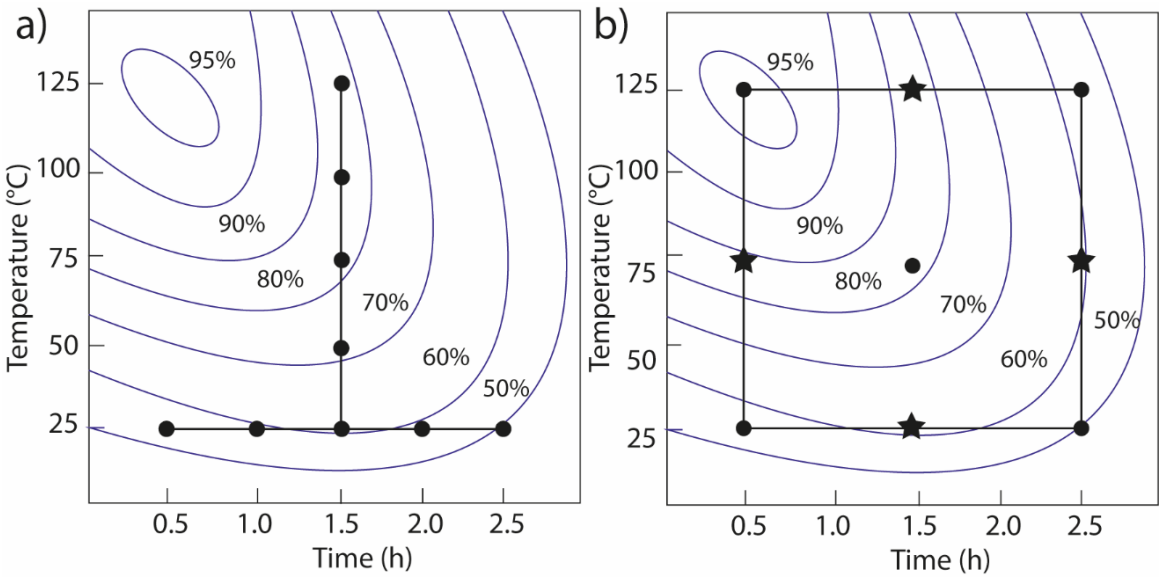

Figure 2. Example of a) OVAT and b) DoE application

Clearly, the OVAT design has failed dramatically because it fails to detect the interaction between temperature and time to the reaction yield. It is evident the OVAT approach does not lead to real optimum taking inefficient, unnecessarily many runs. It provides no information about what happens when factors are varied simultaneously, thereby overlooking potential interactions. Moreover, this approach results in isolated, disconnected experiments, leading to local knowledge acquisition and no comprehensive mapping of the experimental space. To resume:

- DoE takes into account the interactions among the variables, while the OVAT does not;
- DoE provides a global knowledge (in the whole experimental domain), while the OVAT gives a local knowledge (only where the experiments have been performed);
- In each point of the experimental domain, the quality of the information obtained by the experimental design is higher than the information obtained by the OVAT;
- The number of experiments required by an experimental design is smaller than the number of experiments performed with an OVAT approach.

Moreover, systematically exploring the entire experimental domain enables the development of a mathematical model that can accurately predict response values across the domain. This prediction accuracy, given a known experimental variability, can even be estimated before conducting the actual experiments. This means going from a local knowledge to a global knowledge.

Now that it was understand DoE is the best choice, what are the next steps? It's important to clarify that creating the experimental design isn't the most challenging part, as it might seem. The real difficulty lies in carefully understanding the problem and selecting the relevant factors accordingly. Thus, the critical first step is to gain a deep understanding of the problem, carefully choose the relevant factors, and define the response(s) to be analysed. From there, the process moves to selecting an appropriate experimental design, conducting the experiments, analysing the data, and ultimately make conclusions.

It may happen that a single experimental design doesn't yield the desired solution, requiring a follow-up design. I would also like to highlight that no experimental design truly "fails"; each DoE provides valuable and important information necessary to achieving the research goal. Moreover, the insights gained from the first DoE are often crucial for setting up a second one, leading the process toward the desired and real optimum. This is another advantage over the OVAT approach. Thus, considering the potential need for multiple rounds of experimental design, it's advisable to allocate no more than 40% of the available budget to the initial set of experiments.[20] To resume, the goal of experimental design is to maximize information while minimizing the number of experiments. Therefore, the entire process is planned with a focus on maximizing outcomes in terms of both cost-effectiveness and efficiency.

Experimental designs can be arranged according to their objectives:

- **Screening Designs:** These are used to identify the most influential factors among many variables. They are ideal for the initial phases, when it is necessary to reduce the number of factors to focus only on the significant ones. Common examples include the Plackett-Burman design and fractional factorial designs. These designs are efficient in testing many factors with fewer experiments, though they tend to ignore higher-order interactions.
- **Improvement Design:** These designs are used after an initial screening to investigate interactions between factors through linear models, aiming to deepen understanding of the problem at hand. Once validated, they allow for accurate predictions within the defined experimental domain. Common example is the full factorial design.
- **Optimization Designs:** These are used to find the optimal conditions for a response. Once a reduced set of relevant factors has been identified, these designs help explore how the response changes as a function of the factors, allowing for identification of the maximum or minimum point (real optimum). Common designs in this category include the central composite design (CCD), the Box-Behnken design and Doehlert Designs. These are particularly useful for

constructing quadratic models that describe the response surface, enabling identification of the optimal point.

- **D-optimal design:** this design belongs to the family of Optimal Designs and is particularly useful when the number of experiments is large and needs to be minimized, when factors have multiple levels, or when both continuous and categorical factors are involved. In D-optimal design, the objective is to select a subset of experimental conditions that optimizes the determinant of the information matrix, which is a measure of the precision with which model parameters can be estimated.

This work employs various experimental designs to investigate different hydrometallurgical processes. Each design will be explained in relation to a specific case study, allowing for a more detailed and contextual understanding.

2.1.1 Randomization

One of the basic assumptions underlying ANOVA, which is the statistical method typically used to analyze the results of factorial experimental designs, is that the residuals - i.e., the fluctuations introduced by uncontrolled factors - are randomly distributed. This assumption ensures that the variance observed in the response can be correctly attributed to the investigated factors.

However, for measurements conducted over an extended period, variations in uncontrolled factors such as pressure, temperature, stability of the measurement apparatus, calibration standard drift, or operator knowledge may introduce a systematic trend in the results rather than purely random noise. In such cases, randomization of the experimental runs is essential to mitigate these potential sources of bias. By randomly assigning the order of experiments, one can help ensure that any such trends are equally likely to affect all treatment levels, thus preserving the validity of the ANOVA model and enabling correct inference about factor effects.

Let's consider the effect of three factors, A, B, and C. For each factor (or treatment), let's assume that four replicates are performed:

i. **First approach (commonly used):** Conduct four measurements consecutively for A, followed by four for B, and then four for C.
ii. **Second approach (the correct method):** Perform all 12 measurements in a randomized order.

The random sequence of measurements ensures that any errors introduced by uncontrolled factors are distributed randomly across A, B, and C, minimizing systematic biases.

2.2 Mathematical models used in DoE

In the previous paragraph, it was discussed the importance of experimental design and the different types. What is the mathematics behind experimental designs? It is reasonable to assume that the outcome of an experiment (Y) is dependent on the experimental conditions ($X_1, X_2, \dots X_k$). This means that the result can be described as a function based on the experimental variables, that is, there is a relationship between factors and response(s):

$$Y = f(X_1, X_2, \dots X_k) + \varepsilon \quad (1)$$

where ε represents the sources of variability that were not included in the experimental model. These can be linked to uncontrolled or unmeasured phenomena such as environmental fluctuations (e.g., temperature or humidity changes), instrumental drift, operator-related inconsistencies. Thus, it is a random variable supposed to follow a normal distribution with mean 0 and variance σ^2. As the mean of ε is 0, the expected value of the experimental response, E[Y], is precisely the function f because[21]:

$$E[Y] = E[f(X_1, X_2, \dots X_k)] + E[\varepsilon] \quad (2)$$

This function can be approximated by a simplified polynomial function derived from experimental data, resulting in an empirical model that effectively represents the response within the chosen experimental

domain. The experimental domain is the range of the factors within which an experiment is conducted. It includes the boundaries for all variables that are studied. Moreover, the factor can be qualitative or quantitative. In the case of qualitative factors (e.g., different suppliers, different materials, solvent, type of catalyst, etc.), no extrapolations (i.e., predictions) can be performed outside the tested levels. On the other hand, data from tests where the factor is quantitative (such as temperature, voltage, pH, molarity, etc.) can be used for both effect investigation and prediction.

Based on the objective and thus on the type of experimental design used, three main models are employed (Table 1):

i. **first-order linear models'** studies only the main factors and thus the relationship between of each factor with the response. A positive coefficient indicates that as the value of the independent variable increases, the mean of the dependent variable also tends to increase. A negative coefficient suggests that as the independent variable increases, the dependent variable tends to decrease. The coefficient value signifies how much the mean of the dependent variable changes given a one-unit shift in the independent variable while holding other variables in the model constant. Moreover, they are measures of the slopes of the response surface at the origin in the direction of the variables. This model is used in screening design.

ii. **second-order interactions models** that also study the interactions/effect between each factor. An interaction effect occurs when the effect of one variable depends on the value of another variable, that is when the influence of a variable may be modified by the settings of other variables. The response surface can give a twisted plane, where the slope of the surface of a factor depends on the level of the second factor. [22] This model is used for the improvement design.

iii. **Second-order quadratic models** consider non-linear effects and in particular the quadratic effect of each variable. These coefficients describe how the response surface curves, with positive values indicating a convex surface and negative values indicating a concave surface.

This is important for the optimization process to identify maximum or minimum within the experimental domain.

Table 1. Synoptic table with the main models used in design of experiment.

Polynomial functions	Mathematical model
$Y = \beta_0 + \sum_{i=1}^{k} \beta_1 X_1 + \varepsilon$	First-order linear
$Y = \beta_0 + \sum_{i=1}^{k} \beta_i X_i + \sum\sum_{i<j} \beta_{ij} X_i X_j + \varepsilon$	Second-order interactions
$Y = \beta_0 + \sum_{i=1}^{k} \beta_i X_i + \sum\sum_{i<j} \beta_{ij} X_i X_j + \sum_{i=1}^{k} \beta_{ii} X_i^2 + \varepsilon$	Second-order quadratic

β_0 represents the intercept, that is where the regression plane intersects with the Y-axis. It is equal to the estimated Y value when all the independents have a value of 0, which typically corresponds to the central point of the experimental domain.

To analyse each coefficient is necessary to have a number of experiments equal to or greater than the number of coefficients. Therefore, if we want to study two factors using a quadratic model, we will need a minimum of six experiments. This minimum number ensures that there is sufficient data to estimate all terms in the model, including linear effects, quadratic effects, and interactions between the factors.

2.2.3 Multivariate Regression and Response Surface

The polynomial functions discussed earlier can be directly related to the multiple regression model (MLR). It plays a crucial role in experimental design by providing a systematic approach to analyse and interpret the impact of factors on a response(s). These factors, of course, are expressed in different

units and vary across distinct ranges, thus there is a scale factor that impedes the evaluation of the importance of a factor because of the magnitude of the coefficient(s) in the model. Therefore, the natural variables are linearly transformed into coded variables, $X_1, X_2, \ldots X_k$, which are dimensionless quantities with a common range, usually between -1 and +1, which helps in interpreting interactions and main effects more easily. For instance, if a study involves varying temperature and pH, coding these values makes it easier to identify and compare their effects on the response, regardless of their original units.

To apply MLR, it is essential to construct the experimental matrix with the coded values. This matrix organizes all the conditions under which experiments are performed, incorporating the levels of each factor under investigation. Each row in the experimental matrix represents a unique combination of factor levels, or an experimental run, along with the corresponding output or response. The responses are structured as a single-column matrix with the same number of rows as the experimental matrix.

The fit of an MLR model is assessed using several statistical metrics:

- **Coefficient of Determination (R^2)**: This metric indicates the proportion of variance in the dependent variable that is explained by the independent variables. An R^2 value close to 1 suggests that the model explains most of the variability in the data, which is desirable for making accurate predictions.
- **Adjusted R^2**: This metric adjusts R^2 for the number of predictors in the model, providing a more accurate measure of fit when multiple variables are involved.
- **Root Mean Square Error (RMSE)**: RMSE quantifies the average difference between observed and predicted values, offering a clear measure of prediction accuracy.
- **Analysis of variance (ANOVA) for significance of regression**: it is used to determine the statistical significance of each coefficient, helping to identify which variables have a meaningful impact on the dependent variable.

- **Lack of fit test**: ANOVA is often accompanied by a model-validation statistic called a lack of fit (LoF) test. A statistically significant LoF indicates that the model does not fit the data well.

A common challenge in MLR is multicollinearity, where independent variables are highly correlated with each other. This can inflate the variance of the coefficient estimates, making them unstable and difficult to interpret. In chemometrics applications, multicollinearity is addressed by calculating the Variance Inflation Factor (VIF) for each predictor. A Variance Inflation Factor (VIF) of 1 signifies that there is no multicollinearity between the variables, meaning the coefficient accurately represents the effect of a one-unit change in the variable on the response. Although guidelines can vary, VIF values below 4 are typically regarded as acceptable. However, when VIF values exceed 8, it indicates problematic multicollinearity, making the estimation of related coefficients unreliable. In standard experimental designs, VIF values usually approach 1, suggesting minimal correlation between factors. In contrast, historical datasets may display higher covariances between factors, leading to elevated VIF values and resulting in an unstable MLR model.

Based on the mathematical model, it can be interpreted geometrically as a response surface. For example, the relationship between the response and the levels of the two factors can be represented by a surface in three dimensions and this surface is known as the response surface. A more convenient representation is a contour diagram, which is essentially a view of the response surface from above, as it is in two dimensions (X_1 and X_2). These graphical representations are used in the experimental section (CHAPTER 3), particularly using contour plots.

2.3 Application in Metals Recovery

In the field of metallurgical chemistry, Design of Experiments (DoE) is instrumental in optimizing the recovery of metals from ores and secondary sources. By systematically applying DoE principles, chemists can rigorously evaluate how various factors-such as leaching temperature, pH levels, reagent concentrations, and reaction times-affect metal recovery processes. DoE methodologies, such as

factorial designs and response surface methodology, allow for a comprehensive exploration of the interaction effects between multiple variables. This enables the development of detailed response surfaces that illustrate, for example, how different conditions influence the leaching efficiency or the recovery yield. This approach not only improves the precision and accuracy of recovery models but also aids in identifying optimal conditions for scaling up processes from laboratory to industrial scale. By incorporating DoE into metal recovery research, chemists can achieve more reliable, cost-effective, and environmentally friendly extraction processes, driving advancements to develop hydrometallurgical process for metals recovery.

Bibliographic research was conducted on SCOPUS using the search terms: "metals recovery" AND "optimiz*" AND "leaching," with the optional inclusion (and/or not) of "experimental design." When "experimental design" was excluded, 716 documents were retrieved (Figure3). When it was included, the result was to just 24 documents. The application of DoE in this field only begins to appear from 2002 onward (Figure 4). Thus, among the total of 716 documents, only 3.35% apply optimization using DoE.

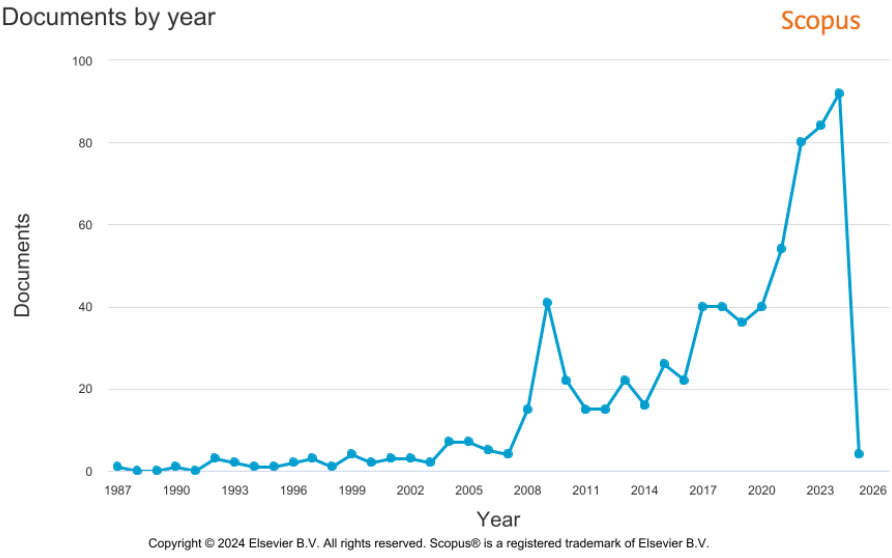

Figure 3. Research articles that do not use experimental design in the optimization of metals recovery.

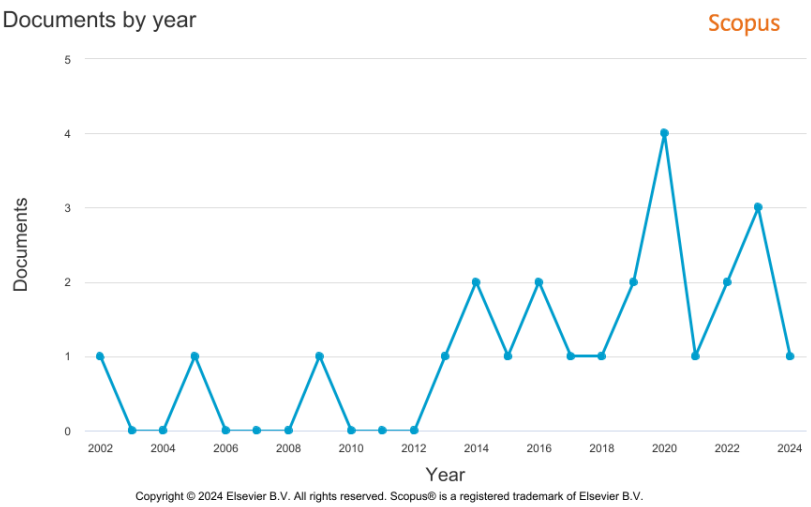

Figure 4. Research articles that use experimental design in the optimization of metals recovery.

2.4 Characterization Methods

2.4.1 ICP-OES

Inductively Coupled Plasma Optical Emission Spectroscopy **(ICP-OES)** is an analytical technique used in metal recovery for the detection and quantification of metals in various matrix types. Here's how ICP-OES is applied in the field of metal recovery. It can detect multiple metals simultaneously, including both major and trace elements, making it particularly useful in complex matrices where multiple metals may be present. During metal recovery, leaching processes are often employed to dissolve metals from solid materials into a solution. ICP-OES is used to monitor metal concentrations in the leachate, helping to assess the effectiveness of the leaching process and to adjust parameters for optimal metal recovery. In this study a Thermo Scientific™ iCAP™ PRO X Duo was used to measure the metal concentrations. The Calibration standards for ICP-OES analysis were assessed by injecting a blank as well as five standard solutions ranging from 1 ppb to 10 ppm. Weighted least squares was used to build a calibration curve. A new calibration curve was measured at the start of each run. To ensure accuracy and precision of the calibration curves, respectively, a coefficient of determination (R^2) greater than 0.990 and relative standard error (RSE) below 20% was required. Limit of detection (LOD) and quantification (LOQ) were automatically computed from the calibration lines by the instrumental software and calculated as $\frac{3\times SD}{m}$ and $\frac{10\times SD}{m}$ where SD is the standard deviation of the black and m is the slope of the calibration curve. Cross standard solutions were used to validate the calibration curve. Samples outside the calibration range were suitably diluted to fall within the calibration. The instrument was tuned yearly with a commercially available tuning solution (Thermo Fisher Scientific) in HNO_3/0.01% CH_3OH. ICP-OES operating conditions are listed in Table 2.

Table 2. ICP-OES operating conditions.

Parameter	Set Value
RF Power	1150 W
Nebulizer Gas Flow	0.50 L/min
Nebulizer Gas Pressure	2.30 bar
Auxiliary Gas Flow	0.50 L/min
Cool Gas Flow	12.5 L/min
Pump speed	45 rpm
Wash Time	30 s
Uptake Time	15s

2.4.2 XRD

X-ray Diffraction **(XRD)** is an analytical technique used to analyse the crystalline structure and composition of materials. In this case it was used to study the real composition of the solid wastes. XRD is used in metal recovery for:

- **Identification of Metal Phases**: it can identify the crystalline phases that contain the metals of interest, such as oxides, sulphides, or pure metals. This helps determine which metals are present and in what forms, which is essential for choosing the most effective leaching method.
- **Determining Structural Changes During Processing**: as metals undergo different recovery stages-such as leaching, smelting, or refining-XRD is used to monitor changes in their crystalline structure. These structural insights are essential for optimizing recovery processes, as they highlight the effects of different treatments on the crystalline structure of metals.

- **Evaluating Residual Metals in Waste**: After processing, XRD can be used to analyse residues to confirm if all valuable metal phases have been successfully recovered. It also helps identify any remaining metal compounds, allowing adjustments in recovery strategies to maximize yield.
- **Characterizing By-products**: In metal recovery processes, by-products are formed, for example the metal salts recovered. Thus, XRD help to identify this secondary raw material.

For the XRD analysis the Cu X-ray tube was operating at 40 kV and 25 mA. Diffractogram was recorded in the 2-theta range from 5 to 75 with a 0.02 step and 2 s counting time. The sample for X-ray diffraction was prepared as finely ground powder mounted in a brass sample holder by side-loading in order to minimize iso-orientation of the grains. Calculated diffraction pattern was obtained using the Cambridge Crystallographic Data Center's (CCDC) mercury software. Phase identification was made with QUALX2.0.[23,24]

2.4.3 XAS

X-ray Absorption Spectroscopy (**XAS**) can offer several key advantages in metal recovery processes, particularly in understanding the oxidation state and speciation of metals. In the case of multiphase mixtures (which is the case for many of the wastes studied here) understanding in which phase a critical element is located, and determining its which oxidation state/structural location is essential for planning a recovery method and also for optimising the recovery procedure.[25]Absorption Spectroscopy (XAS) and spectra were collected in fluorescence mode at the LISA CRG Beamline (BM08) of the European Synchrotron (ESRF) in Grenoble, France.[26] In this research work, XAS was employed to confirm the presence of metallic copper within the photovoltaic panels (See 3.3).

2.4.4 SEM-EDX

Scanning Electron Microscopy with Energy-Dispersive X-ray Spectroscopy **(SEM-EDX)** is a combination of techniques used to analyse the morphology, composition, and distribution of metals within various materials. SEM-EDX is applied in metal recovery for:

1. **Morphological Analysis**: SEM provides high-resolution images of waste surfaces, revealing details about particle size, shape, and structure. In metal recovery, this helps to understand the physical characteristics of metal-bearing particles, aiding in the selection of effective recovery methods.

2. **Elemental Composition Identification**: EDX, used in conjunction with SEM, detects the elemental composition of materials by analysing X-rays emitted from the sample's surface. In metal recovery, EDX identifies the metals present in the sample and provides information on impurities or unwanted elements that may affect recovery efficiency.

3. **Mapping Elemental Distribution**: SEM-EDX enables elemental mapping, showing the distribution of metals across a sample's surface. For an example, it is useful as it reveals how metals are associated with other minerals.

4. **Characterization of By-products and Residues**: During and after recovery processes, SEM-EDX can analyse by-products and residues to ensure that valuable metals are not being lost and to optimize recovery conditions.

SEM-EDX, Zeiss Sigma 300 (Scanning Electron Microscope-Energy Dispersive X-ray) was used to study surface morphologies of the spent catalyst and to validate the use of the kinetic model.

3

Metal Recovery Processes

3.1 Closed-Loop Lithium Recovery from $LiFePO_4$ Batteries Using Tartaric Acid Leaching

INTRODUCTION

Lithium-ion batteries (LIBs) have become indispensable in modern technology due to their high energy density, long cycle life, and low self-discharge rates.[27] Since their commercial introduction by Sony in 1991,[28] LIBs have been widely adopted in portable electronic devices, electric vehicles, and renewable energy storage systems. Among the various types of LIBs, lithium iron phosphate ($LiFePO_4$) batteries are particularly noteworthy due to their high safety, thermal stability, and environmental friendliness. [29–31] However, the rapid increase in the consumption of $LiFePO_4$ batteries has resulted in a growing volume of spent batteries, posing significant environmental concerns. For this reason, there is a need to

develop of efficient and sustainable recycling methods to recover valuable metals and mitigate environmental impacts. Lithium, as well iron, phosphorus and vanadium, are a critical component of LIBs and essential for battery performance. The escalating demand for lithium, driven by the expanding EV market, underscores the need for effective recycling strategies to ensure a stable supply of this vital metal. Several studies have reviewed the latest techniques for recovering materials from spent lithium-ion batteries (LIBs).[32] Generally, the recycling process can be categorized into discharging and dismantling, pretreatment, metals leaching, and metal separation. Pretreatment methods, such as mechanical separation, ultrasonic cleaning, solvent dissolution, and ionic liquid dismantling, are crucial for isolating cathodic materials from the aluminum foil.[32] Hydrometallurgical methods have emerged as a promising approach for the recovery of metals from spent LIBs. These methods involve the use of aqueous solutions to selectively leach metals from the battery materials. Compared to pyrometallurgical processes, hydrometallurgical methods are more energy-efficient and generate less secondary pollution.[33] In recent years, researchers have increasingly used natural organic acids as leaching agents to mitigate adverse environmental impacts.[34] For example, citric acid has been used to achieve high recovery efficiencies for lithium, nickel, cobalt, and manganese from spent lithium nickel manganese cobalt oxide (NMC) batteries.[35] Similarly, oxalic acid has shown promising results in selectively recovering lithium and iron from spent LiFePO4 batteries, with lithium leaching efficiencies reaching up to 98%.[28] Tartaric acid has also been effective in the recovery of lithium from spent LIBs.[36] Among all these studies on the use of organic acids there is no available literature on the recovery of tartaric acid, to the best of our knowledge.

This research focuses on the use of tartaric acid, derived from agri-food waste, as a leaching agent for the recovery of lithium from spent $LiFePO_4$ batteries. Tartaric acid ($C_4H_6O_6$) is a naturally occurring organic acid commonly found in grapes and other fruits.[37] It is widely used in various industries, including food and beverage production, pharmaceuticals, and chemical manufacturing.[38] Its effectiveness as a leaching agent for metal extraction is due to its capability to form complexes with metal ions.[36] This study was inspired by one of the fundamental principles of chemistry, articulated by

Antoine-Laurent Lavoisier: "Nothing is created, nothing is destroyed, everything is transformed". Therefore, this research is dedicated to optimizing the recovery process to ensure that all possible components, including the initial leaching acid, are efficiently recovered. The goal is to enable the continuous reuse of the starting tartaric acid in subsequent leaching cycles, thus enhancing the overall sustainability and efficiency of the extraction process and contributes to a circular economy. This comprehensive recovery strategy not only maximizes resource utilization but also adheres to green chemistry principles by minimizing waste production and reducing the demand for new reagents in each cycle. Through this approach, the study gets to establish a more sustainable and resource-efficient method for hydrometallurgical applications. The influence of several process parameters on the leaching efficiency of lithium was systematically investigated. Additionally, the leaching kinetics were thoroughly analysed. Following the leaching process, both tartaric acid and lithium were recovered. These comprehensive studies provide valuable insights into the efficient and sustainable recovery of lithium from spent batteries.

METHODS

Materials and Chemicals

The discharged $LiFePO_4$ pouch cells used in this study were provided by Orim S.p.a., a company specializing in metal recovery from solid waste in the Marche (Italy). We examined the cathodic active material extracted from these cells. Reagents and chemicals including HNO_3 (65% pure), HCl (37% pure), and H_2O_2 (35%) were purchased from Sigma-Aldrich and used without further modification. NaOH, $CaCl_2$ and Li_3PO_4 were purchased by Sigma-Aldrich while Na_3PO_4 by ThermoScientific. Tartaric acid ($C_4H_6O_6$) was obtained from Distillerie Mazzari S.p.a., an industry involved in recycling marc to recover the acid. Lithium, vanadium, iron and phosphorous standards were purchased from Carlo Erba and Sigma Aldrich. Deionized water was employed in the leaching process and for the preparation of solutions for ICP-OES analysis.

Experimental plan

An experimental design approach was used to optimize the industrial hydrometallurgical process. A full factorial design with five factors varied at two levels would require at least $2^5 = 32$ analysis and would give information on the main effect of each factor and on all interactions between the different factors.[20,39] To limit sample analysis time and cost, a fractional factorial design $2^{(5-1)}$ with resolution V was performed. Total 16 experiments were carried out in the fractional design matrix with the high and low levels represented by +1 and−1, respectively (Table 3). Thus, a fractional factorial design was utilized to screen all the variables that can influence the system along with the respective range of variability. We examined five independent variables (factors) with the aim of discriminating the significant ones from those with a negligible effect. The factors include the solid/liquid ratio (S/L) in g/L, the working temperature (T) expressed in degrees Celsius (°C), the reaction time (t_r) of the leaching process expressed in minutes (min), the concentration of tartaric acid ($[C_4H_6O_6]$) expressed in molarity (mol/L) and the concentration of hydrogen peroxide (H_2O_2) in volume %. According to the number of factors and their respective levels, the postulated multiple linear regression model is composed of 16 terms (1 constant,5 linear terms and 10 two-interactions terms) without confounding (aliasing):

$$y = b_0 + b_1x_1 + b_2x_2 + b_3x_3 + b_4x_4 + b_5x_5 + b_{12}x_1x_2 + b_{13}x_1x_3 + b_{14}x_1x_4 + b_{15}x_1x_5 + b_{23}x_2x_3 + b_{24}x_2x_4 + b_{25}x_2x_5 + b_{34}x_3x_4 + b_{35}x_3x_5 + b_{45}x_4x_5 + \varepsilon \quad (3)$$

The factors were selected based on experience and classical leaching processes described in the literature.[36,40] Subsequently, two-factors central composite design circumscribed was developed to optimize the lithium leaching process, with a total of 13 experiments with 5 replicates of the central point. It was chosen only the significant variables. Thus, according to the number of factors and the respective levels, the postulated model is the full quadratic model composed of 6 terms:

$$y = b_0 + b_1x_1 + b_2x_4 + b_{14}x_1x_4 + b_{11}x_1^2 + b_{44}x_4^2 + \varepsilon \quad (4)$$

Table 3 lists the variables together with their respective levels, both fractional design and central composite design.

Table 3. Independent variables and their coded and actual values used for experimental design for the optimization of the lithium leaching process. It shows both fractional factorial design and central composite design.

Fractional factorial design

Factors	Coded variables	Actual values and coded levels	
		-1	1
Sample (g/L)	X_1	100	500
T (°C)	X_2	25	80
Reaction time (min)	X_3	60	180
$[C_4H_6O_6]$ (mol/L)	X_4	0.4	1.8
H_2O_2 (%)	X_5	1	4

Central composite design

Factors	Coded variables	Actual values and coded levels				
		-α	-1	0	1	α
Sample (g/L)	X_1	583	100	300	500	17
$[C_4H_6O_6]$ (mol/L)	X_4	0.1	0.4	1.1	1.8	2.1

α is an axial level also known as the "star point" which is specific to composite center designs (α = 1.414)

For the recovery of tartaric acid, a full factorial design was used to study the effect of three variables: the stoichiometric ratio between lithium and precipitating agent (1:1 and 1:2, x_1), the physical state of the added salt: (solid or liquid, x_2), and the washing process after filtration (with or without washing x_3). The percentage yield of calcium tartrate was determined using gravimetric analysis and used as response. Concurrently, the purity of the precipitate was monitored to evaluate potential inclusions, occlusions, or coprecipitations of lithium at pH 7. This dual approach ensured a comprehensive assessment of both the yield and the purity of the calcium tartrate precipitate. Table 4 shows the variables with their respective levels. The postulated mathematical model with main and interactions effects is:

$$y = b_0 + b_1X_1 + b_2X_2 + b_3X_3 + b_{12}X_1X_2 + b_{13}X_1X_3 + b_{23}X_2X_3 + \varepsilon \quad (5)$$

The first variable was chosen to enhance tartaric acid recovery efficiency. The other two categorical variables were selected for the same purpose and to mitigate the dilution effect caused by adding water, which reduces lithium concentration. Several studies indicate that high lithium recovery is achieved with concentrated solutions, so maintaining solution concentration was a key objective.[41] As for lithium precipitation, a DoE approach was not applied, as this process has already been widely investigated in the literature due to its high efficiency.[41–44]

All the experiments of each experimental design were conducted in a randomized order to eliminate any potential systematic biases that could affect the results.

Table 4. Independent variables and their coded and actual values used for experimental.

Factors	Coded variables	Actual values and coded levels	
		-1	1
Stoichiometric ratio	X_1	1	2
Precipitating agent	X_2	liquid	solid
Washing	X_3	without	with

To clarify the overall experimental approach and the rationale behind the chosen methodologies, the following schematic (Figure 5) summarizes the DoE strategies applied across different stages of the process development. Three different DoE methodologies were employed, each designed to the specific objective of the corresponding step:

- **Leaching of lithium**: A two-step approach was adopted. First, a fractional factorial design was used to screen five variables and identify the most significant factors. Then, the main factors were further investigated using a circumscribed central composite design for optimization.

- **Tartaric acid precipitation**: A full factorial design involving three factors was applied directly, as the number of variables was manageable, and no preliminary screening was necessary.

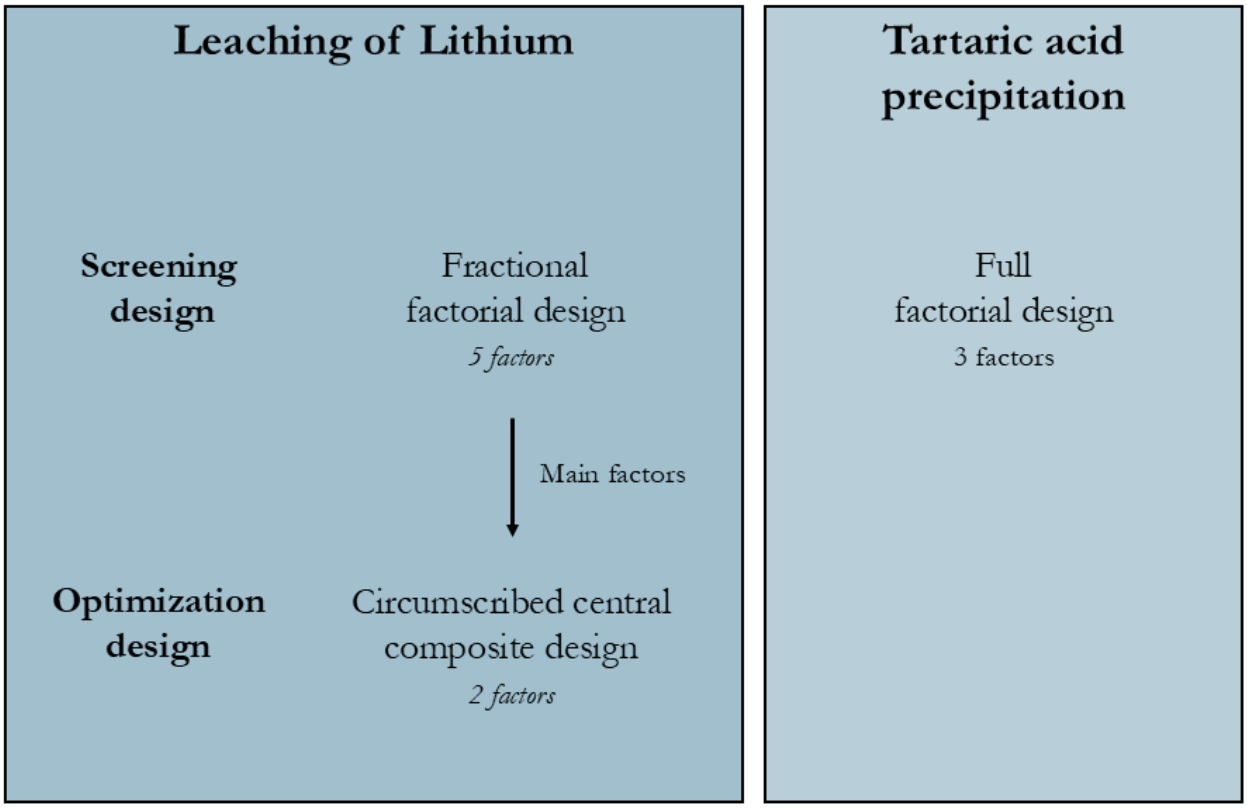

Figure 5. Summary scheme of the Design of Experiments (DoE) strategies applied during the different steps of the process: lithium leaching and tartaric acid precipitation. A two-step approach (screening and optimization) was adopted for leaching, while a full factorial design was applied for precipitation.

Experimental Procedure

The pouch cells were disassembled, and a product analysis was conducted. The cathodic active material (containing lithium) was recovered through a mechanical abrasion. This one was thoroughly characterized and used as the primary subject of the research. Aqua regia was used to dissolve it to measure the total amount of the metals (wt% total). Specifically, three tests were conducted with the heating plate set at 350°C. Consequently, the total metal content was calculated as an average of these three trials. For the optimization of leaching process, each experiment was carried out using the same leaching starting solution to maintain uniformity in measurement's errors. A condenser was used to prevent an increase in tartaric acid concentration when the temperature was set to high, while the

stirring rate was kept constant at 300 rpm. Upon completion of the reaction, the solution was filtered and then filled up to the desired volume in a volumetric flask. The metal content (wt% leaching) of the resulting leaching solution was then measured through ICP-OES. The Leaching Efficiency (LE) of each metal was calculated using:

$$LE = \frac{\text{wt\%(leaching)}}{wt\%(total)}\ x\ 100 \qquad \text{where} \qquad wt\% = \frac{[M] x\ V\ x\ DF}{w}\ x\ 100 \tag{6}$$

whereas: wt% (leaching) is the metal content leached and wt% (total) is the total metal content in the batteries. M, V, DF, and w are the metal concentrations in leach liquor (mg/L), the volume of leach liquor (L), the dilution factor for the ICP-OES analysis and the weight of sampling (mg), respectively.

After determining the optimum experiment with the highest lithium leaching efficiency, the precipitation processes for tartaric acid and lithium were examined in detail. The initial phase of the study involved the preparation and testing of synthetic leaching solutions, formulated to replicate the chemical composition found in real leachates from spent $LiFePO_4$ batteries. These model solutions allowed for a controlled evaluation of the precipitation behaviour and process parameters. Once the method was validated, the experiments were extended to real leaching solutions obtained directly from the treatment of cathodic materials extracted from dismantled lithium-ion batteries, to assess the practical applicability of the proposed recovery strategy under realistic conditions. To maintain solution concentration and prevent excessive dilution, 10 M NaOH was used to adjust the pH to 7.0. At this pH, $CaCl_2$ was introduced as the precipitating agent. The resulting precipitate was filtered and dried for 24 hours under low vacuum conditions. Subsequently, the pH of the filtrate obtained after calcium tartrate precipitation was adjusted to 10.0 using additional NaOH, and Na_3PO_4 was added to precipitate Li_3PO_4. The precipitation experiment was conducted at 80 °C for 2h with a stirring speed of 300 r/min and was repeated several times. Since the solubility of Li_3PO_4 decreases with increasing temperature, a higher temperature can make more Li precipitate. The precipitated Li_3PO_4 then collected through filtrating and washed with 80 °C deionized water to eliminate the excess Na_3PO_4. The Li

contents before and after precipitation were measured by ICP-OES for the calculation of Li_3PO_4 precipitation %.

RESULTS AND DISCUSSION

Disassembly and characterizations

Product analysis was conducted on five pouch cell batteries, providing both qualitative and quantitative information. This analysis allows a comprehensive understanding of the waste material under investigation. In this context, the analysis is aimed at obtaining a detailed overview of the waste and facilitating the planning of its recycling process. The operational procedure involves the separation of all the components of each individual battery. At first, pouch cells were weighed before manual disassembly. Each component was then weighed using an analytical balance, providing detailed measurements of each component's mass. This approach offers a comprehensive view of the sample being analysed, allowing for a detailed assessment of the waste material. Figure 6 show the product analysis.

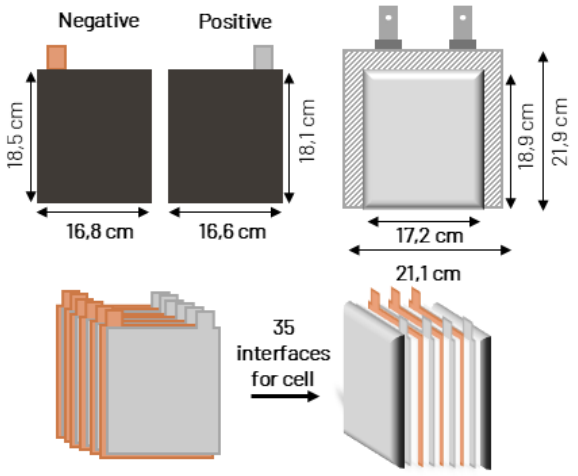

Component	Average (g)	IC 95%
Pounch Cell	774,88	4,18
Without Casing	732,93	4,20
Casing, Tabs	42,02	0,35
Collector +	12,26	0,18
Collector-, Separator	9,00	0,07

Figure 6. Product analysis of the pouch cells.

The dimensions of the electrode sheets and casing are shown on the left, including the internal stack of 35 layers forming the electrochemical cell. The table on the right provides the average mass (in grams) and associated 95% confidence intervals (CI) for each major component:

- **Pouch Cell**: Total mass of the complete, sealed battery cell.
- **Without Casing**: Mass of the internal electrochemical components, excluding the aluminium casing and tabs.
- **Casing**, **Tabs**: Combined mass of the external aluminium pouch and tab connectors.
- **Collector +**: Mass of the current collector associated with the positive electrode (typically aluminum foil).
- **Collector –**, **Separator**: Combined mass of the negative current collector (typically copper foil) and the separator layers between electrodes.

The active material average of a cathode, calculated from three representative samples, was determined to be 10.51g(±0.08). Given the total cathode mass of 12.26g (Figure 6), it can be concluded that 86% of the cathode consists of active material, specifically the component containing $LiFePO_4$.

The total metal content was determined through ICP-OES. It measured 5.54 ± 0.18 wt % of lithium, 19.91 ± 1.62 wt % of phosphorus, 32.37 ± 2.51 wt % of iron and 0.25 ± 0.02 wt % of vanadium. The reported error refers to the ICP analysis and is based on three replicates. The XRD analysis, shown in Figure 7a, confirms the presence of a single crystalline phase in the sample. The calculated pattern of $LiFePO_4$ is represented by the blue line, while the experimental one is depicted by the black line. The comparison between the two lines demonstrates a close match, indicating $LiFePO_4$ as the only crystalline phases in agreement with literature.[45] SEM-EDX analysis (Figure 7b) shows that the sample consists of small, sub-spherical particles with a homogeneous particle size distribution (≤ 5um). This information is important to study the kinetics of the process for applying the so-called model "Shrinking Core, a widely used approach to describe solid-fluid reactions where the unreacted core of a particle gradually shrinks as the reaction proceeds.[30,46,47] Furthermore, the metals exhibit a uniform

distribution across the sample (Figure 6c-e). Table 5 shows the elemental analysis. The content of Phosphorus, Iron and Vanadium was compared with the ICP-OES analysis shown below. Accounting for errors, both techniques indicate an identical percentage composition. Vanadium is used in batteries like a doping agent to improve performance.[48]

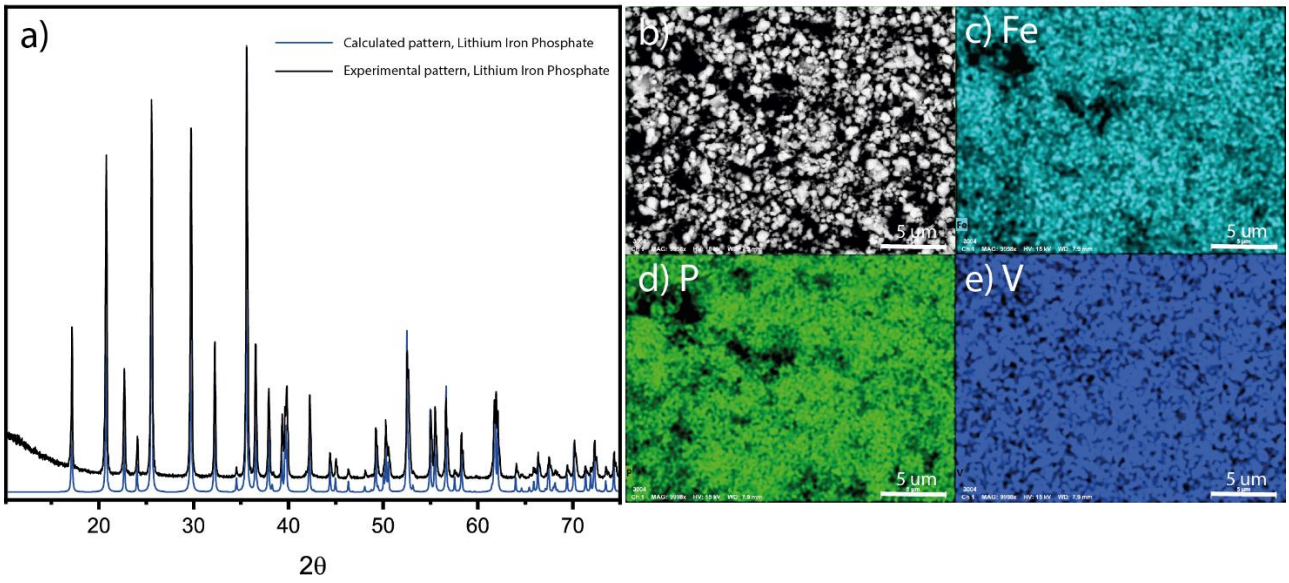

Figure 7. a) XRD pattern of the active material of cathode. b) SEM image without EDX map, c) iron EDX map, d) phosporous EDX map, and e) vanadium EDX map. Magnification 9998x and bar = 5µm

Table 5. SEM-EDX analysis.

Elemento	Mass Norm. [%]	abs. error [%]	rel. error [%]
P	15.501	0.371	2.379
V	0.254	0.011	4.219
Fe	27.722	0.476	1.708

Leaching and recovery mechanism

Tartaric acid is a diprotic, dicarboxylic acid and its dissociation reactions can be represented as:

$$H_2C_4H_4O_6 + H_2O \rightleftarrows H_3O^+ + HC_4H_4O_6^- \quad (7)$$

$$HC_4H_4O_6^- + H_2O \rightleftarrows H_3O^+ + C_4H_4O_6^{2-} \quad (8)$$

The pK_a values of tartaric acid are pK_{a1} = 2.72 and pK_{a2} = 4.79 calculated by MarvinSketch developed by Chemaxon.[49] Theoretically, the leaching products can contain Li^+, Fe^{3+}, PO_4^{3-} and vanadium. The

leaching process can be described as a complexation and/or chelation phenomenon, where tartaric acid molecules envelop and bind to metals ions, forming stable complex compounds.[36,50–53] Computational studies have proposed complexes of tartaric acid with various metals, including lithium, for their potential use as leaching agents.[36] For the recovery of tartaric acid by precipitation, it was chosen the salt with the lowest solubility constant (K_{sp}) to achieve a high-yield precipitate. Consequently, calcium tartrate was used by adding $CaCl_2$. The precipitation reaction was conducted at pH 7, where the molecular fraction $\alpha_{C_4H_4O_6^{2-}}$ is maximized, ensuring that almost 100% of the tartaric acid as the tartrate ion ($C_4H_4O_6^{2-}$). This approach ensures efficient precipitation and maximizes recovery. The precipitation reaction can be written:

$$C_4H_4O_6^{2-} + Ca^{2+} \rightleftarrows CaC_4H_4O_6 \downarrow \qquad K_{ps} = 1.48 * 10^{-7} \tag{9}$$

where K_{ps} was calculated from the solubility of calcium tartrate, which is 0.1 g/L.[54]

For the recovery of lithium, a similar approach was utilized. An anion was chosen to form a salt with a low solubility product constant (K_{ps}). Specifically, Na_3PO_4 was selected as the precipitating agent to form Li_3PO_4, which has a low K_{ps} of 2.37×10^{-11},[55] (equation 10). The pH of the precipitation reaction was carefully selected based on the pK_a values of phosphoric acid, H_3PO_4 (pK_1 2.15, pK_2 7.20, and pK_3 12.15). These values indicate that a pH above 12 is necessary to maximize the concentration of PO_4^{3-} ions, which is crucial for effective lithium precipitation. Additionally, Na_3PO_4, derived from a strong base and a weak acid, undergoes basic hydrolysis in solution (equation 11-12), which increases the pH. Thus, the solution pH was adjusted to 10 using NaOH. Subsequently, Na_3PO_4 was added, exploiting its hydrolysis to further raise the pH to 12 without diluting the solution. As OH^- ions form and the pH increases, the hydrolysis reaction is inhibited, thereby facilitating the precipitation of Li_3PO_4.[41] This method ensures that the solution remains concentrated, optimizing the lithium recovery process gained a pH about of 10.

$$PO_4^{3-} + 3Li^+ \rightarrow Li_3PO_4 \tag{10}$$

$$Na_3PO_4 \rightarrow 3Na^+ + PO_4^{3-} \quad (11)$$

$$PO_4^{3-} + H_2O \rightleftarrows HPO_4^{2-} + OH^- \quad (12)$$

Optimization of hydrometallurgical process

The leaching step was first addressed using a fractional factorial design (FFD) to identify the significant factors affecting the process. Following this, a circumscribed central composite design (CCC) was employed to optimize these factors.

Table 6. Synoptic table with FFD experiments and relative response.

N° exp	Run	x_1	x_2	x_3	x_4	x_5	% Li
1	1	-1	-1	-1	-1	1	60.57
2	4	1	-1	-1	-1	-1	12.73
3	13	-1	1	-1	-1	-1	35.17
4	3	1	1	-1	-1	1	13.6
5	9	-1	-1	1	-1	-1	46.24
6	8	1	-1	1	-1	1	16.62
7	15	-1	1	1	-1	1	55.23
8	6	1	1	1	-1	-1	9.47
9	2	-1	-1	-1	1	-1	70.02
10	19	1	-1	-1	1	1	33.31
11	17	-1	1	-1	1	1	66.06
12	5	1	1	-1	1	-1	44.29
13	10	-1	-1	1	1	1	67.28
14	11	1	-1	1	1	-1	38.76
15	16	-1	1	1	1	-1	73.81

After conducting all the FFD experiments and collecting the results (expressed as a percentage of lithium leached) shown in Table 6, a MLR analysis was performed. Figure 8a illustrates the coefficient

plot of the derived model, highlighting the impact of each factor on the leaching efficiency. This approach ensured a systematic and thorough investigation, enabling the identification and optimization of critical parameters for the leaching process. As observed, the variables x_1 (solid-liquid ratio) and x_4 (tartaric acid concentration) play a significant role in the generated model. Specifically, an increase in the solid-liquid ratio correlates with a decrease in leaching efficiency, as indicated by the negative coefficient. Conversely, an increase in tartaric acid concentration correlates with an increase in leaching efficiency, as reflected by the positive coefficient. These findings highlight the importance of optimizing both the solid-liquid ratio and the tartaric acid concentration to enhance the overall efficiency of the leaching process.

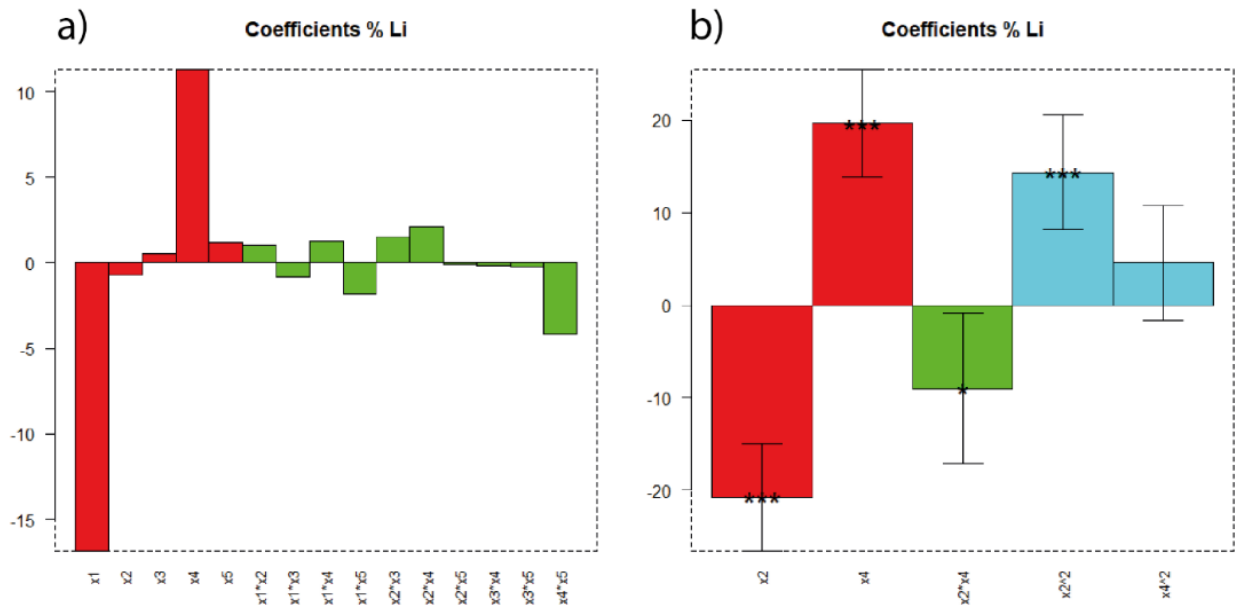

Figure 8. a) Coefficients plot of fractional factorial design. b) Coefficients plot of central composite design: the number of asterisks indicate the significance of coefficients while the error bars indicate confidential interval error of the coefficients.

Thus, it was carried out a CCC design only with x1 and x4. After running all the experiments and collecting the results (Table 7), a MLR was carried out:

$$y = 18.3 - 20.7x_1(***) + 19.6x_4(***) - 9.0x_1x_4(*) + 14.3x_1^2(***) + 4.6x_4^2 \quad (13)$$

Stars represent the statistical significance (p-value; * = 0.05, ** = 0.01, *** = 0.001). Figure 8b shows the coefficients plot for this model with the relative confidential error bar. The model has a SD of residuals of 6.9 (10 d.o.f), an experimental SD of 4.0 (4 d.o.f), an explained variance of 93.4 and an

explained variance in prediction of 80.0. Since the residual standard deviation and the experimental standard deviation were not significantly different, there is no lack of fit.

Table 7. Synoptic table with CCC experiments and relative response.

N°exp	Run	x_1	x_4	% Li
1	11	-1.00	-1.00	20.37
2	6	1.00	-1.00	5.35
3	9	-1.00	1.00	79.30
4	4	1.00	1.00	28.32
5	2	-1.41	0.00	85.93
6	1	1.41	0.00	15.55
7	7	0.00	-1.41	4.95
8	3	0.00	1.41	57.79
9	10	0.00	0.00	15.05
10	5	0.00	0.00	16.24
11	8	0.00	0.00	16.55
12	13	0.00	0.00	24.98
13	12	0.00	0.00	18.72

The linear terms for solid-liquid ratio (x_1) and tartaric acid molarity (x_4) variables are highly significant (both x_1 and x_4 at $p<0.001$). Additionally, the interaction term for solid-liquid ratio and tartaric acid molarity (x_1x_4) is also significant ($p<0.05$). The linear terms indicate that a more favourable response is achieved at lower solid-liquid ratios and higher tartaric acid molarities. Furthermore, the quadratic term of x_1 is also significant ($p<0.001$). This suggests that lower solid-liquid ratios and higher tartaric acid concentrations result in improved leaching efficiency, likely due to the increased availability of the acid to interact with the solid material, thereby enhancing the leaching process. Figure 9 presents the response iso-surface plot for the two variables considered.

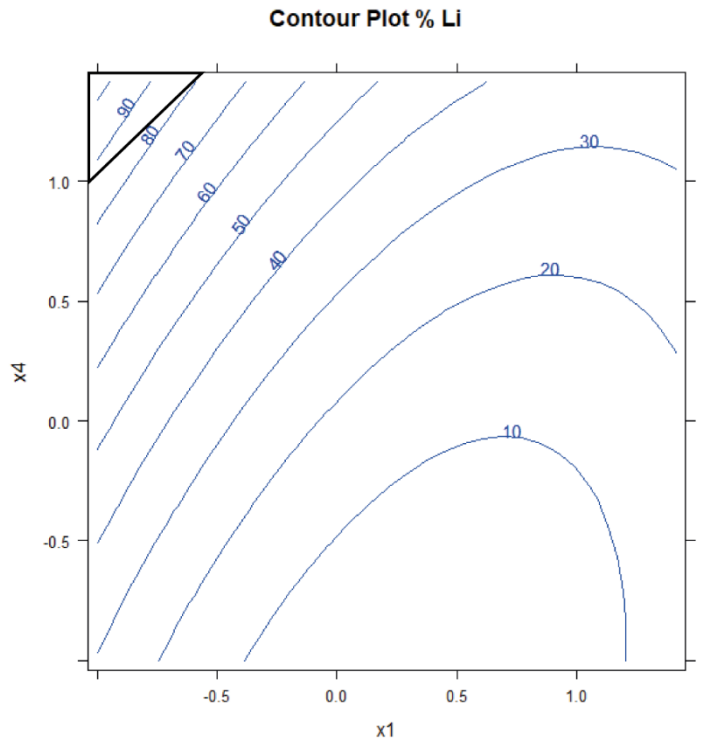

Figure 9. Countour plot between x1 (solid-liquid ratio) and x4 (tartaric acid concentration).

The optimal conditions for achieving high leaching efficiencies were identified in the upper left of the isosurface plot (black triangle in the figure 9), with a tartaric acid concentration of 2.1 M and a solid-liquid ratio of approximately 100 g/L. Using the predictive model, three experiments were conducted with 2.1 M tartaric acid and 110 g/L of active material, showing a leaching efficiency of 95.0% (±2.3).

Recovery of tartaric acid

After the leaching optimization, the recovery process of tartaric acid was studied to enable its reuse in subsequent leaching cycles. Following this, the recovery of lithium was also examined. This dual focus ensured that the process was both efficient and sustainable, maximizing resource utilization and minimizing waste. Before to study the precipitation process, a 2.1M solution with added $CaCl_2$ was prepared. This experiment was useful to obtain a precipitate of calcium tartrate, which was used as a reference. An IR spectrum was conducted on this sample to confirm correct precipitation of the calcium tartrate, followed by XRD analysis to identify the crystalline phase.

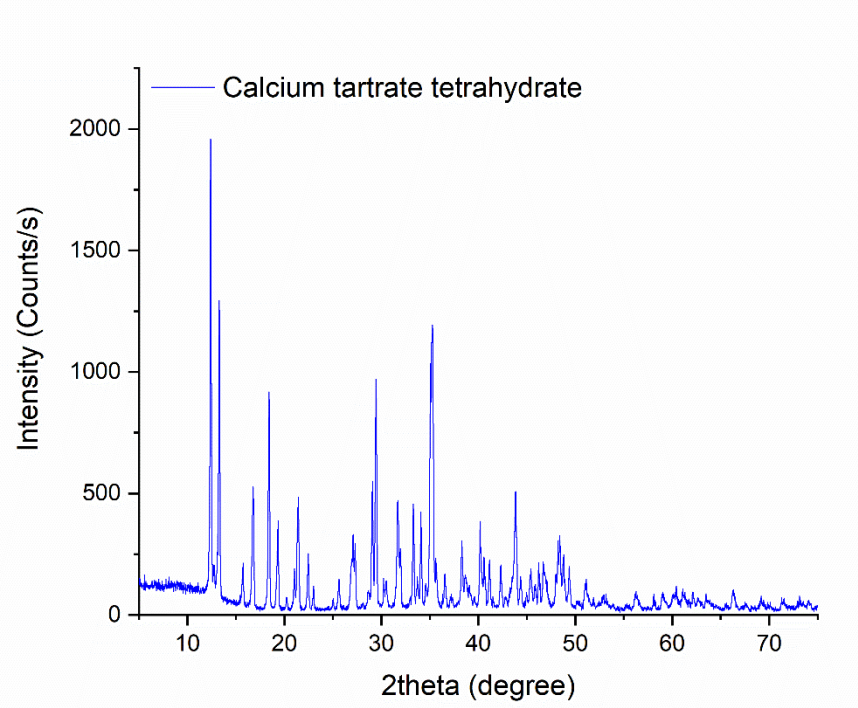

Figure 10. XRD pattern of calcium tartrate reference.

XRD pattern (Figure 10) was confirmed by ICDD database that indicate a tetrahydrate calcium tartrate. This information was crucial as it allowed us to calculate the right precipitation yield.

Table 8. Synoptic table with full factorial design and relative responses.

Run	N° exp	x1	x2	x3	% $CaC_4H_4O_6$	% Purity
1	1	−1	−1	+1	92.28%	99.94%
2	6	+1	−1	−1	100.25%	99.95%
3	5	−1	−1	−1	94.04%	99.92%
4	8	+1	+1	−1	99.03%	99.89%
5	2	+1	−1	+1	98.36%	99.96%
6	7	−1	+1	−1	93.24%	99.89%
7	3	−1	+1	+1	91.79%	99.91%
8	4	+1	+1	+1	102.94%	99.94%
9	8R	1	1	−1	100.51%	99.93%

After performing all the experiments, a MLR analysis was conducted:

$$Y = 96.5 + 3.7X_1 + 0.3X_2 - 0.2X_3 + 0.6X_1X_2 + 0.6X_1X_3 + 0.7X_2X_3 \quad (14)$$

with an explained variance equal to 87.97%. Table 8 presents the experiments and their corresponding experimental responses. Figure 11 show the coefficient plot. Notably, x_1 exhibits a larger magnitude compared to the other factors, indicating a stronger influence on the response variable y. This suggests that x_1 plays a critical role in driving the outcome. Specifically, it is reasonable to hypothesize that an increase in the stoichiometric ratio would positively affect the precipitation yield, which aligns with the underlying process dynamics. Thus, solid $CaCl_2$ was added in a stoichiometric ratio of 1:2 without washing, thereby preventing lithium dilution. Another experiment under these conditions was conducted to study repeatability, yielding a recovery rate of 99.8% (±2.8). All experiments consistently demonstrated a high purity of approximately 99.93% (±0.03) (Table 8). Purity was assessed by ICP-OES analysis after mineralizing each sample in aqua regia. This response is not used to obtain a MLR model because for low variability.

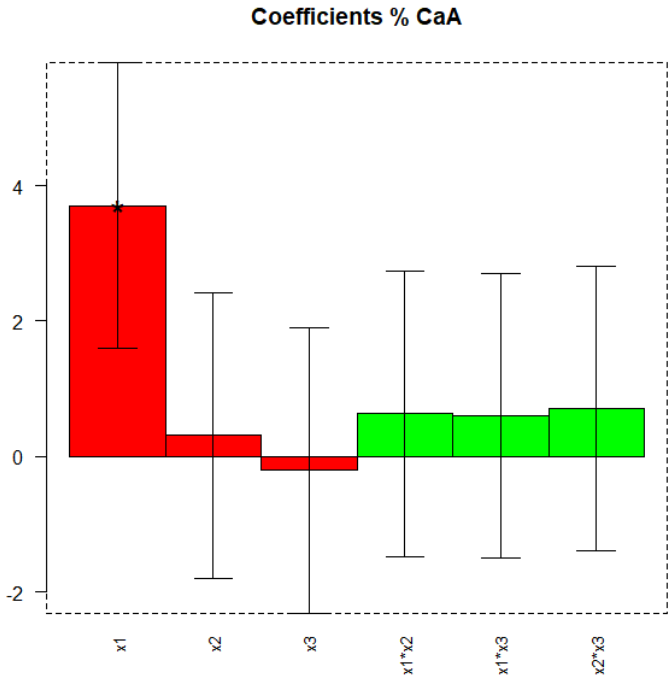

Figure 11. Coefficient plot based on MLR on D-optimal design.

An FTIR spectrum was acquired to confirm the successful precipitation and was subsequently compared with the reference spectrum for validation (Figure 12). The IR spectra obtained are similar to the previously reported IR spectrum of calcium tartrate crystals.[56,57] The absorption bands in the range of 3600 cm–1 to 3400 cm^{-1} are attributed to the O–H stretching mode. The absorption at 2987 cm^{-1} corresponds to the C–H stretching mode. The bands near 1581 cm^{-1} and 1487 cm^{-1} are associated with the C=O stretch of the carbonyl group. The strong peak around 1383 cm^{-1} is linked to the symmetric C=O stretch combined with δ (O–C=O) mode. The absorption near 1330 cm^{-1} is attributed to C–O stretching. The absorption at 1282 cm–1 is due to C–H bending. The peak around 1147 cm^{-1} is associated with C–H vibrational modes. Peaks at 1061 cm^{-1} and 1011 cm^{-1} of varying intensities are due to out-of-plane O–H deformation and C–O stretching vibrations, respectively. Absorptions between 815 cm^{-1} and 530 cm^{-1} are due to calcium–oxygen bonding.[56,57]

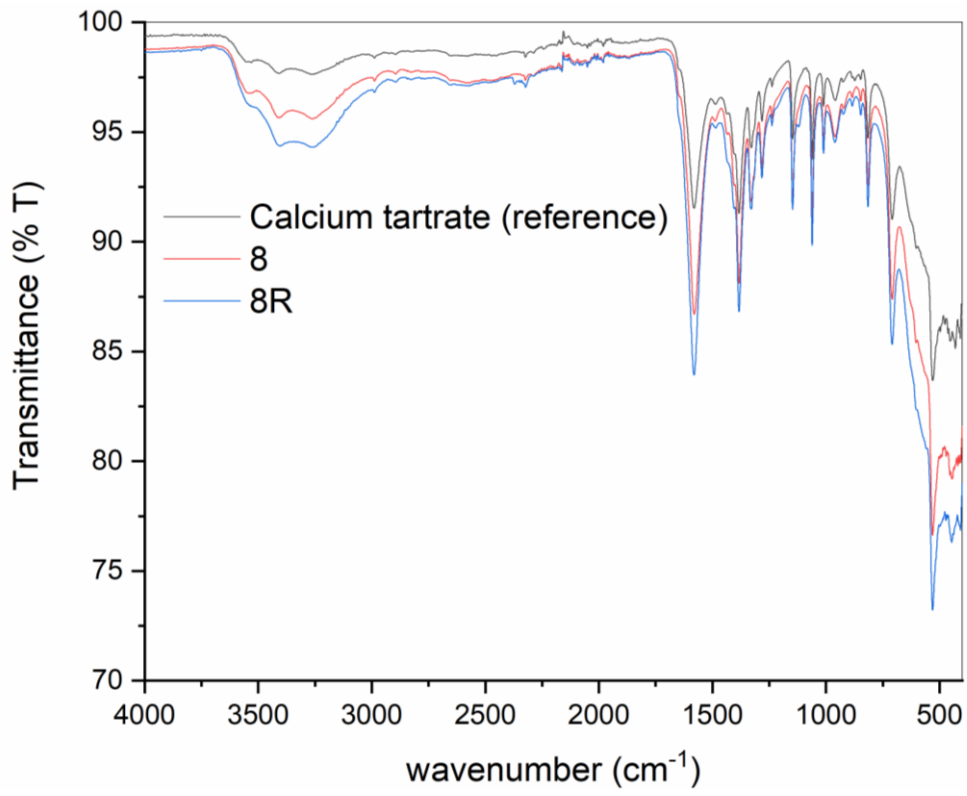

Figure 12. FTIR spectrum of calcium tartrate reference (black line), and two precipitation trials in synthetic solution (red and blue line).

Recovery of lithium

An IR spectrum of the starting material Li_3PO_4, was recorded and used as reference (Figure 13). Thus, for subsequent trials (in synthetic and real solution) each precipitate was compared by performing IR spectroscopy and comparing the results with the standard IR spectra. In the pure Li_3PO_4 spectra 1015 and 586 cm^{-1} represents vibration of PO_4 group.[58,59] Subsequently, lithium was precipitated as lithium phosphate in synthetic solutions. In this study, it achieved a recovery yield of 94.0%(±1.8). The error in these steps indicate the standard deviation calculated in two replicates. An FTIR spectrum was acquired to confirm the successful precipitation and was subsequently compared with the standard spectrum for validation (Figure 13).

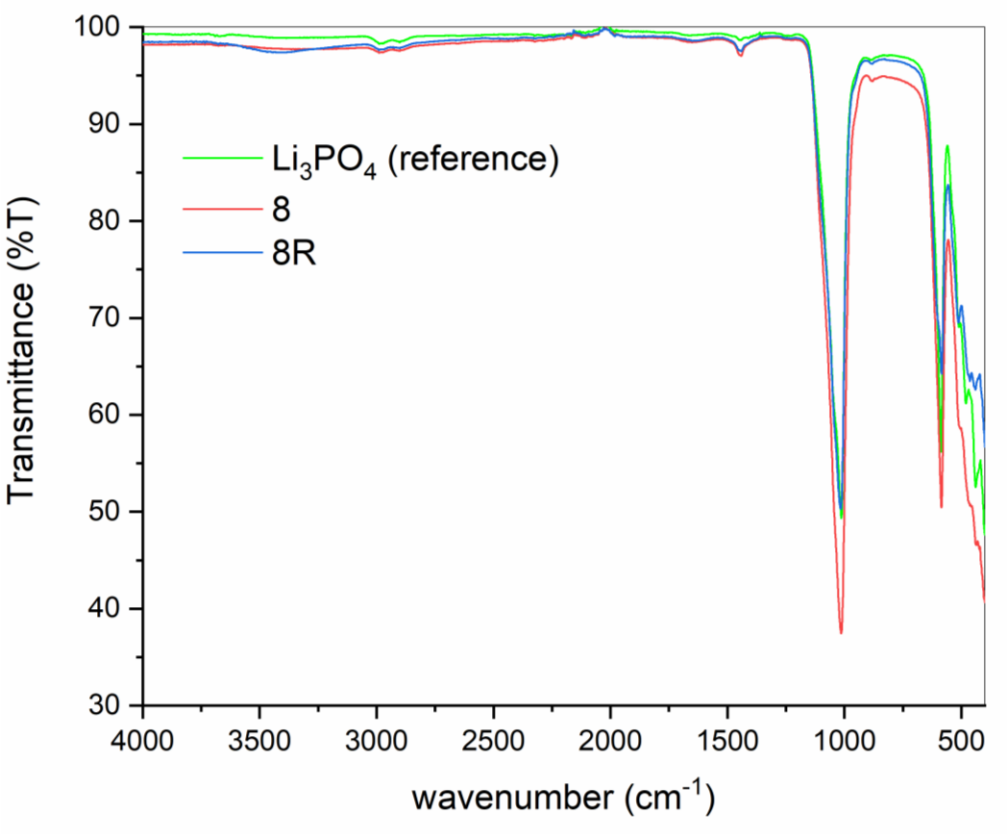

Figure 13. FTIR spectrum of lithium phosphate reference (green line), and two precipitation trials in synthetic solution (red and blue line).

From Synthetic to Real System

The developed precipitation process was then applied to the real leaching solution obtained from the leaching optimization procedure. Comparable recovery efficiencies were achieved, confirming the robustness and reproducibility of the process. It was recovered 98.0% (±1.9) of calcium tartrate and

97.7% (±3.6) of lithium phosphate. Figures 14-15 present the FTIR spectra from the real-case test. The transition to real leaching solutions demonstrated the practical applicability of the optimized conditions. Moreover, the successful implementation of this method not only confirms its efficacy but also provides a viable pathway for efficient lithium recovery in industrial applications.

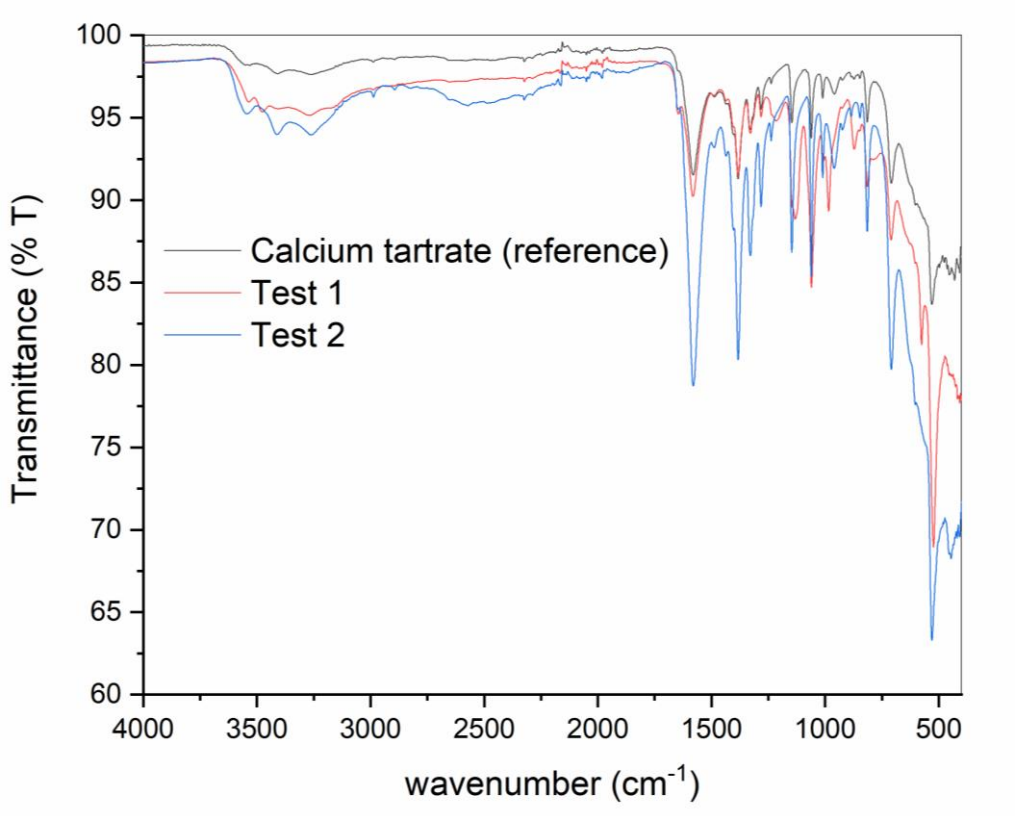

Figure 14. Real-Process Evaluation on calcium tartrate precipitation.

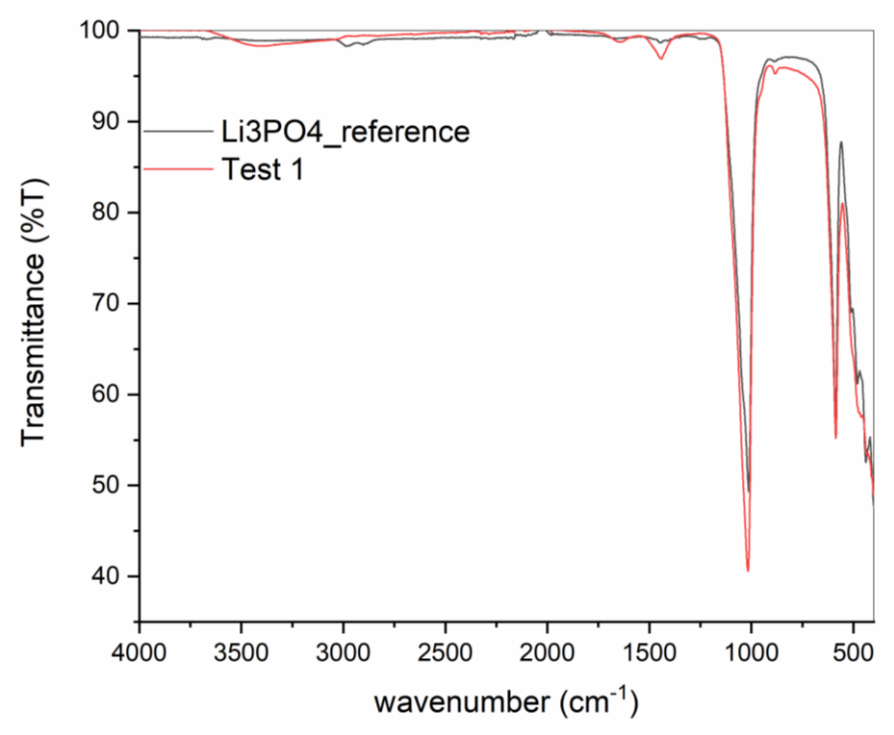

Figure 15. Real-Process Evaluation on lithium phosphate precipitation.

Kinetics and Determination of the Rate-Controlling

To study the leaching kinetics, a test was conducted using optimized conditions for lithium recovery. The objective was to analyse the leaching rate within a specific timeframe. The shrinking core model (SCM), widely used for leaching kinetics, was applied here to describe consecutive steps in the leaching process: diffusion of the reagent through a liquid film around the particles, diffusion through a solid product layer, and the dissolution reaction at the unreacted core surface, leading to metal mobilization. Each step has corresponding kinetic equations that describe the process rate, with the equation best fitting the experimental data considered the rate-controlling step:

Film diffusion control:

$$t \propto X \tag{15}$$

Product layer diffusion control:

$$t \propto 1 - 3(1 - X)^{\frac{2}{3}} + 2(1 - X) \tag{16}$$

Chemical reaction control:

$$t \propto 1 - (1 - X)^{\frac{1}{3}} \quad (17)$$

where, t is the reaction time and X is the fraction of leached metal. The kinetic data obtained from the different mechanism equations (Eqs. 15-17) are presented in Figure 16a indicating a change in slope around 3 minutes, suggesting a shift in the leaching mechanism. Thus, the kinetic data was analysed in two phases. During the initial 3 minutes, the kinetic plots from Eqs. 15-17 are displayed in Figure 16b, showing the chemical reaction and film diffusion control equations with the highest R^2 value, indicating their dominance. The rate constant up to 3 minutes was calculated as an average resulting 0.14 min^{-1}. For the second phase, starting at 5 minutes, new equations derived by Aarabi-Karasgani et al. were used (Eqs. 18-20),[60] capturing the leaching process behaviour beyond the initial 5 minutes:

$$t - t_1 \propto X \quad (18)$$

$$t - t_1 \propto 3\left[(1 - X_1)^{\frac{2}{3}} - (1 - X)^{\frac{2}{3}}\right] - 2(X - X_1) \quad (19)$$

$$t - t_1 = (1 - X_1)^{\frac{2}{3}} - (1 - X)^{\frac{2}{3}} \quad (20)$$

where, X is the fraction of leached metal in the second stage, t_1 is the time at which the second stage is started, and X_1 is the fraction of leached material at time t_1. Figure 16c shows R^2 values for liquid film, product layer diffusion, and chemical control, which are very close, suggesting a mixed control mechanism. The rate constant was thus calculated as an average of each mechanism, resulting in 0.009 min^{-1}.

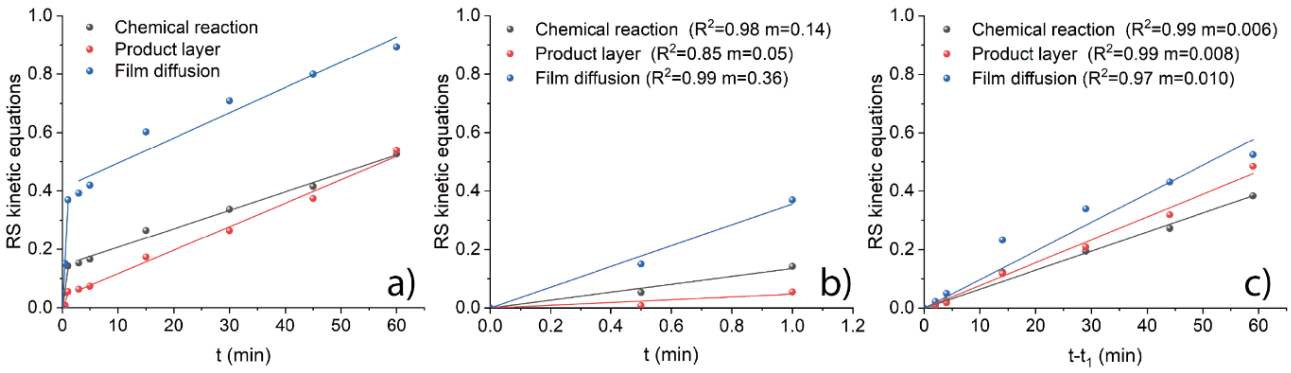

Figure 16. The right side (RS) of rate-controlling equations as a function of time at optimum conditions; a) Eqs. 15-17, b) Eqs. 15-17 (step 1), c) Eqs. 18-20 (step 2).

CONCLUSIONS

This study successfully demonstrated the sustainable recovery of lithium from $LiFePO_4$ batteries using tartaric acid derived from agri-food waste, in line with green chemistry principles by promoting resource efficiency and waste valorisation. The optimized lithium leaching process achieved an efficiency of 95.0%(±2.3). Additionally, tartaric acid recovery demonstrated a high yield of 98.0%(±1.9), allowing for its reuse in subsequent leaching cycles. Lithium precipitation as lithium phosphate resulted in a recovery yield of 97.9%(±3.6%), further confirming the efficiency and robustness of the method. The SCM demonstrated a good fit with the experimental data, allowing for the determination of the rate constant for the leaching process. It was possible to accurately describe the kinetics of the process and extract meaningful information about the rate at which the desired reaction occurs. Overall, the optimized process offers a scalable and viable solution for lithium recovery, enhancing resource utilization and minimizing waste, thus contributing to the development of sustainable industrial practices. The application of experimental design techniques, such as fractional factorial and central composite designs, was crucial in efficiently identifying and optimizing key process parameters, significantly improving the process's overall performance and reproducibility.

3.2 Hydrometallurgical Molybdenum Recovery Using Tartaric Acid from Agrifood Waste

INTRODUCTION

Molybdenum is used in a variety of industrial and chemical applications including steel production, lubricants, electrical components, and catalysts.[61] Despite not being classified as a critical raw material by the European Commission in 2023, molybdenum can be considered potentially critical due to its position on the threshold between non-critical raw materials and the criticality zone, with a notably high supply risk score (0.8).[62] Half of the global molybdenum supply originates from the treatment of molybdenite, powellite, and wulfenite ores, while the remaining fifty percent is obtained as a by-product during copper smelting.[63] At present, molybdenum sulphide concentrate undergoes an initial roasting process on a global scale leading to its transformation into industrial molybdenum oxide. Subsequently, soluble molybdate salt is extracted from this oxide, which is later used for the smelting of molybdenum metal or its alloys.[64,65] The focus of this research is on a specific catalyst based on molybdenum to produce formaldehyde, which is an important industrial chemical used in the manufacturing of resins, adhesives, and other products. Formaldehyde is typically produced by the catalytic oxidation of methanol. Molybdenum catalysts are often used in this process due to their capability to withstand the high temperatures and pressures required for the reaction. Additionally, they exhibit good activity and selectivity for the production of formaldehyde.[66,67] The formaldehyde market is expected to witness significant growth in the foreseeable future because of various factors such as increasing industrial applications and expanding end-use industries. In Europe it is expected to reach 13.1 million metric tons by 2027.[68] It is important to focus on these numbers because the production of formaldehyde is proportional to the generation of spent catalyst. As formaldehyde production increases, significantly huge proportion of catalyst will be discarded. So, it is crucial and useful to recover the main metal

within it. Several hydro and pyrometallurgical techniques have been proposed to recover molybdenum catalysts.[69] However, the use of pyrometallurgy processes is somehow restricted to higher energy expenses, secondary environmental impacts like waste gas emissions, and the production of less valuable products like polymetallic alloy.[70] Conversely, hydrometallurgical ones approaches are favoured for their notable benefits such as reduced energy consumption and lower treatment costs compared to pyrometallurgy.[70,71] Hydrometallurgical processes facilitate the transformation, migration, and enrichment of valuable metals through techniques like low-temperature roasting, strong inorganic or alkali leaching, chemical precipitation, solvent extraction, and ion exchange.[70] However, the main processes use high temperature and strong acids (e.g., H_2SO_4, HNO_3) and bases (e.g., NaOH).[72] To the best of our knowledge, no literature is available regarding the recovery of molybdenum from this type of catalyst, which is extensively utilized in the industry. The recovery of any type of raw material, mainly those with a high supply risk score,[62] is essential for various reasons. Environmentally traditional metal extraction methods such as open-pit mining, can cause significant damage to the environment and surrounding ecosystems.[73] Thus, the recovery process through recycling or other, more sustainable methods, can reduce the environmental impact of metal production. Additionally, metal recovery requires less energy compared to extracting metals from ore, leading to lower energy consumption and carbon emissions.[74] The Global molybdenum reserve base in 2022 was 12,000,000 mt, with distribution predominantly from Chile, Peru, USA, and China.[64] This critical aspect in the supply chain stability and recovering metals from existing sources can help to ensure a stable supply of metals, by reducing reliance on a sole ore source (International Molybdenum Association reported that global molybdenum extracted in 2022 was 286,440 tonnes from mine production only and does not include material recovered from spent catalysts).[75]

In this work, a green and sustainable hydrometallurgical process is developed to recover molybdenum from a spent oxidation catalyst based on tartaric acid. It is a diprotic acid that is found in many plants, particularly in grapes and tamarinds. It has the chemical formula $C_4H_6O_6$, and it is used in a variety of applications, including food and beverage production, pharmaceuticals, and chemical manufacturing.[37]

It is an effective leaching agent for metal extraction because of its ability to form complexes with metal ions.[38] In this study, the recovery was carried out from agri-food waste, specifically from wine lees produced as waste from Italian wineries. [36,76] According to an estimate provided by the International Organisation of Vine and Wine (OIV), in 2014, 44.4 Mhl of wine were produced in Italy, resulting in 8 million quintals of marc, including grape seeds (equivalent to 15% of grapes vinified), and 2,250,000 hectolitres of lees (equivalent to 5% of wine produced). [77] It is evident that in regions or countries, with high wine production, like Italy, a process that involves the recovery of tartaric acid from winery waste to leach industrial waste becomes feasible. Thus, agri-food waste can be repurposed to treat industrial waste, facilitating the retrieval and reintegration of valuable metal compounds. This practice contributes to the advancement of an effective circular economy, where the waste of one process becomes the raw material for another. The goal is to prolong the utilization of resources, extracting their utmost value before they are reclaimed and regenerated.

EXPERIMENTAL SECTION

Materials

Samples of spent catalyst waste were collected from Orim S.p.a., a solid waste recycling company in Marche (Italy). The reagents and chemicals i.e., nitric acid (69% Hiperpur), and hydrochloric acid (37% puriss) were purchased, from PanReac AppliChem and Sigma-Aldrich, respectively, and used as received. Tartaric acid used in this study was sourced from an industry that recycles wine lees to recover the acid (Distillerie Mazzari S.p.a) and was used as received. Deionized water was used in the leaching process and to prepare solutions for the analysis.

General Procedure

Aqua regia was used to dissolve samples to measure the total amount of the metals. Specifically, three tests were conducted with the heating plate set at 350°C. A condenser was used to avoid evaporation of water. Consequently, the total metal content was calculated as an average of these three trials. For the

leaching experiments, a 25 mL round bottom flask was placed on a magnetic stirrer set at a speed of 300 rpm. The temperature was fixed at 25 °C or 80°C (depending on the experiments) and a condenser was used to prevent an increase in tartaric acid concentration. Once the reaction was completed, the solution was filtered and adjusted to the desired volume in a volumetric flask. The metal content of the resulting solution was then measured through ICP-OES. The Leaching Efficiency (LE) of each metal was calculated using:

$$LE = \frac{\text{wt\%(leaching)}}{wt\%(total)}\ x\ 100 \qquad \text{where} \qquad wt\% = \frac{[M]x\ V\ x\ DF}{w}\ x\ 100 \tag{21}$$

whereas: wt% (leaching) is the metal content leached and wt% (total) is the total metal content in the spent molybdenum catalyst. M, V, DF, and w are the metal concentrations in leach liquor (mg/L), the volume of leach liquor (L), the dilution factor for the ICP-OES analysis and the weight of sampling (mg), respectively.

RESULTS AND DISCUSSION

Characterization of the spent catalyst powder

Figure 17 shows the XRD pattern of spent catalyst powder. It exhibits a large amount of amorphous phases and, mainly, the presence of $Fe_2(MoO_4)_3$ and MoO_3. Commercially available iron molybdate catalysts always contained $Fe_2(MoO_4)_3$ and MoO_3.[66,67] Knowing the crystalline phases present within the catalyst is crucial for understanding the reaction mechanism of tartaric acid during the leaching process and evaluating the acid's capability to dissolve metals that are present in specific crystalline phases.

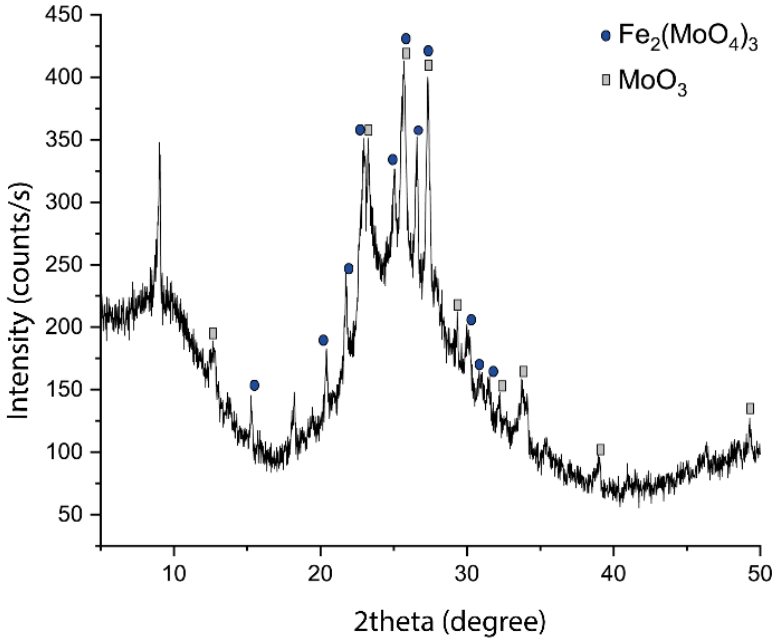

Figure 17. XRD pattern of spent molybdenum catalyst.

The QualX software identified non-indexed peaks as organic compounds. For this reason, were performed various analyses such as elemental microanalysis, FTIR, TGA/DTA. An elemental microanalysis of the catalyst show the presence of 1.72% carbon and 0.67% hydrogen (Figure 18).

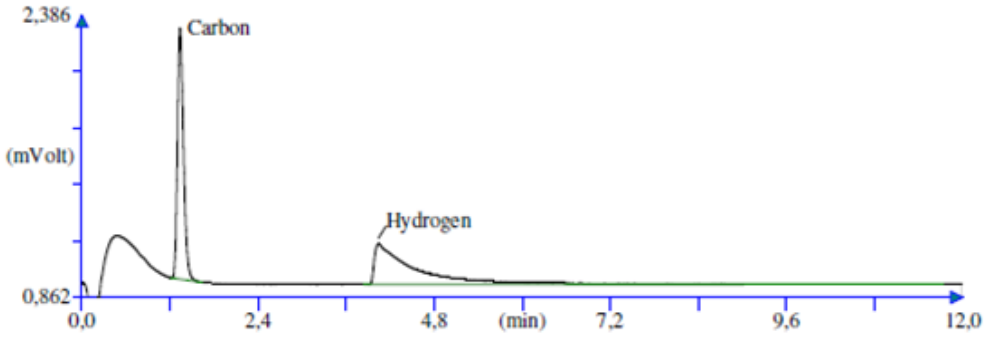

Element Name	%	Ret.Time
Carbon	1.7229	80
Hydrogen	0.6713	243
Totals	2.3942	

Figure 18. Elemental microanalysis of the catalyst.

The FT-IR spectrum of the catalyst (Figure 19) also confirms the presence of organic compounds, as indicated by the stretching peaks at 2918 and 2850 cm^{-1}, which correspond to the possible stretching of C-H bonds in alkanes or alkenes.

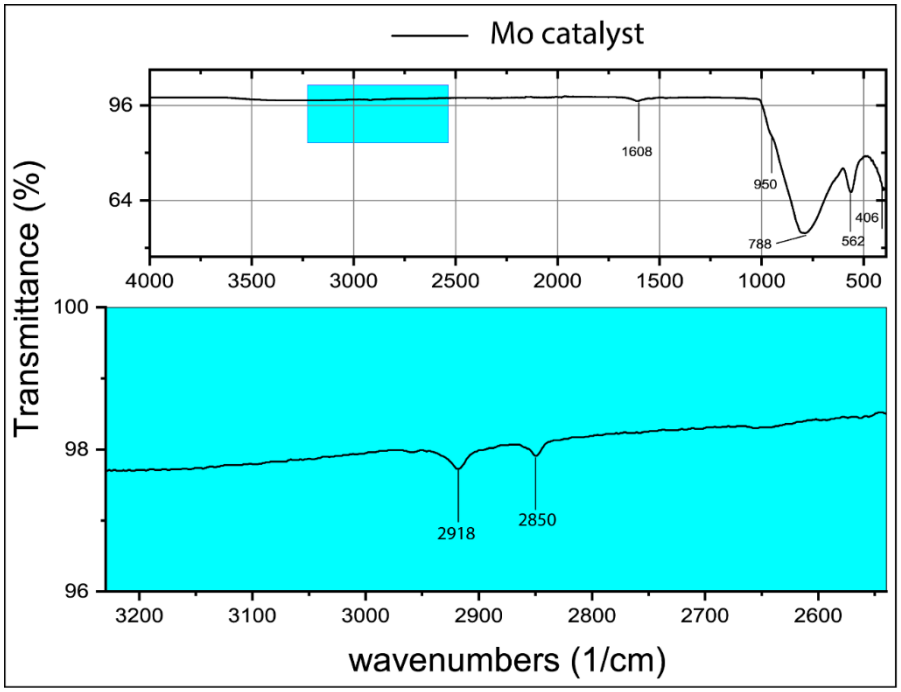

Figure 19. FT-IR spectrum of the catalyst. Up the full-spectrum; below the zoom in the region of 3000cm-1.

It is known that metals do not emit signals at these wavelengths. A broad band ranging from 700 and 900 cm^{-1} is attributed to the vibrations of Mo–O bond within the tetrahedral MoO4 present in the $Fe_2(MoO_4)_3$ catalyst. The band at 554/562 cm^{-1} can be assigned to the vibrations of bridging oxygen bonds (Mo–O–Mo), while the weak band observed at 963/950 cm^{-1} can be assigned to the vibrations of the bridging oxygen (Fe–O–Mo) bonds.[78,79] The presence of a narrow band at 990/992 cm^{-1} and a broad one at 624/614 cm^{-1} in IR spectra of the sample heated at 400 °C (Figure 20) is characteristic of MoO3.[79]

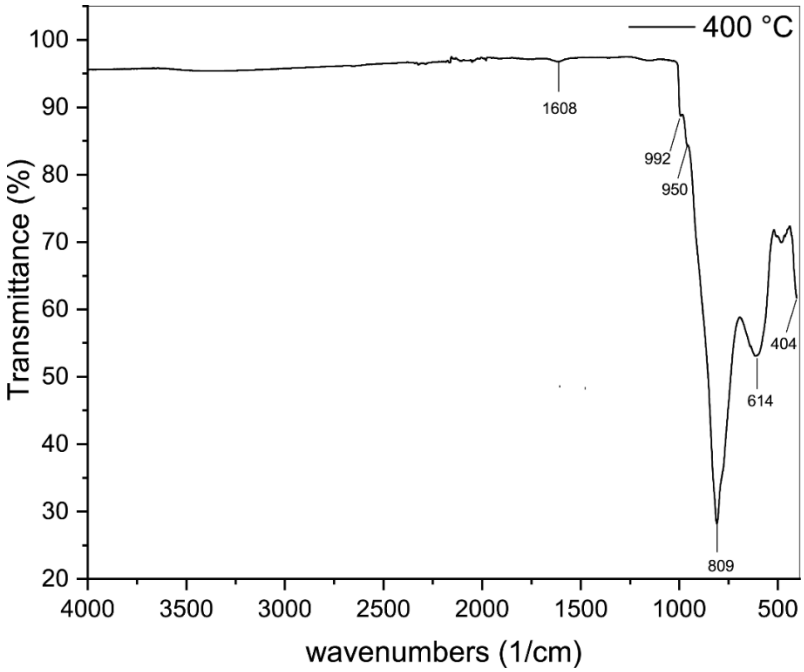

Figure 20. FT-IR spectrum of the catalyst at high temperature (400 °C).

To evaluate the existence of organic compounds, a thermogravimetric analysis (TGA/DTA) was performed by heating the sample from 30°C to 870°C at a rate of 10°C/min and holding it at the final temperature for ten minutes (Figure 21).

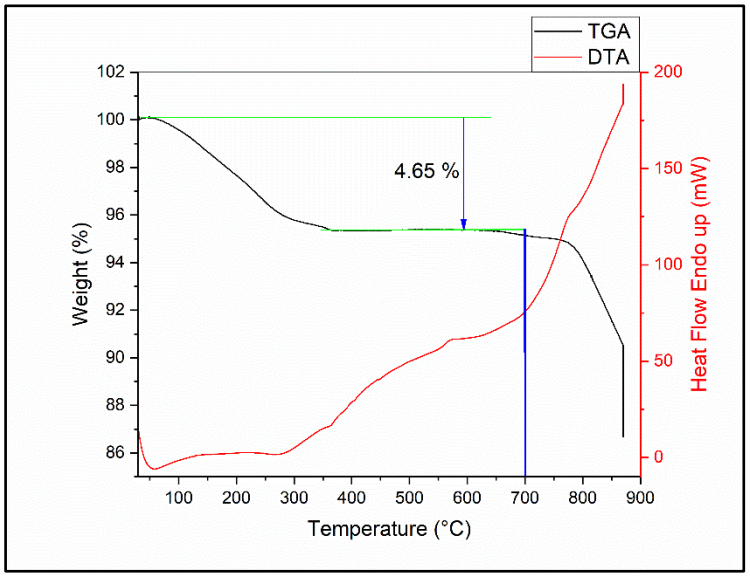

Figure 21. TGA and DTA analysis of the catalyst.

It was reported that MoO_3 reaches its sublimation point at temperatures above 700 degrees. [80] The TGA data shows a decrease in weight with increasing temperature, accompanied by an endothermic peak in the DTA, which confirms sublimation. Additionally, it reveals a negligible weight loss of 4.65%

between 350/400 °C up to 700 degrees. This weight loss can be attributed to a desolvation process, potentially leading to the release of water and/or organic compounds used in the methanol oxidation process to formaldehyde, as evidenced by the endothermic peaks in the DTA. Based on this information, the spent catalyst was heated to 400 °C and subsequently subjected to XRD analysis (Figure 22).

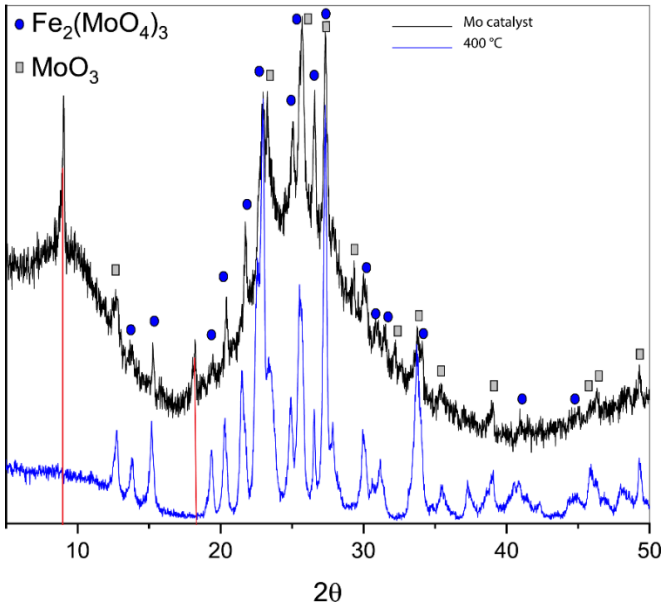

Figure 22. Comparison of XRD pattern at difference temperature: 25 °C (black line) and 400 °C (blue line).

The disappearance of unindexed peaks in the catalyst treated at 400 degrees (shown in red lines) confirms the presence of organic compounds in the sample. Furthermore, the transformation of amorphous phases into crystalline ones can be observed in the heated sample. XRD, FTIR, and TGA analysis collectively validate the presence of organic compounds, but the focus of this study is not on identifying the specific organic compounds but rather on confirming their presence. The SEM images in Figure 23 reveals the presence of iron and molybdenum and demonstrate a correlation between the sites of the two metals. The presence of the $Fe_2(MoO_4)_3$ phase and the remaining amount of molybdenum oxide can be confirmed by the ratio of iron to molybdenum in the phase, as confirmed in the SEM-EDX analysis in Table 9.

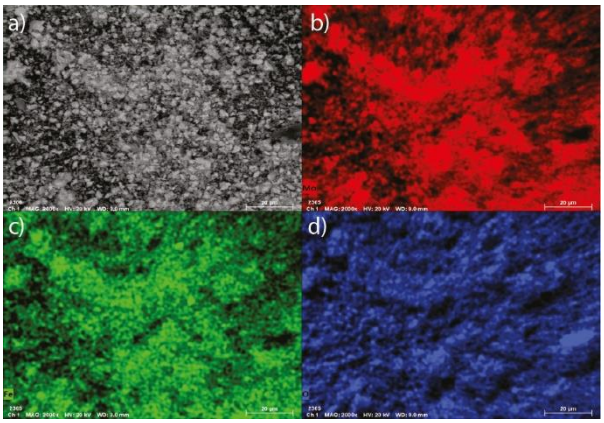

Figure 23. *SEM images of spent catalyst powder: a) without EDX map b) molybdenum EDX map; c) iron EDX map; d) oxygen EDX map. Magnification 2000X and bar=20µm.*

Table 9. *EDX analysis of spent catalyst powder. Rel.error is the relative error associated to the atom %.*

Element	Atom [%]	rel. error [%]
Oxygen	82,79	5,12
Aluminium	0,44	4,64
Calcium	0,06	10,25
Iron	5,03	1,40
Copper	0,20	4,95
Molybdenum	11,48	2,00
SUM	100,00	

In this study, SEM analysis was also performed to assess the applicability of the shrinking core model (SCM) and to validate its assumptions, as it relies on the particles maintaining their size and integrity throughout the leaching process.[81] Figure 24 represents SEM images of the spent catalyst powder before the leaching process and the residue remaining after leaching experiments. The images revealed that there is no significant alteration in the core particle distribution between the pre-leaching state (Figure 24a) and the post-leaching residue (Figure 24b). Additionally, both images demonstrated the

presence of some agglomerates. These observations suggested that the leaching process did not cause substantial changes in the particle distribution, and it was possible to apply the SCM.

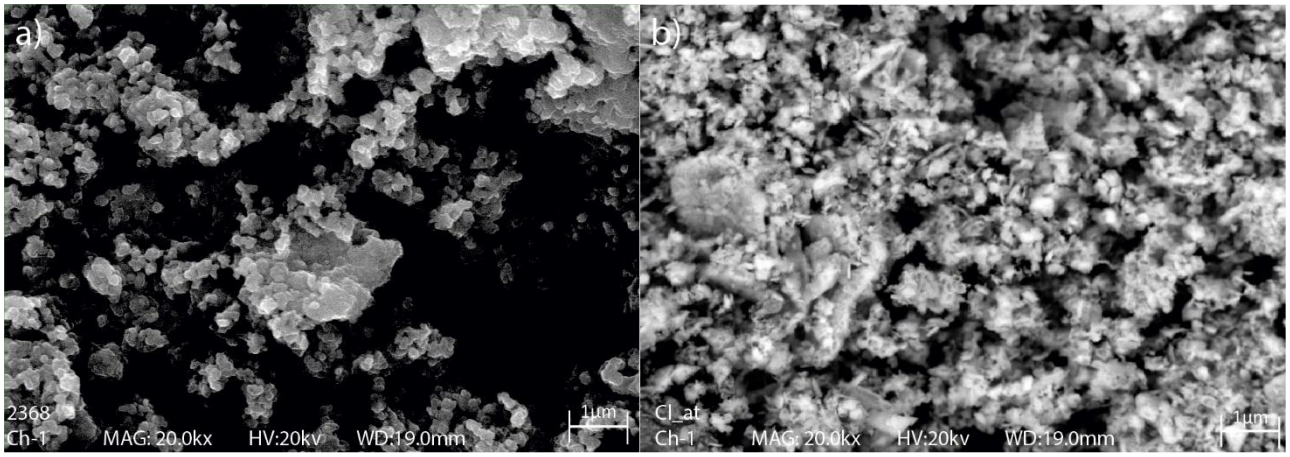

Figure 24. SEM images of the spent catalyst powder a) before leaching and b) after leaching; magnification 20.0kx and bar=1µm).

The total metal content in the spent catalyst was determined through ICP-OES. It measured 58.01±2.71 wt% of molybdenum and 13.81±0.54 wt% of iron content. All the other metals are below LOD of the technique, except for aluminium and copper, which account for only 0.5% and 0.03%, respectively, relative to the sum of molybdenum and iron.

Leaching process and mechanism

In leaching process and mechanism, the following factors were investigated: concentration of tartaric acid (0.1 M - 2.5 M), solid-liquid ratio (33 g/L - 200 g/L), temperature (25 °C - 80 °C), and time reaction (1 - 110 min). Tartaric acid contains two carboxyl groups in one molecule. Its dissociation reactions can be represented as:

$$H_2C_4H_4O_6 + H_2O \rightleftarrows H_3O^+ + HC_4H_4O_6^- \quad (22)$$

$$HC_4H_4O_6^- + H_2O \rightleftarrows H_3O^+ + C_4H_4O_6^{2-} \quad (23)$$

The pK_a values of tartaric acid are pK_{a1} = 2.72 and pK_{a2} = 4.79 calculated by MarvinSketch made by Chemaxon. Theoretically, the leaching products can contain Fe^{3+}, Mo^{6+} or MoO_4^- derived from

$Fe_2(MoO_4)_3$ and MoO_3 (see figure 1). Moreover, MoO_3 can react with water, lowering the pH of the leachate: [82]

$$MoO_3 + H_2O \rightleftarrows H_2MoO_4 \quad (24)$$

$$H_2MoO_4 + 2H_2O \rightleftarrows MoO_4^{2-} + 2H_3O^+ \quad (25)$$

The leaching process can be understood as a complexation/chelation phenomenon, where the tartaric acid molecules surround and bind to the molybdenum and iron ions, forming a complex compound. Several works have shown the system to be complex, and that the nature of species in solution depends upon several factors including pH, temperature, total concentrations, and the M:L ratio, where M are Fe^{3+}, Mo^{6+}, or MoO_4^- species and L the potential ligand. [52,53,83–85]

Influence of various factors on the leaching process

To examine the effect of tartaric acid concentration on molybdenum leaching efficiency, experiments were carried out with variations in tartaric acid molarity of 0.1, 0.7, 1.3, 2.0, and 2.5 M (Figure 25a). The other experimental conditions i.e., solid-liquid ratio (75 g/L), temperature (25 ◦C) and reaction time (60 min) were kept constant throughout the experiment. The recovery of molybdenum increased significantly from 12.06±3.68% at 0.1 M to 87.36±2.94% with tartaric acid molarity of 1.3 M. This phenomenon can be explained by the fact that a higher concentration of tartaric acid leads to enhance the collision frequency among reactants, consequently accelerating the reaction rate.[36] Figure 25b shows the effect of the solid-liquid ratio (g/L) on the leaching process. Increasing the solid-liquid ratio has a negative effect on the leaching efficiency. This trend is associated with the reduction of the available surface area per unit volume of the solution, which occurs as the solid-liquid ratio increases.[86] The amount of spent catalyst powder was varied from 30 to 200 g/L. In this experiment, all other conditions, such as molarity (1.3 M), temperature (T = 25 ◦C), and reaction time (60 min) were kept constant. The leaching efficiency decreases from 87.20±1.46% to 76.87±1.61% with the increase in pulp density from 30 to 200g/L, respectively. The process was optimized to include a solid-liquid ratio

of 75 g/L, which resulted in a recovery rate of molybdenum equal to 87.36±2.94 %. This value was chosen because it is beneficial in an industrial setting, leading to lower water consumption, a smaller reactor size, and a smaller solid-liquid separation system. This ultimately reduces the capital and operating expenses of the process. As shown in Figure 25c, the impact of the reaction time on the leaching efficiency of molybdenum was studied under the following conditions: solid-liquid ratio of 75 g/L, temperature of 25°C, and molarity of 1.3 M. The leaching efficiency of molybdenum was found to increase with the reaction time. Further increasing the reaction time to 110 min resulted in a plateau of leaching efficiency. Thus, 60 min was established as the optimal reaction time for the leaching of Mo. A temperature range of 25°C to 80°C was examined (Figure 5d), with a solid-liquid ratio of 75 g/L and a tartaric acid concentration of 1.3 M, over a 1-hour leaching duration to evaluate the impact on the leaching efficiency of molybdenum. Based on the observations in Figure 25d, the recovery of molybdenum shows an insignificant increase from 87.36±2.94% at 25 °C to 90.91±2.90% at 60 °C. Considering cost efficiency in industrial applications, it is preferable to operate at low and room temperature. In this way, energy consumption and associated costs can be reduced, making the process more economically viable. Therefore, for these reasons, the optimal condition was determined to be at room temperature. Generally, higher temperatures promote the leaching reaction because, typically, metal leaching involves an endothermic process. [36] In this case, as it can be seen, temperature does not play a significant role in molybdenum extraction.

Black lines represent iron leaching, showing a parallel trend with the molybdenum trend. Thus, tartaric acid is not selective for the Molybdenum leaching over Iron and we can observe the same atom ratio (Mo/Fe) in the spent catalyst and in the leachate in the optimized condition.

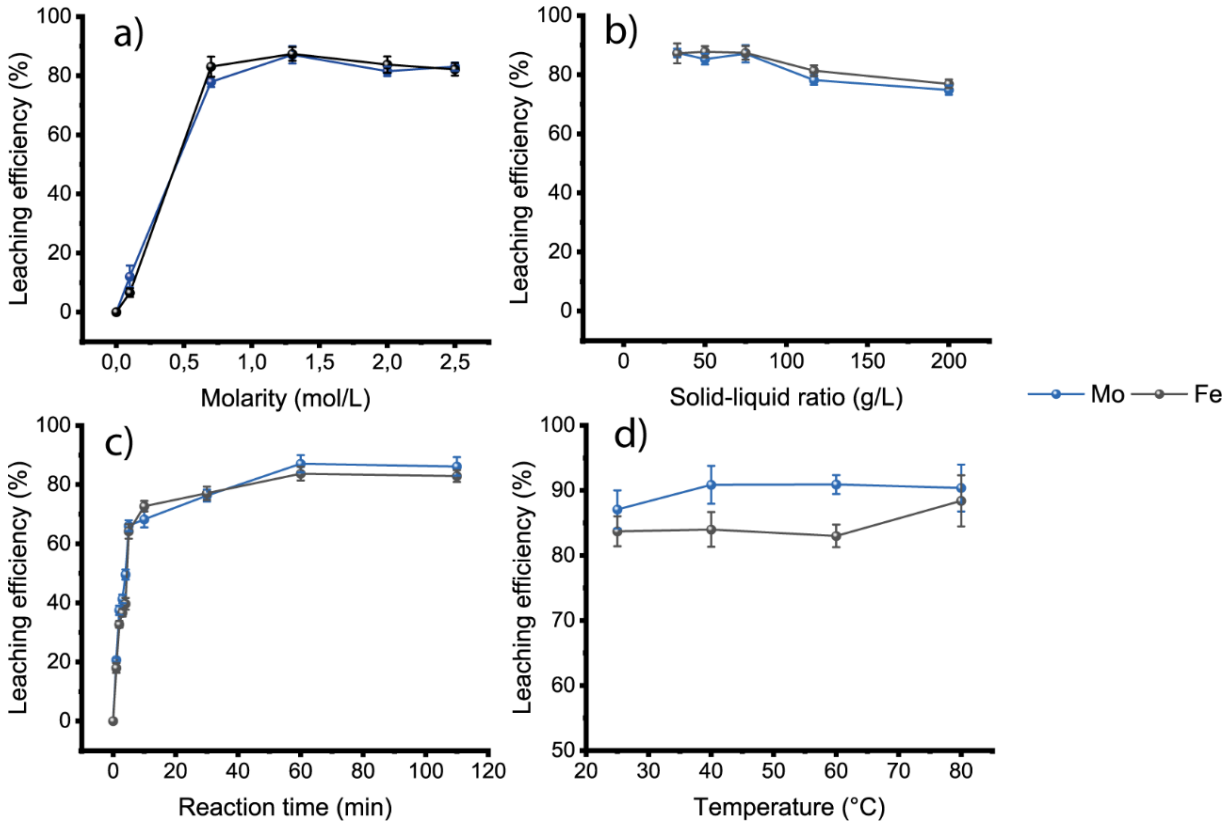

Figure 25. Synoptic graph that shows the effects of each factor on the leaching efficiency: a) molarity of the tartaric acid, b) solid-liquid ratio, c) reaction time, and d) temperature. In black and blue, respectively, the iron and molybdenum leaching trend at the same conditions. The error bars indicate the analytical error associated to the leaching process.

A series of tests was conducted to recover molybdenum from the solution. To extract molybdenum from the tartrate complexes, an initial attempt was made to precipitate the acid as calcium tartrate at pH 7. Calcium chloride ($CaCl_2$) was selected for this purpose due to its cost-effectiveness, high solubility, and its ability to precipitate as calcium carbonate ($CaCO_3$) when exposed to CO_2, thus obtaining tartaric acid. [87] This approach would contribute to the reduction of harmful emissions into the environment. To the best of our knowledge, no literature is available about the reuse of tartaric acid after the leaching process. Consequently, molybdenum precipitation can be performed using the conventional method: addition of NH_4Cl, acidification with HCl to achieve pH 2, and heating to 90°C. This temperature facilitates the formation of precipitates of ammonium molybdate. [65]

Kinetic and determination of the rate controlling step

To investigate the kinetics of leaching, a test was conducted using the optimized conditions for molybdenum recovery. The test aimed to analyse the rate at which leaching occurred within the specified timeframe. The shrinking core model is the most commonly used model for describing the kinetics in leaching processes.[46] The shrinking core model employed in this work accounts for consecutive steps in the leaching process, including the diffusion of the reagent through a liquid film surrounding the particles, the diffusion through a solid product layer surrounding the particles, and the dissolution reaction taking place on the surface of the unreacted core, leading to metal mobilization. For each step, there are corresponding kinetic equations (Eqs. 6-8) that describe the rate of the process. The equation that best fits the experimental data is considered to be the rate-controlling step.[81]

Film diffusion control:

$$t \propto X \tag{26}$$

Product layer diffusion control:

$$t \propto 1 - 3(1 - X)^{\frac{2}{3}} + 2(1 - X) \tag{27}$$

Chemical reaction control:

$$t \propto 1 - (1 - X)^{\frac{1}{3}} \tag{28}$$

where, t is the reaction time and X is the fraction of leached metal. The kinetic data obtained from the different mechanism equations (Eqs. 6-8) are presented in Figure 26a. The plot clearly indicates a change in slope at approximately 5 minutes for each equation, suggesting a shift in the leaching mechanism at this point. Therefore, the kinetic data needs to be analysed in two steps. In the first step, encompassing the initial 5 minutes, Eqs. 6-8 were utilized, and the corresponding kinetic plots are displayed in Figure 26b. The plot demonstrates that the chemical reaction control equation exhibits the highest R^2 value, indicating its dominance in this stage. The value of the rate constant for chemical

control kinetics up to 5 min is 0.06 min^{-1}. However, it is worth noting that film and product layer diffusion processes are also occurring concurrently to some extent. To explore the kinetics of the second step, which begins at 5 minutes and onwards, a new set of equations derived by Aarabi-Karasgani et al are employed.[60] Eqs. 9 to 11 are the equations for film diffusion, product layer diffusion, and chemical reaction control, respectively. These equations capture the behaviour of the leaching process beyond the initial 5-minute period:

$$t - t_1 \propto X \tag{29}$$

$$t - t_1 \propto 3\left[(1 - X_1)^{\frac{2}{3}} - (1 - X)^{\frac{2}{3}}\right] - 2(X - X_1) \tag{30}$$

$$t - t_1 = (1 - X_1)^{\frac{2}{3}} - (1 - X)^{\frac{2}{3}} \tag{31}$$

where, X is the fraction of leached metal in the second stage, t_1 is the time at which the second stage is started, and X_1 is the fraction of leached material at time t_1. R^2 values observed in Figure 26c are very close to each other for liquid film, product layer diffusion, and chemical control. Therefore, kinetics is probably governed by a mixed control mechanism. [46,88] For this reason, the rate constant was calculated as an average of each mechanism with a result of 0.018 min^{-1}.

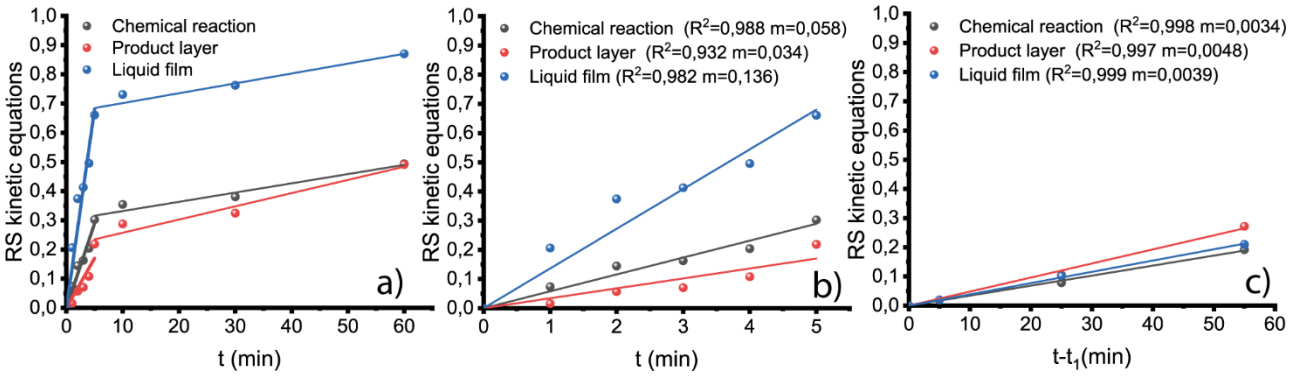

Figure 26. The right side (RS) of rate-controlling equations as a function of time at optimum conditions; a) Eqs. 6-8, b) Eqs. 6-8 (step 1), c) Eqs. 9-11 (step 2).

CONCLUSIONS

A simple, efficient, and sustainable process was developed to recover molybdenum from a specific spent catalyst. Tartaric acid is sourced from winery waste and employed in the leaching of the spent molybdenum catalyst. This approach allows for the recovery of secondary raw materials from industrial solid waste by utilizing another one generated by the winery industry. Furthermore, when comparing tartaric acid to inorganic acids, it has a lower environmental impact. The use of organic acids, as tested in this work, allows for efficient extraction of molybdenum. The latter eliminates the need for hard acids or bases, which can be hazardous to both the process and the operators. Furthermore, the use of organic acids derived from agri-food waste not only reduces waste production, but also makes it possible to recover the valuable metal of molybdenum. The reproducibility of the developed process was studied, and the results indicated a molybdenum recovery rate of 87.36% ± 2.94, under the optimal conditions previously determined: 1.3 M of tartaric acid, 75 g/L of solid-liquid ratio, a reaction time of 60 minutes, and a temperature of 25 ◦C. The SCM demonstrated a good fit with the experimental data, allowing for the determination of the rate constant for the leaching process. It was possible to accurately describe the kinetics of the process and extract meaningful information about the rate at which the desired reaction occurs. From an economic standpoint, evaluating the market price of tartaric acid in comparison to the commonly used inorganic acid in hydrometallurgy (e.g., H_2SO_4), the developed process using tartaric acid would be more expensive. Nevertheless, if tartaric acid is sourced from agri-food waste and integrated into a circular economy, this would significantly lower the cost and render the process more economically viable.

3.2.1 D-optimal design: a practical case study

D-optimal design is referenced in Section 2.1; however, here it will be explained in more detail. It is a sophisticated experimental design strategy used to efficiently estimate model parameters with minimal experimental runs while maximizing the information gained from each experiment. As previously mentioned, in D-optimal design, the objective is to select a subset of experimental conditions that optimizes the determinant of the information matrix, which is a measure of the precision with which model parameters can be estimated.

If X is the model matrix and X' its transposed, the matrix X'X is the information matrix, and its inverse $(X'X)^{-1}$ is the dispersion matrix. They are square matrices, having as many rows and as many columns as the coefficients of the model. The values of the main diagonal of the dispersion matrix, multiplied by the experimental variance, correspond to the variances of the coefficients, while the extra diagonal values, multiplied by the experimental variance, correspond to the covariances among the coefficients. It is therefore possible, for each experimental matrix, to evaluate a priori (i.e., before performing the experiments) the precision of the coefficients and how much they covary. This forms the basis of all experimental design. One of the criteria for selecting the experiments is the maximization of the determinant of the information matrix. The experimental design obtained by applying this criterion to select the "best" submatrix is therefore known as D-optimal design. Thus, given the number of experiments to be performed (n) and the postulated model with p factors, the D-optimal design will find the subset of candidate points leading to the highest information (the subset leading to the X'X matrix having the highest determinant).[89] The direct comparison of the determinant is possible only for matrices having the same number of experiments. To compare experimental matrices having a different number of experiments the normalized determinant is used:

$$M = \frac{\det (X'X)}{n^p} \tag{32}$$

An increase in the number of experiments influences both the numerator and denominator of this calculation. The value of M grows when adding an experiment improves the quality of information more than it increases the required experimental effort. For each quantity of experiments, the algorithm identifies the optimal subset based on the normalized determinant. In practical, the normalized determinant "weighs" the increase of information (connected with the increase of the number of experiments) by the experimental effort, and therefore suggests the best compromise.[21,89]

The D-optimal designs are also employed to "repair" data matrices whose experiments had been previously performed without following adequate designs, for example in a OVAT way. This process is particularly significant, as companies frequently consult a chemometrics expert specializing in DoE after conducting hundreds of experiments in a random or inadequate manner. The consultant's primary objective is to extract valuable insights from the existing dataset, even if it was generated without a structured design. This approach is crucial because it enables the company to reduce both costs and time. If the analysis reveals gaps in the data, additional experiments can then be strategically incorporated using D-optimal design to enhance the datasets.

Before analysing it, I'd like to mention that this project was undertaken at the beginning of my doctoral studies, at a time when I didn't know so well the application of DoE. As a result, a DoE was conducted, but all experiments consistently yielded the same efficiency (about 90%). What was this indicating? It suggested that none of the variables significantly impacted the leaching process due to the low variability of the response. In figure 2a-b we were within the curve of the optimal. In other words, it was as if I were in a potential well, and every experimental domain I chose fell within this potential well. Thus, consider the coded dataset obtained using the OVAT method for molybdenum recovery (Table 10).

Table 10. OVAT experiments.

N° exp	Time	Molarity	S/L	%Mo	y_{exp}	y_{calc}	leverage	y_{exp}- y_{calc}
1	-1.000	0.000	-0.497	39.8	-	-	-	-
2	-0.905	0.000	-0.497	73.1	73.1	45.47	0.78	27.67
3	-0.524	0.000	-0.497	76.3	76.3	64.40	0.58	11.91
4	0.048	0.000	-0.497	85.8	85.8	82.04	0.72	3.75
5	1.000	0.000	-0.497	82.8	-	-	-	-
6	0.048	-1.000	-0.497	12.1	-	-	-	-
7	0.048	-0.500	-0.497	77.9	77.9	55.67	0.56	22.26
8	0.048	0.000	-0.497	85.8	85.8	82.04	0.72	3.75
9	0.048	0.583	-0.497	81.5	81.5	91.02	0.54	-9.51
10	0.048	1.000	-0.497	83.1	-	-	-	-
11	0.048	0.000	-1.000	87.4	-	-	-	-
12	0.048	0.000	-0.796	81.9	81.9	85.03	0.65	-3.10
13 (x5)	0.048	0.000	-0.497	85.8	85.8	82.04	0.72	3.75
14	0.048	0.000	0.006	78.2	-	-	-	-
15	0.048	0.000	1.000	74.8	-	-	-	-

With this background, the data matrix consisting of 15 experiments was analysed, excluding those performed solely for reproducibility studies. Assuming an approximate model without interaction terms, we obtain a simplified model with 7 coefficients to investigate: linear terms, quadratic terms, and the intercept. By applying the D-optimal algorithm, we observe (see Figure 27a) that 7 experiments

provide the optimal number needed to construct this model. This is because the original data matrix was generated using the OVAT approach, and any additional experiments beyond these 7 only diminish the model's quality, as indicated by a decrease in the logarithmic value rather than the expected increase. The output also provides the VIF relative to the number of experiments (figure 27b). Section 2.2.3 discusses the ideal VIF range necessary to obtain reliable coefficient estimates for the model, with values closer to one indicating better precision.

Once the 7 optimal experiments were selected, the experimental response was introduced, and the model was calculated. Figure 27c and 27d show the coefficients magnitude of the model and the response surface, respectively. As shown, reducing the dataset from 15 to just 7 experiments retained the same information. To validate this pseudo-model, it was used experiment 13 that was repeated five times in the OVAT process, resulting in an average of 84 ± 2.7. The model predicted a value of 85.8, demonstrating that the experimental and predicted values align closely within the error.

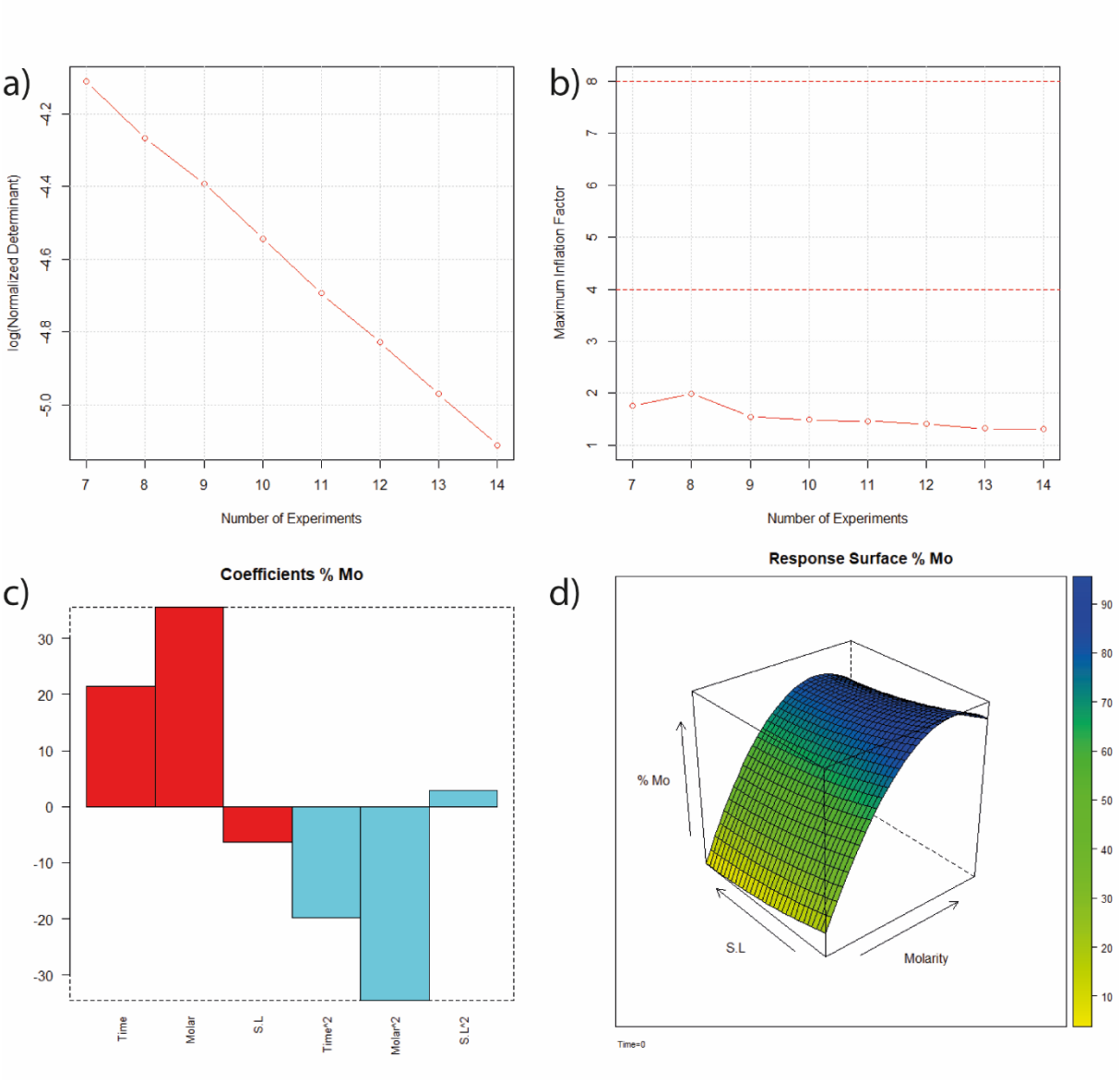

Figure 27. a) Normalized Determinant (logarithmic scale) plot; b) VIFs plot with the maximum variance inflation factor for each solution; c) coefficients plot; d) Response surface. The normalized determinant 'weighs' the increase of information (connected with the increase of the number of experiments) by the experimental effort, and therefore suggests the best compromise.

Now, the aim is to incorporate interaction effects by using the algorithm to expand the existing dataset, adding experiments in a way that maximizes the accuracy and precision of the information obtained. Figure 28a show the number of additional experiments required, approximately 15. As illustrated (Figure 28b), experiments beyond this 15-experiment threshold also achieve an optimal VIF.

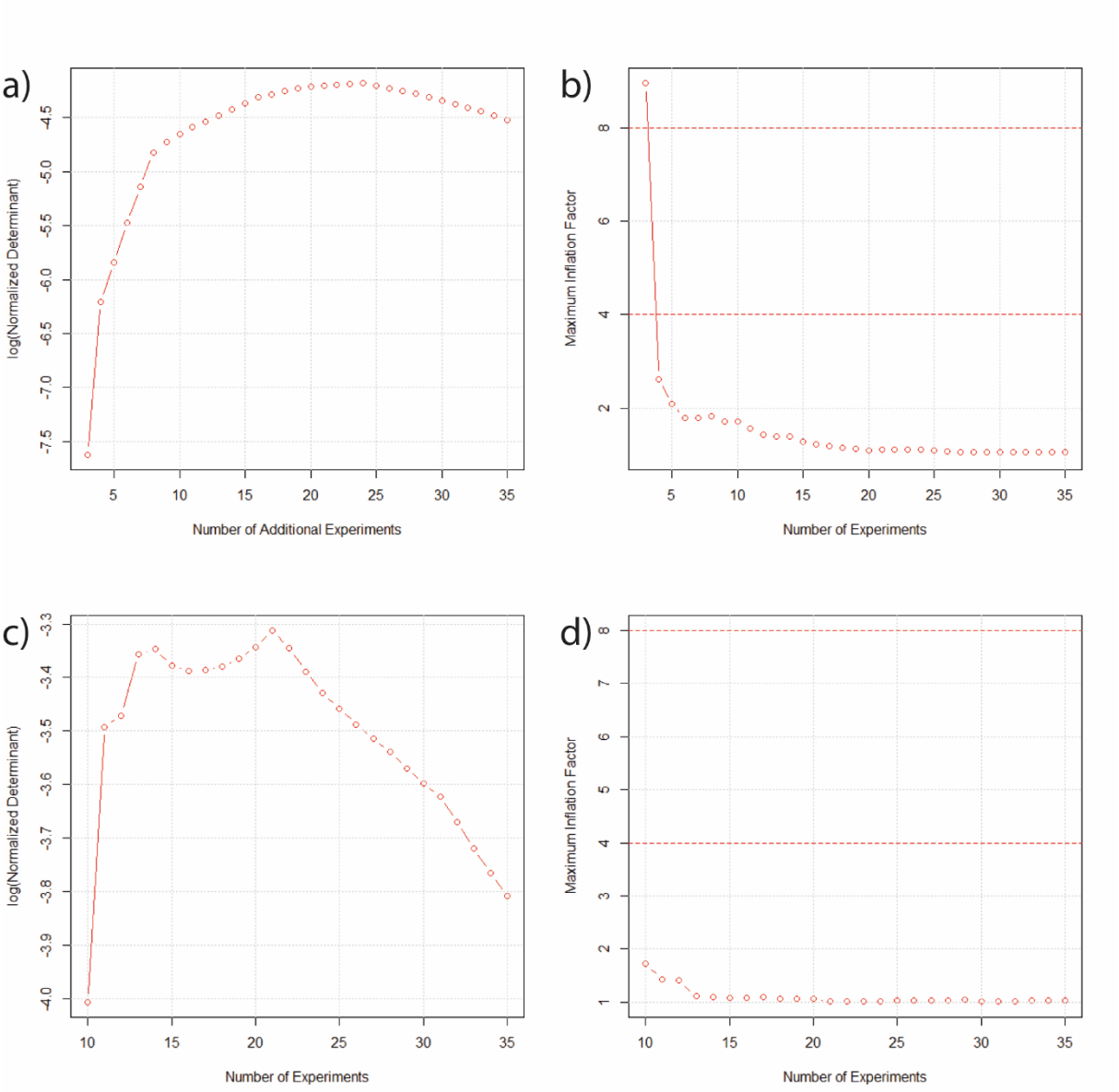

Figure 28. a) Normalized Determinant (logarithmic scale) plot for addition experiments; b) VIFs plot with the maximum variance inflation factor for each solution for addition experiments; c) Normalized Determinant (logarithmic scale) plot for new experiments; d) VIFs plot with the maximum variance inflation factor for each solution for new experiments.

When working with datasets that were not created using a DoE approach, it's important to evaluate whether it is more beneficial to continue analysing the existing dataset or to generate a new one. How can this be evaluated? By estimating the number of experiments required. In this case, starting from the same experimental domain would require 14 experiments (as shown in Figures 28c and 28d), whereas building on the existing dataset would require adding 15 more experiments.

In conclusion, the DoE approach yields substantially more information than conducting experiments based on subjective and daily intuition and using the OVAT method. Here, we were able to obtain the

same insights with only seven experiments as we did with 15 or more in the initial dataset. Additionally, the process of refining and optimizing experimental data matrices is extremely valuable for companies that face challenges in reaching their target and request guidance from chemometric consultants. This method enables the extraction of essential information, which is crucial for developing effective DoE strategies. As a result, it helps optimize experimental conditions reaching the minimum or maximum points on the response surface.

3.3 Silver Recovery from Silicon Solar Cell Waste Using Hydrometallurgical and Electrochemical Techniques

INTRODUCTION

Silver, being one of the precious metals, holds significance across various aspects of human life due to its distinctive physical and chemical properties.[90] In the production of photovoltaic modules, silver is utilized in the metallization process on the front side of silicon solar cells through screen-printing techniques.[91] While the European Commission did not classify silver as a critical raw material in 2023, its potential criticality should not be overlooked. Silver, positioned on the threshold between non-critical raw materials and the criticality zone, is notable for having a significantly high supply risk score (0.8).[92]

A crystalline silicon solar panel usually consists of an aluminium frame, tempered glass, polymeric sheets of Ethylene Vinyl Acetate (EVA) binding the solar cells together, a junction box, and a polymer back sheet. It also contains valuable elements like silver (Ag) and aluminium (Al) in the form of contacts, silicon (Si) as a wafer, copper (Cu), lead (Pb), and tin (Sn) as constituents of connecting wires.[93,94]

At an industrial level, the recycling of crystalline silicon solar panels primarily emphasizes the retrieval of bulk materials such as glass and aluminium frames. The resulting waste is typically processed at established recycling facilities dedicated to laminated glass and metal.[95,96] Consequently, valuable materials like silver and copper are often overlooked or disregarded. The significance of recovering silver from spent silicon solar cells cannot be overstated, particularly in light of the increasing demand for silver and the strict environmental regulations in place.[97] Moreover, the retrieval of raw materials is crucial for multiple reasons. Conventional metal extraction techniques, such as open-pit mining, can inflict substantial harm on the environment and neighbouring ecosystems. Therefore, employing a metal recovery process based on industrial wastes can mitigate the environmental impact associated

with metal production. Additionally, metal recovery generally requires less energy than extracting metals from ore, leading to reduced energy consumption and lower carbon emissions, especially if the recovery rate is comparable to or higher than traditional extraction methods.[98]

The annual PV market experienced substantial growth, reaching 236 GW worldwide in 2022, marking a 35% increase compared to the annual capacity in 2021.[99] As the production and deployment of photovoltaic systems continue to rise, there is a corresponding increase in end-of-life photovoltaic modules, prompting a growing interest in their recycling. Therefore, disposing of end-of-life solar panels in landfills would be a hazardous approach, displaying a direct threat to the environment.[93]

From an economic and productivity perspective in the recovery of silver from solar cells, the chemical leaching presents a viable technique. At present, the predominant method for leaching is the utilization of nitric acid, succeeded by precipitation with either NaCl or NaOH or by electrochemical refining. An alternative method involves subjecting the silver to thermal treatments to prepare it before undergoing treatment with nitric acid and subsequently precipitate with NaCl. Additionally, leaching with HCl and the direct precipitation of Ag are also employed as leaching methods.[100–102]

This study, in partnership with ORIM s.p.a, (a company specializing in metal recovery from solid waste in the Marche, Italy) aims to develop a highly selective process for leaching silver particles and subsequently electrodepositing them through environmentally friendly electrochemical methods. The presence of copper poses a challenge, acting as an antagonist and impeding the achievement of highly pure silver due to the close values of their standard reduction potential (Ag=0.8 V vs SHE and Cu=0.3 V vs SHE).[103] To address this issue, a combined base-activated persulfate and ammonia system was tested in the leaching process. Persulfate acts as an oxidizing agent and its strong oxidation properties can be activated using a strong base (NaOH). This system is designed to generate a protective hermetic layer of copper (II) oxide, preventing the leaching of copper.[104] Design of experiment (DoE) was carried out to find better conditions for silver leaching. In this way the precision is maximized, and specific conclusions can be drawn regarding a hypothesis statement.[20,105] Subsequent to the leaching

process, an electrochemical method was employed to recover purest silver metal. Electrochemical recovery of precious/valuable metals includes the deposition of metals onto solid, inert electrodes. In most cases, the concentration of metallic impurities in a solution far exceeds that of the target metals. The prevention of co-deposition of contaminant metals poses a significant challenge when the reduction potentials of these metals are in close proximity. This proximity results a decline in the purity of the recovered product. Thus, the present scenario requires further purification.[106] The electrodeposition-redox replacement (EDRR) approach successfully resolves this issue by applying a pulsed electrodeposition method. This technique, previously reported in the literature, enables the recovery of highly pure silver metal from hydrometallurgical leachate containing copper ions.[107] This procedure allows for the electrodeposit of extremely pure deposits of small quantities of rare metals while keeping their purity intact.[108] This would be completely consistent with the concepts of sustainable growth and the circular economy.[109] The key to the method's effectiveness is the spontaneous redox reaction between the less noble and more noble metals. Metallic elements with a lower electrode potential are responsible for the reduction of a dissolved metal (with a higher electrode potential) to zero valence.[108] Metals dissolved in a solution can be recovered (spontaneously reduced) using this method (Figure 1). In summary, the aim of this study is to identify the best experimental conditions for the leaching and recovery of silver without impurity.

MATERIALS AND METHODS

Materials and reagents

The silicon solar cells waste used in this study was provided by Orim S.p.a. Reagents and chemicals including nitric acid (65% pure) and hydrochloric acid (37% pure) were purchased from Sigma-Aldrich, while ammonia (25% pure) and Potassium PerSulfate (PPS) from Fluka and sodium hydroxide (pure) from Merck. All reagents and chemicals were used without further modification. Deionized water was employed in the leaching process and for the preparation of solutions for inductively coupled plasma analysis. Multi-element standards (IQC-26) were employed by Agilent.

Experimental Procedure

The silicon solar cells waste was in the form of powders. We opted to utilize it without undergoing additional processing, thereby avoiding unnecessary increases in time and cost. In order to measure the total amount of the metals (wt% total), aqua-regia was used to dissolve the waste in a duplicate at 350°C, whilst the silver content was measured after the digestion with only HNO_3 (65%) to avoid its precipitation as AgCl and thus inaccurate analysis. In accordance with the experimental design, two solutions were prepared for the leaching experiments, each with the specified molarity derived from the starting solution (see table 12). NaOH was added to achieve a theoretical pH of about 13. This step is necessary to increase the oxidation properties of persulfate salt. Temperature and stirring rate were kept constant to 25°C and 300 rpm, respectively. Upon completion of the reaction, the solution was filtered and then filled up to the desired volume in a volumetric flask. The metal content (wt% leaching) of the resulting leaching solution was then measured through ICP-OES. The Leaching Efficiency (LE) of each metal was calculated using equation 1:

$$LE = \frac{\text{wt\%(leaching)}}{wt\%(total)}\ x\ 100 \qquad \text{where} \qquad wt\% = \frac{[M]x\ V\ x\ DF}{w}\ x\ 100 \tag{33}$$

whereas: wt% (leaching) is the metal content leached and wt% (total) is the total metal content in the silicon solar cell waste. M, V, DF, and w are the metal concentrations in leach liquor (mg/L), the volume of leach liquor (L), the dilution factor for the ICP-OES analysis and the weight of sampling (mg), respectively.

Following the leaching process, an electrochemical technique was used to recover silver in a conventional three electrode system including reticulated vitreous carbon (RVC) as the working, a platinum plate as counter, and an Ag/AgCl (3M KCl) for the reference electrode. The pH was adjusted using a pH meter. Cyclic voltammetry (CV) and electrodeposition-redox replacement (EDRR) techniques were used to efficiently recover metals from the silicon solar cell waste. The determination

of metal concentrations was carried out utilizing ICP-OES analysis, while SEM was employed to examine the physical structure of the deposited metal.

RESULTS AND DISCUSSION

Characterization of the spent silicon solar cells

The total metal content in the solar cell waste was determined through ICP-OES (Table 11):

Table 11. *ICP-OES analysis of the total amount of metals. The error is relative only to ICP-OES measurements.*

Al (wt%)	Ag (wt%)	Cu (wt%)	Fe (wt%)	Sn (wt%)	Pb (wt%)
1.85±0.03	0.65±0.08	0.23±0.07	0.71±0.04	1.10±0.07	0.240±0.008

All the other metals are below LOQ of the technique or present in trace amounts, a few mg/kg. Figure 29 shows the diffractogram of the starting sample, displaying diffraction peaks of silicon with minor peaks due to the presence of metallic silver, copper, iron, tin, and lead. As reported in the Table 12, many metals phases and overlapping peaks making phase identification challenging. The small broad peak at about 26 degree is possible to presence small amount of graphene, whereas the very large band at the beginning of XRD pattern is attributed to the presence of an amorphous phase.

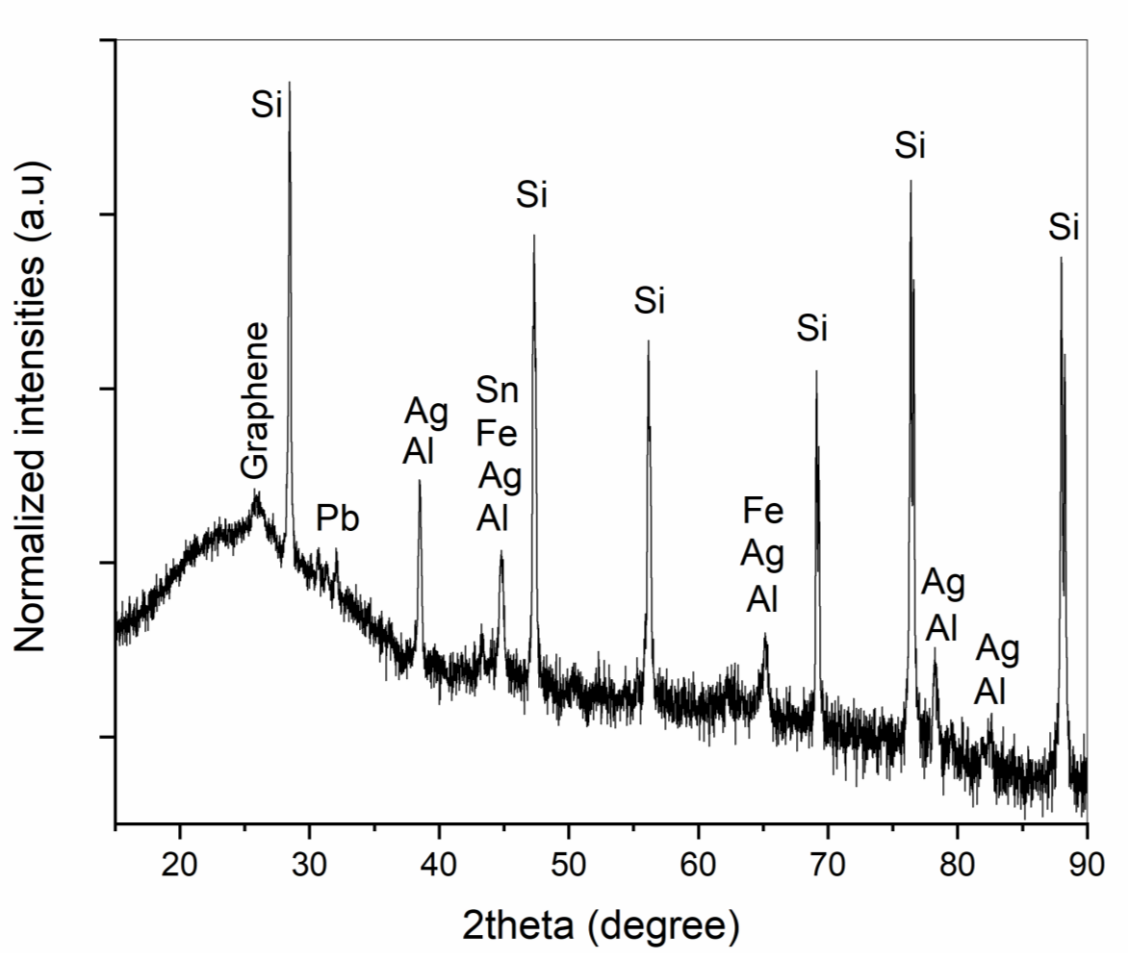

Figure 29.XRD patterns of silicon solar cells waste.

Table 12. Schematic table with main metal phases in the waste.

2theta	d-spacing (Å)	Si	Al	Ag	Cu	Fe	Sn	Pb	Graphene
25.87	3.44	--	--	--	--	--	--	--	X
28.47	3.13	X	-	-	-	-	-	-	-
30.70	2.91	-	-	-	-	-	X	-	-
31.37	2.85	-	-	-	-	-	-	X	-
32.07	2.79	-	-	-	-	-	X	-	-
38.54	2.33	-	X	X	-	-	-	-	-
43.32	2.09	-	-	-	X	-	-	-	-
44.86	2.02	-	X	X	-	X	X	-	-
47.40	1.915	X	-	-	-	-	--	-	-
56.11	1.637	X	-	-	-	-	-	-	-
65.25	1.43	-	X	X	-	X	-	-	-
69.13	1.358	X	-	-	-	-	-	-	-
76.47	1.246	X	-	-	-	-	-	-	-
78.27	1.22	-	X	X	-	-	-	-	-
82.52	1.168	-	X	X	-	X	-	-	-
88.02	1.109	X	-	-	-	-	-	-	-

Identifying the metal crystalline phases present within the waste is crucial for planning an effective leaching process and evaluating the leaching solution's ability to dissolve metals. In literature is reported that a silver paste is commonly used for electrical contacts in silicon solar cells. The paste typically comprises three constituents: silver powder, organic vehicle, and glass frit. The shape and size of the silver powder particles, the primary component in this type of conductor, may vary based on the process parameters during its preparation.[110,111] The SEM-EDX analysis in Back-Scattered Electron (BSE) reveals and confirm silver particles with oval shapes and diverse sizes (ranging from 20-100 μm) (Figure 30a shows a typical silver particle). EDX analysis of these particles (Figure 30b) confirm the presence of metallic silver. Furthermore, examination of the residue post-leaching reveals the presence of relict silver (~10%, see below) in the form of a dendritic shell rimming an oxide core (Figure 30c-d). The pre- and post-leaching photos (Figure 30a-c) highlight how the leaching solution corrodes the silver, dissolving it into the solution.

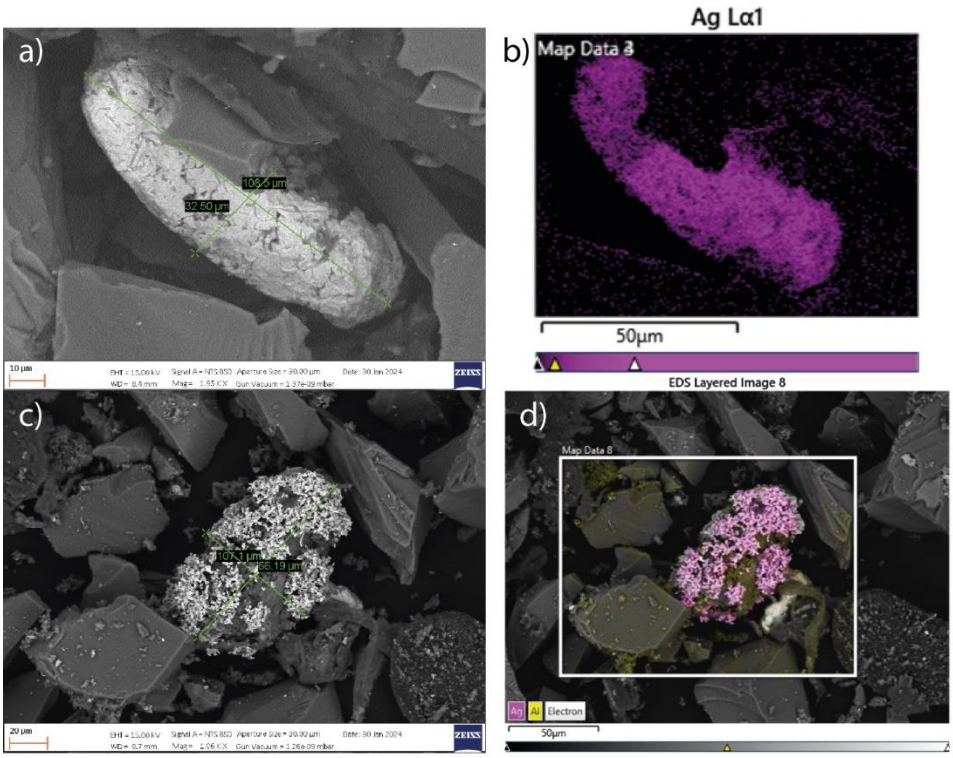

Figure 30. SEM-EDX analysis: a,b) silver particle in silicon solar cell waste before leaching; c,d) silver particle in silicon solar cell waste after leaching

ICP-OES, XRD and SEM-EDX analyses yielded no information concerning the oxidation state of copper. Thus, XAS analysis played a crucial role in studying the oxidation state of copper, a prerequisite for the application of the leaching process employed. X-ray Absorption Near Edge Structure (XANES) spectra (Figure 31) of Cu-solar cell in blue displays edge energy peak positions and relative peak intensities compatible with that of metallic copper, thus indicating that copper is mainly in the metallic state and not as oxide.

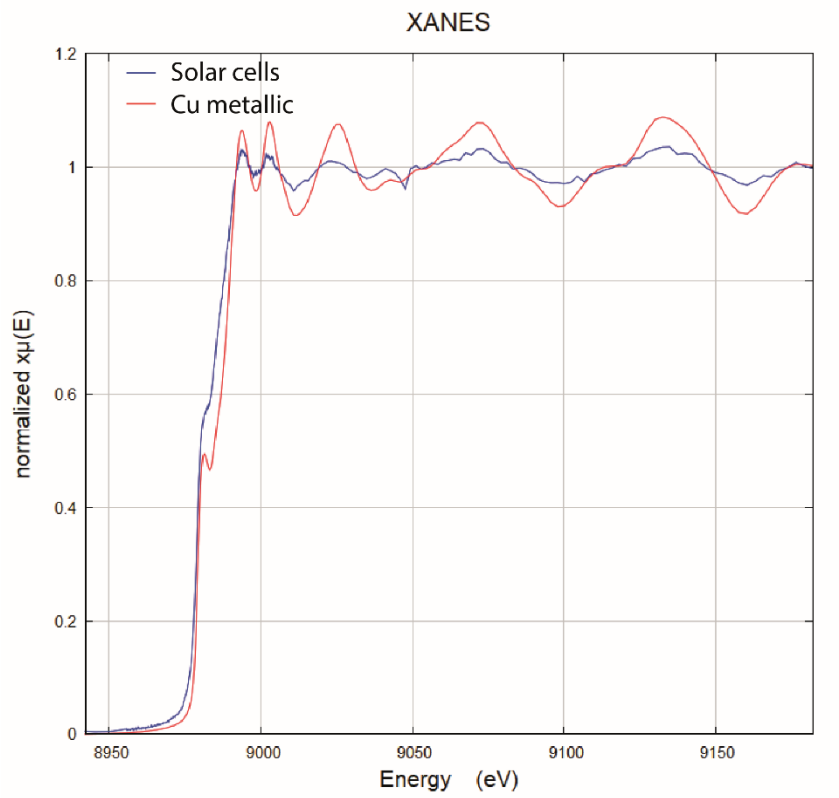

Figure 31. XANES Spectra of waste at Cu K-edge. Cu metallic was recorded in transmission mode while Solar cells was recorded in fluorescence mode.

Leaching process: mechanism and development

Silver can be oxidized in the presence of a suitable oxidizing agent with a standard electrode potential (E_0) value of 0.8 V vs SHE. In our case we utilized a persulphate activated by a base with a E_0 equal to 2.01 V, which is higher than that of hydrogen peroxide (1.8 V) but lower than ozone (2.1 V).[103,112,113] Subsequently, in the leaching process, metallic silver undergoes to chemical oxidation, leading to the formation of silver(I) oxide (Eq.34-35). At this point, Ag_2O readily dissolves in an excess of NH_3,

forming a cationic silver-ammonia complex (Eq.6). The formation of this complex in solution will enhance the dissolution of Ag from the containing materials. Eq.37 shows the sum of the reaction involved in the leaching process:

1° reaction: $$2Ag + S_2O_8^{2-} \rightarrow 2SO_4^{2-} + 2Ag^+ \quad (34)$$

2° reaction: $$2Ag^+ + 2OH^- \rightarrow Ag_2O * H_2O \quad (35)$$

3° reaction: $$Ag_2O * H_2O + NH_3 \rightarrow 2[Ag(NH_3)_2]^+ + 2OH^- \quad (36)$$

Sum: $$2Ag^+ + S_2O_8^{2-} + 4NH_3 \rightarrow 2[Ag(NH_3)_2]^+ + 2SO_4^{2-} \quad (37)$$

Regarding copper, which has a lower potential than silver (0.3V),[103] it undergoes oxidation by the persulfate present in the solution, leading to the formation of a copper(II) oxide layer that prevents leaching, aided by the strong alkaline solution. [104] Copper and silver do not precipitate in a high basic environment due to the formation of soluble complexes with ammonia. The leaching experiments aimed to find the best conditions of the industrial hydrometallurgical process were conducted using a chemometric approach.

We examined four independent variables (factors) with the aim of distinguishing the significant ones from those with a negligible effect. The factors considered in modelling and designing the leaching process include the solid/liquid ratio (S/L) of the waste in g/L, the concentration of PPS in mol/L, the reaction time (t_r) of the leaching process expressed in minutes (min) and the concentration of ammonia expressed in molarity (mol/L). The actual values of the factors have been coded to dimensionless levels, as outlined in Table 13. Table 13 also shows the experimental domain of interest (-1 to +1). The experimental domain was carefully chosen, considering both prior experience and relevant literature.

Table 13. Independent variables and their coded and actual values used for experimental design of the leaching process.

Factors	Coded variables	Actual values and coded levels		
		-1	**0**	**+1**
NH_3 (mol/L)	X_1	0.5	0.9	1.2
Sample (g/L)	X_2	50	75	100
PPS (mol/L)	X_3	0.04	0.10	0.2
Time (min)	X_4	30	45	60

An experimental design based on 2^4 full factorial design was utilized (Table 14).[114] Repeated tests (in bold text in table 14) were carried out between one experimental design and another, and between two experimental groups of the same design to estimate the variance of the experimental error. Moreover, the experiments were randomized to minimize the effects of the uncontrolled factors.

Table 14. Experimental designs used for planning the leaching experiments.

Day	N° Exp	Run	X_1	X_2	X_3	X_4	Cu (%)	Ag (%)
First half - Fractional Factorial Design								
one		6	1	1	-1	1	-1	17.74	71.11
		2	2	1	-1	-1	1	3.24	2.35
		8	3	1	1	1	1	31.96	36.93
		7	4	-1	1	1	-1	14.88	28.72
two		1	5	-1	-1	-1	-1	1.64	0.09
		3	6	-1	1	-1	1	0.93	0.78
		5	7	-1	-1	1	1	14.08	83.88

	4	8	1	1	-1	-1	1.53	1.03
three	**6a**	9	1	-1	1	-1	17.63	59.10
	1a	10	-1	-1	-1	-1	2.50	1.22
Second half - Fractional Factorial Design								
	9	11	1	1	1	-1	50.59	37.17
	12	12	1	-1	-1	-1	7.20	1.52
	15	13	-1	-1	1	-1	17.01	61.40
four	10	14	1	-1	1	1	37.46	75.57
	5a	15	-1	-1	1	1	23.17	87.22
	13	16	-1	1	-1	-1	1.66	0.42
	16	17	-1	1	1	1	30.79	37.36
	14	18	-1	-1	-1	1	3.75	0.94
Five	11	19	1	1	-1	1	1.72	0.45
	13a	20	-1	1	-1	-1	0.19	0.08
Used to validate the model in prediction								
	17		0	0	0	0	41.45	28.48
Six	**17a**		**0**	**0**	**0**	**0**	**55.98**	**29.90**

The mathematical model to this design is the following:

$$Y = \beta_0 + \sum_{i=1}^{k} \beta_1 x_1 + \sum \sum_{i<j}^{k} \beta_{ij} x_i x_j \quad (38)$$

where, Y is the response of interest (leaching efficiency of Ag), β_0 a constant, β_i the main effect of the factor i and β_{ij} the interaction coefficients between the i and j factors; the different coefficients will be estimated by multi-linear regression from the results of the experimental design. We considered that three-(or more) factor interactions are neither likely nor important, so it was able to determine the main effects with more degree of freedom.

The expected response is the silver and copper leaching efficiency of the base-activated persulfate and ammonia system. These responses have made it possible to orient our experiments to obtain a leachate with high concentration of silver and low concentration of copper. Table 12 also show the experimental point in which the model was validated (coded point 0 of the experimental domain).

Before conducting the analysis of the DoE, silver and copper efficiency was plotted (Figure 32-33). The scatter plots indicate that the silver efficiency of experiments yielding the highest leaching is not correlated with the copper response, as evidenced by the low efficiencies of the latter. However, at low leaching of both metals, a correlation becomes apparent. Furthermore, the scatter plots, which highlight points based on the concentration of each response, reveal this trend where low copper leaching efficiency corresponds to high silver leaching yields (e.g. point 7,15,14 experimental point).

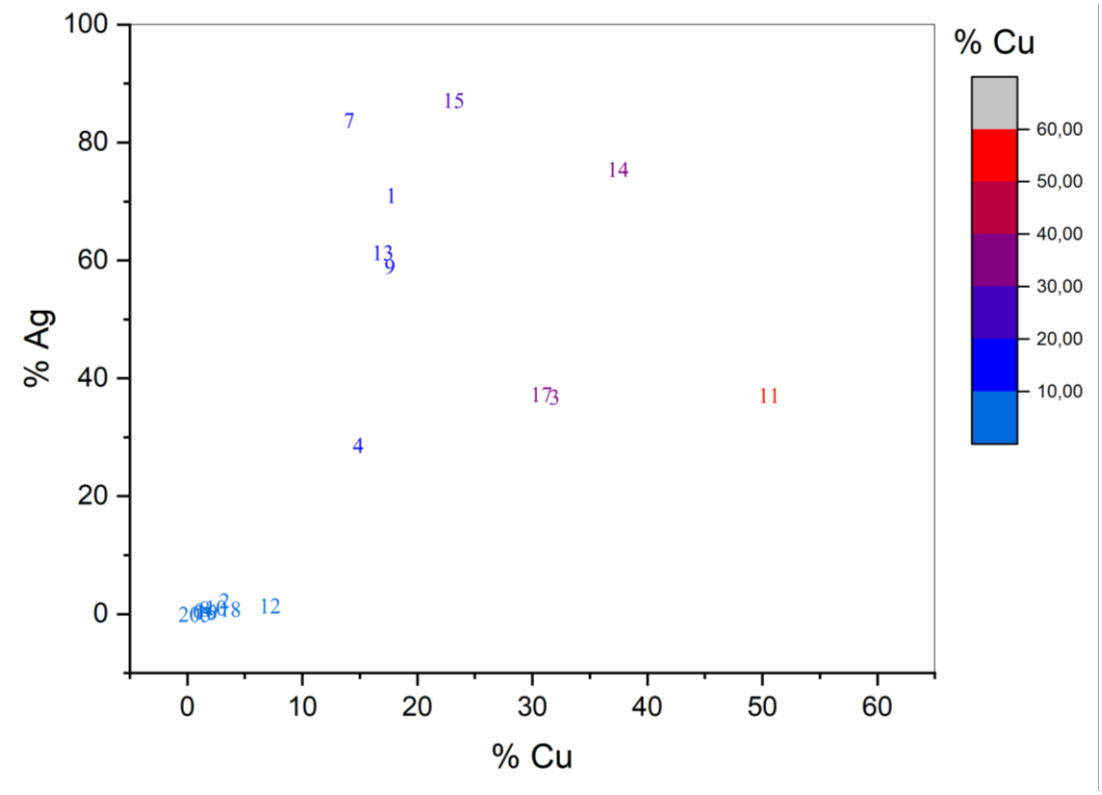

Figure 32. Scatter plot %Cu versus %Ag (number points correspond to run order). %Cu color map.

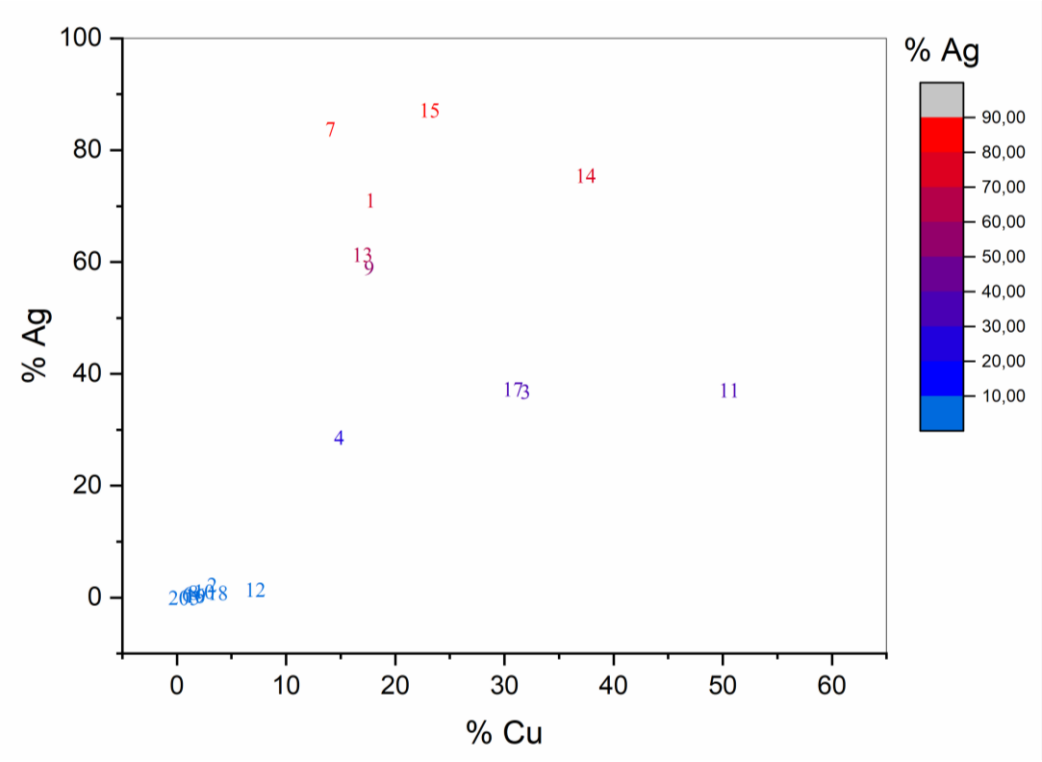

Figure 33. Scatter plot %Cu versus %Ag (number points correspond to run order). %Ag color map.

Based on experimental design matrix and observed response the polynomial model with coded variables was constructed by MLR. The model presents a R^2 equal to 98.1% and a R^2_{pred} about 95.0%. ANOVA was used to interpret the effects between the factors and the responses, and to estimate the statistical parameters. The F-values were utilized to assess the statistical significance of the regression equation, while p-values were employed to determine the significance of individual coefficients. Lower p-values indicate a greater significance of the corresponding variables.[115] The model term effects for X_2, X_3, X_4, X_2X_3 and X_3X_4 were significant and had an impact on silver leaching. In contrast, the others model terms were not considered significant, as its p-value exceeded to 0.05. In Figure 34 is shown the coefficients plot, providing a clear explanation of the points mentioned above.

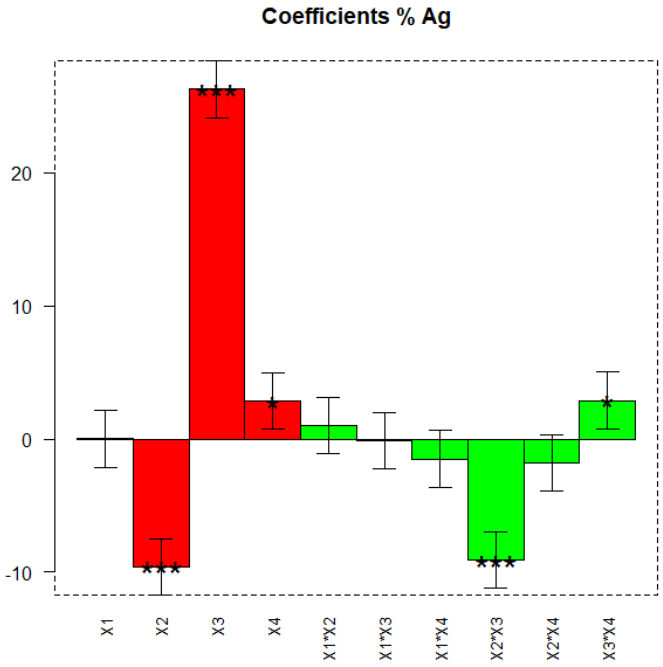

Figure 34. Coefficients plot of full factorial design. The number of asterisks indicate the significance of coefficients while the green error bars indicate confidential error at 95% of the coefficients.

Thus, in this model the S/L ratio of the sample and the concentration of PPS have strong significance in the model and so in the silver leaching. As evident from the negative and positive signs, respectively, an increase in the weight of the sample per litre of solution results in a decrease in recovery efficiency. Conversely, increasing the concentration of PPS per litre of solution leads to a high increase in leaching efficiency. Hence, it is rational to choose for the low level of the first factor (50 g/L of sample) and the

high level of the second factor, which is 0.2 mol/L of PPS. While time exhibits low significance, increasing the reaction time enhances leaching efficiency. Thus, 60 minutes is chosen as better condition. The molarity of NH_3 is not significant, so the low level can be chosen (0.5 M). As regard NH_3 molarity, the maximum value was determined based on findings from the literature, indicating that concentration exceeding 1.2M generally leaches more copper.[104] The minimum molarity was selected to avoid working with an overly large experimental domain and to ensure an excess of ammonia. Ammonia generates a silver precipitate that is soluble only with a significant excess of ammonia. Thus, it is crucial to work with a significant excess of ammonia to dissolve the silver into solution effectively. It was also calculated the stoichiometric ratio of ammonia and the metals (it was considered only Cu and Ag ammonia complexes). Upon analyzing the DoE, two additional experiments were conducted to validate the best choice (0.5M). These experiments were conducted with NH_3 molarity of 0.05 (representing the minimum stoichiometric ratio), and 0.1 (twice the minimum stoichiometric ratio) resulting in low silver leaching. Factors such as S/L ratio, PPS concentration, and reaction time were maintained constant at 50 g/L, 0.2 M, and 60 minutes, respectively, to ensure an ideally occurence of the reaction with high yields, thereby confirming the suitability of 0.5 M NH_3.

Moreover, there is a notable significance in the interaction between the S/L ratio and mol/L of PPS, while the interaction between mol/L of PPS and time demonstrates lower significance. Thus, the following conditions was chosen as best: 0.5 M of NH_3, 0.2 mol/L of PPS, S/L ratio to 50 g/L and reaction time set to 60 min. Two additional experiments were conducted under these conditions to assess reproducibility. When combined with the two previous tests from the experimental design, an average of 85.0±2.6% was achieved at a 95% confidence interval. Additionally, by determining the ratio of extracted silver to leached copper it shows that the silver leaching is 8-10 times higher than that of copper. This outcome aligns well with the utilized leaching process, showcasing successful results. Thus, the low copper content, respect to the silver, was employed as a sacrificial metal for the EDRR process as described after. In conclusion, the model was validated at the central points of the experimental domain, and the experiment was replicated twice. The obtained average was then compared with the

predicted value of 27.5±2.4. The validation results showed an average silver leaching efficiency of 29.2±1.0. As evident, the experimental value aligns perfectly with the predicted value.

Cyclic Voltammetry

Prior to conducting EDRR experiments, a cyclic voltammogram was performed using a Glassy Carbon Electrode (GCE). This was done to examine the oxidation and reduction peaks of Ag and Cu, as well as to identify the ideal deposition potential (E_1) and cutoff potential (E_2) for enriching Ag. Figure 35a illustrates a real solution cyclic voltammogram with a potential range where Ag and Cu oxidation/reduction peaks are predicted. The GCE indicates two reduction peaks in the cathodic scan; the first peak denotes the reduction of Cu^{2+}/Cu at -0.17V and the second is the reduction of Ag^{+}/Ag at -0.90V vs. Ag/AgCl, respectively:

Peak-1: $Cu^{2+} + 2e^{-} \rightarrow Cu^{0}$ (34)

Peak-2: $Ag^{+} + e^{-} \rightarrow Ag^{0}$ (35)

The open circuit potential (OCP) or equilibrium potential of the real solution was determined to be +0.2V vs Ag/AgCl. Consequently, the cutoff potential (E_2) in EDRR was established to be precisely at +0.2V vs. Ag/AgCl. To verify these peaks' behaviour, a CV analysis of synthetic solution (0.5mM $Cu(NO_3)_2.2.5H_2O$; 0.5mM $AgNO_3$) was also performed. These results are perfectly aligned with the outcomes obtained from synthetic solution as shown in Figure 36 and are also in good agreement with the literature.[116] The parameters obtained from CV analysis were utilized for the enrichment of Ag on RVC electrode in EDRR measurements.

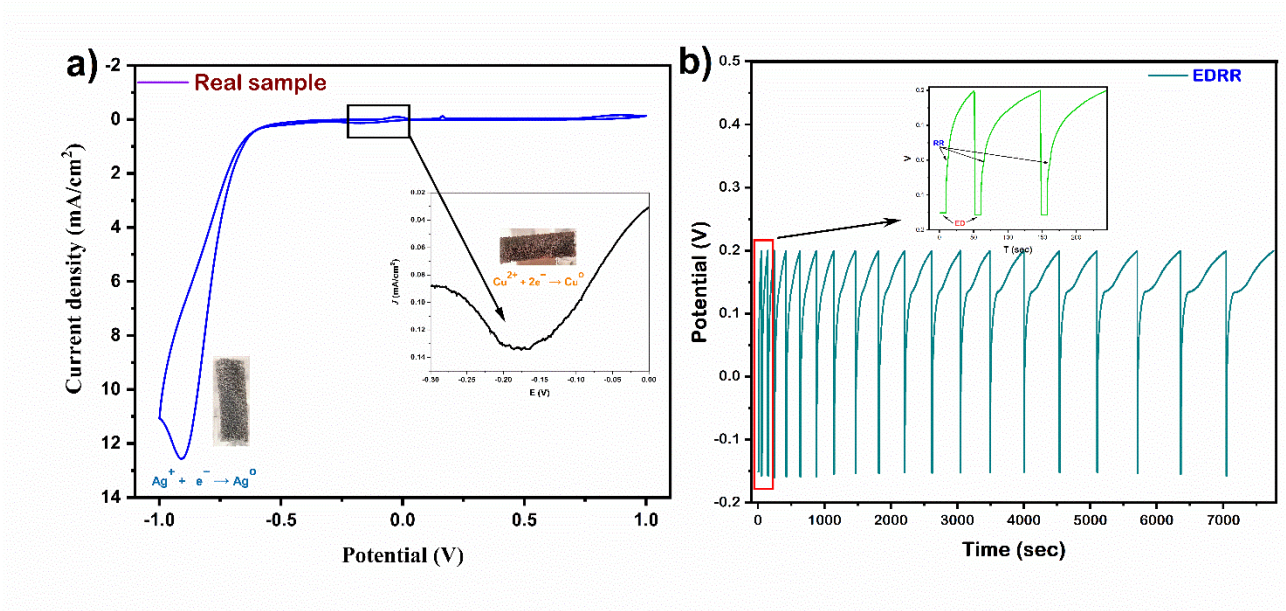

Figure 35. a) Cyclic voltammetry measurement (0.0V→ -1.0V→ 1.0V→0.0V vs. Ag/AgCl) of a real solution containing 35ppm Ag and 11ppm Cu (Concentration of metals were confirmed through ICP-OES analysis) performed with GCE at a scan rate of 20 mVs-1; b) The potential profile of the RVC electrode during EDRR measurements may be described using the following parameters: E1 = -0.17V and E2 = +0.2 V vs. Ag/AgCl, t1 = 10 s, and n = 20.

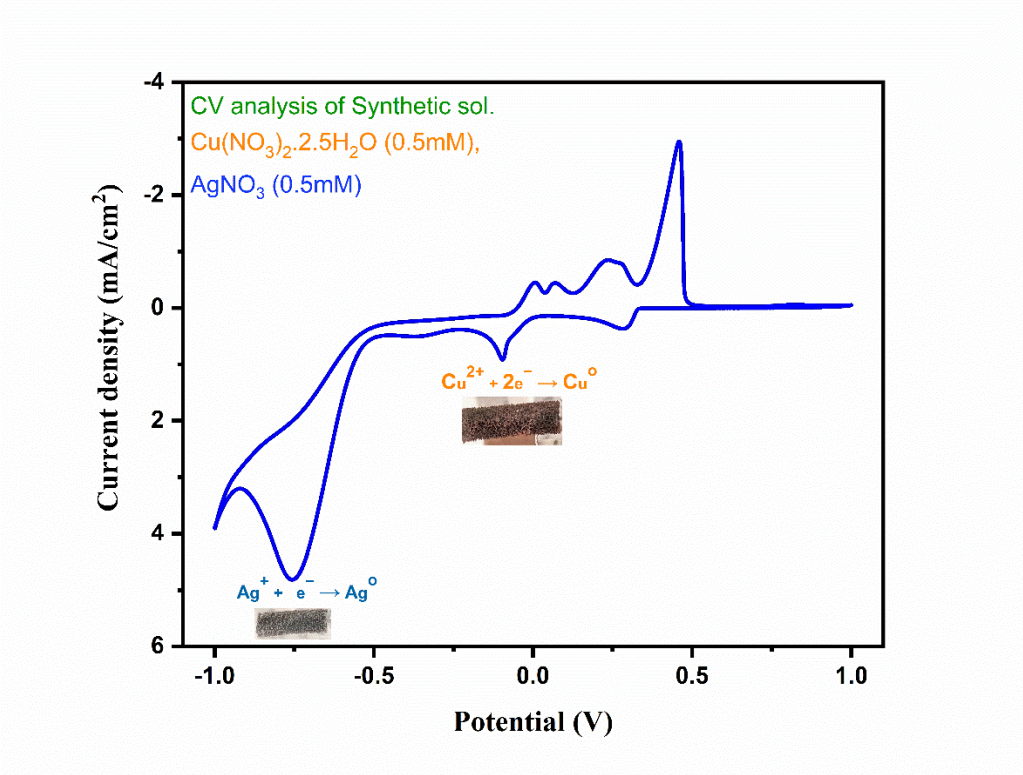

Figure 36. Cyclic voltametric response of synthetic solution (0.5mM $Cu(NO_3)_2$; 0.5mM $AgNO_3$) performed with GCE at a scan rate of 20mVs-1.

Recovery of Ag by EDRR

In light of the results obtained from the CV investigations, an EDRR experiment was carried out with copper serving as the sacrificial metal. An illustration of potential with respect to time is presented in Figure 35b. As evident, during a single EDRR cycle, Copper (Cu) was first deposited using a short potential pulse at E_1 = -0.17V vs Ag/AgCl for 10 s (t_1). This potential is sufficiently cathodic for Cu to deposit onto the RVC electrode surface long enough for the confirmation of redox replacement (RR) with Ag. The deposition time (t_1) is an adjustable parameter that can be utilized to control the amount of Cu that is deposited onto the RVC electrode during each pulse. In the parameter range examined, it was found that this deposition time (t1 = 10 s) offered the best level for Cu deposition, which was replaced by Ag. Due to a higher concentration of Ag in the solution, Ag was co-deposited onto the electrode surface during the electrodeposition (E1). SEM-EDS analysis revealed that the weight percentage ratio of Cu to Ag (Cu/Ag) on the electrode surface after step 1 was 0.88. Since the redox replacement process can only happen at the deposit/solution interface, it is advantageous to produce a thin layer of imperfect sacrificial metal to get a greater Ag enrichment. Deposition times influence surface purity because, as the deposition time rises (20 s), the thickness of the formed Cu layer grows.[117] Following the ED step, there was an instantaneous redox replacement (RR) step. During the RR step, the Cu that has been deposited is replaced by Ag^+ ions because of the greater positive potential of the Ag^+/Ag redox pair compared to the Cu^{2+}/Cu redox pair

Moreover, SEM-EDS analysis performed after the EDRR process showed that the electrode had the purest Ag metal deposited on it, with no detectable Cu impurities. Additional details regarding the methodology are elaborated upon in a prior publication.[118] It is evident that there is a direct relationship between the number of cycles and the time needed to reach the cut-off potential. This occurs due to the accumulation of Cu on the surface of the electrode, which leads to the process of Ag replacement being more time-consuming. The study proposes that by employing the EDRR approach, it is possible to achieve the highest level of purity for precious metals like Ag, without any concurrent deposition of

Cu. According to the literature,[119] researchers investigated the problems associated with the simultaneous deposition of Cu, which leads to the production of impure products that need additional treatment. A potential advantage of the EDRR method described in this study is that, under optimal deposit duration conditions, precious Ag can predominantly substitute Cu, resulting in the formation of pure surfaces. The EDRR strategy has the advantage of requiring short deposition periods and facilitating the substitution of Ag in open cell systems, depending upon the redox potential difference between the metals.

However, as EDRR is performed by cycling between two steps and electrodeposition using only one step with constant parameters, EDRR could be considered as more complicated, expensive, and time-consuming compared to simple electrodeposition of metals. But EDRR in comparison to direct electrodeposition of Ag, offers high purity with fewer defects. Following the EDRR technique, CV and SWV (square wave voltammetry) analyses were conducted to assess the concentrations of metals in the real solution, as seen in Figure 37a, and Figure 37b, respectively.

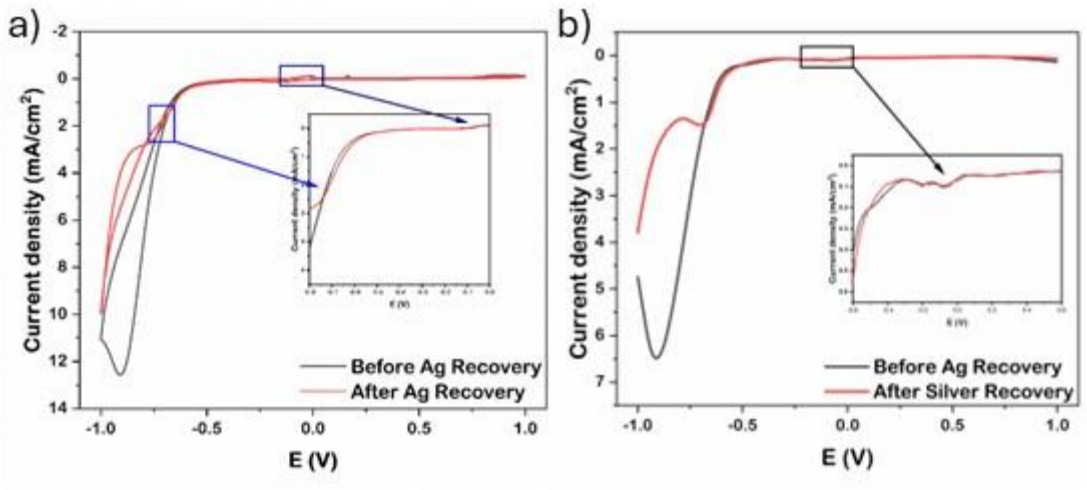

Figure 37. a) Real solution CV analysis before and after EDRR treatmen; b) Behaviour of real solution via square wave voltametric (SWV) analysis before and after Ag recovery.

The EDRR process was carried out four times and ICP-OES analysis was conducted before and after the EDRR process resulting in a recovery yield of 98.7±1.4%, which is in agreement with the literature.[120] Also, Elomaa et al.[107] studied the silver recovery from hydrometallurgical bottom ash

leachant. The silver was extracted from the leachate as Ag metal with a purity of 99.8%. The comparison of CV and SWV before and after EDRR treatment provides a clear description of the effectiveness of the EDRR investigation. Metals dissolved in a solution can be recovered (spontaneously reduced) using this method (Figure 38)

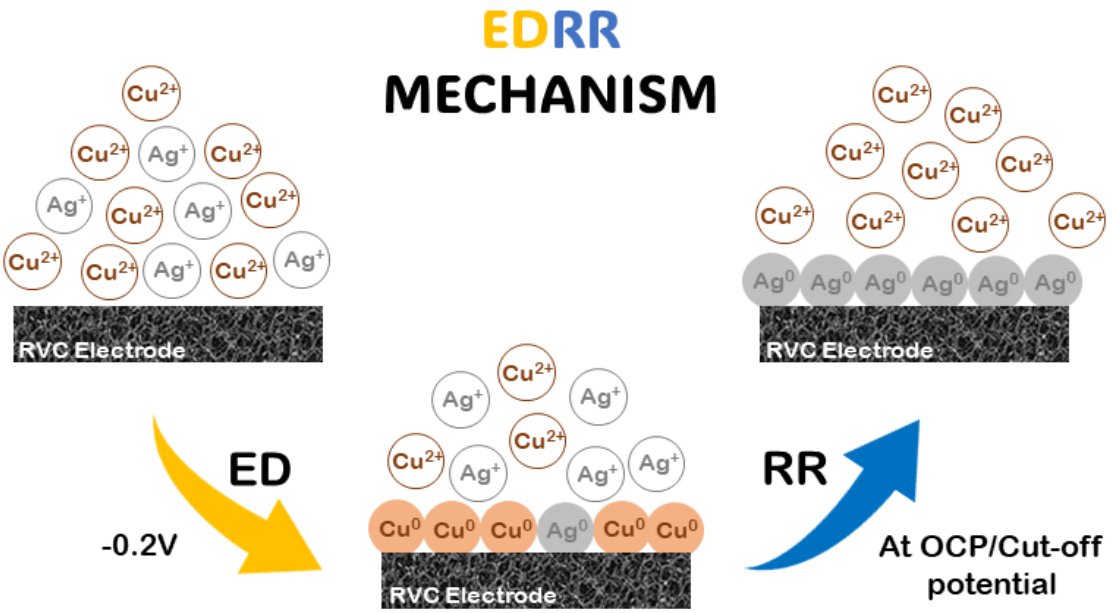

Figure 38. Mechanism of the electrodeposition-redox replacement.

Deposition Mechanism and surface morphology

SEM-EDX analysis (Figure 39a-b) shows the morphology at different magnification levels of the sponge-like structure of the RVC electrode. Figure 39c shows the spatial distribution of silver $L_{\alpha 1}$ peak while Figure 39d shows a composite image with a spatial distribution of different elements superimposed to the morphology.[107,121–123] Moreover, figure 39c-d revealed that a small number of agglomerates on the electrode surface inside the analysis region were brought on by the presence of potassium and sulphur in the solution, which also deposited alongside silver. The presence of these elements depends on starting materials (PPS). The deposition process based on EDRR yields a more uniform distribution of metals with less agglomeration, in contrast to the cementation method, as reported in the literature.[109,124] The presence of copper was also checked with SEM-EDX, and no

copper particles were found. Moreover, Cu concentration was measured by ICP-OES which confirmed the same values (inside the error) before and after silver deposition.

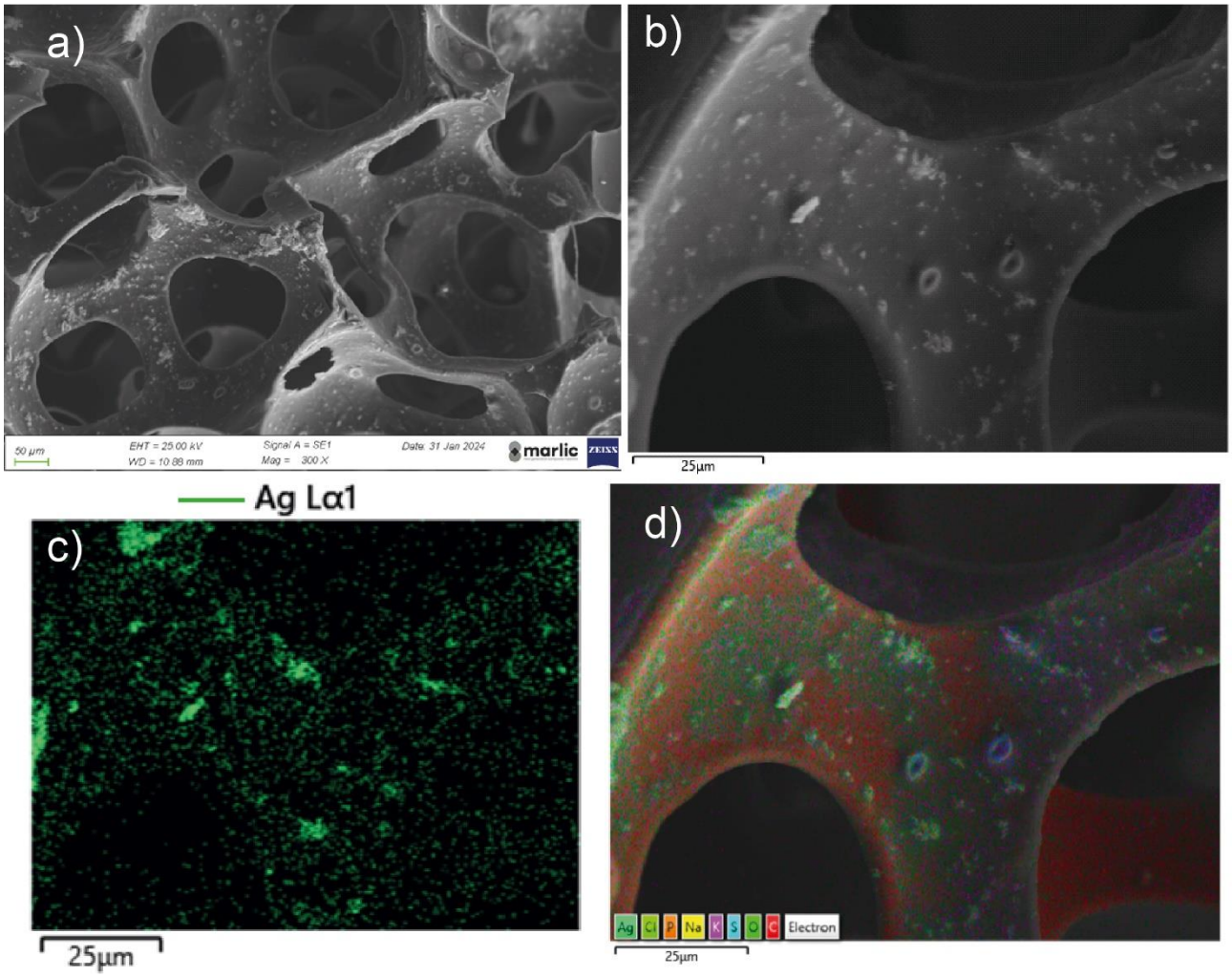

Figure 39. a,b) SEM images of electrode morphology; c) Ag-deposited EDX map after 20 EDRR cycles using Cu as a sacrificial metal (E_1 = -0.2V vs. Ag/AgCl); d) multi-elemental SEM-EDX map.

Conclusions

In this study, a simple and efficient process was developed to recover silver from silicon solar cells waste. The leaching process was studied through a design of experiment (DoE) and were found the best conditions. Electrodeposition-redox replacement (EDRR) process was used to recover silver from hydrometallurgical solution originating from silicon solar waste leached by a combined base-activated persulfate and ammonia solution. The main objective of the electrochemical characterization analysis was to achieve silver recovery, effectively mitigate the problem of co-deposition, and provide a feasible

strategy for recovering precious metals from hydrometallurgical solutions. The best conditions for silver recovery by EDRR were determined to be E_1 = -0.17V, E_2 = +0.2V vs. Ag/AgCl, and t_1 = 10s, and was recovered by 98.7±1.4%. Additionally, it is noteworthy to mention that this approach proves to be selective in its recovery of silver and does not require any chemical addition. This unique feature renders this methodology competitive in comparison to conventional processes. Furthermore, SEM-EDX also verified the enrichment of silver on the surface of the reticulated vitreous carbon electrode with no detectable Cu impurities. Overall, EDRR's energy efficiency and feasibility make it an exceptionally competitive approach for silver recovery from side streams of hydrometallurgical processes, with the potential to have a significant influence on the circular economy.

4

Conclusions

The main objective of this thesis was the development of potential hydrometallurgical processes. Three types of waste were studied: a spent catalyst used in the organic chemical industry; the black mass resulting from the recycling process of photovoltaic panels; and cathodes from $LiFePO_4$ batteries.

These studies collectively underscore the potential of green hydrometallurgical techniques to address critical challenges in waste management and material recovery. By prioritizing the use of renewable reagents, mild operating conditions, and circular economy, these methods cover the way for more sustainable industrial practices. The integration of agri-food waste as a key resource in these processes showcases a practical application of cross-sectoral circular economy principles, where the byproducts of one industry become the raw materials for another.

From a broader perspective, these findings are fundamental in the context of rising global demand for critical metals such as molybdenum, silver, and lithium, driven by their essential roles in renewable

energy, electronics, and emerging technologies. These processes reduce dependency on primary raw materials, mitigate environmental harm associated with mining, and provide scalable, economically viable solutions for industrial adoption. By addressing both material lack and waste accumulation, these innovations contribute to global efforts in transitioning toward a sustainable, circular economy while aligning with key environmental, social, and governance goals.

The application of Design of Experiments played a key role in these studies, ensuring systematic and efficient exploration of experimental variables. By using DoE methodologies, the processes were optimized to achieve maximum recovery rates and leaching efficiencies while minimizing environmental impact. This approach allowed for the identification of key parameters and their interactions. The integration of DoE demonstrates its value as a critical tool in process optimisation.

Moreover, during the second year of doctoral studies, the news emerged about an Italian start-up which developed an eco-friendly process to recover valuable metals from spent lithium batteries using orange peels. This method utilizes the citric acid found in citrus waste as a key reagent for metal extraction, offering a sustainable alternative to traditional methods. Citric acid has one more carboxylic group respect to tartaric acid, used in this research. The creation of this start-up demonstrates how this research conducted with a very similar acid can have a tangible impact on everyday life.

Acknowledgments

We sincerely thank Engr. Alfredo Mancini, Engr. Roberta Vecchiola, and the entire research group of Orim S.p.a. for providing us the solid wastes and for kindly hosting me during my PhD, creating a welcoming and collaborative environment. I also wish to thank Distillerie Mazzari S.p.A. for providing the tartaric acid recovered from winery industry wastes. The PhD grant of R.E.R. has been financed by PON funds from MIUR (CUP: J19J21018790001). This project was also partially supported by MITE funds to G.G. and M.B. ('Ministero dell'Ambiente e della Tutela del Territorio e del Mare – Direzione Generale per l'Economia Circolare', 'Recupero di materiali critici da rifiuti elettronici', CUP: J13C22000320001) and UNICAM FAR funds to G.G. ('Recovery of critical metals (Pd, Ni, V, Cu, Ag, Sn, Au) from industrial waste (REMINE)', CUP: J15F22000020001).

Bibliography

1. Grohol, M. & Veeh, C. *Study on the Critical Raw Materials for the EU 2023 – Final Report*. (2023).

2. Cozma, P., Beţianu, C., Hlihor, R.-M., Simion, I. M. & Gavrilescu, M. Bio-Recovery of Metals through Biomining within Circularity-Based Solutions. *Processes* **12**, 1793 (2024).

3. Cesaro, A., Gallo, M., Moreschi, L. & Del Borghi, A. The hydrometallurgical recovery of critical and valuable elements from WEEE shredding dust: Process effectiveness in a life cycle perspective. *Resour Conserv Recycl* **206**, (2024).

4. Gorman, M. R., Dzombak, D. A. & Frischmann, C. Potential global GHG emissions reduction from increased adoption of metals recycling. *Resour Conserv Recycl* **184**, (2022).

5. Ryter, J., Fu, X., Bhuwalka, K., Roth, R. & Olivetti, E. Assessing recycling, displacement, and environmental impacts using an economics-informed material system model. *J Ind Ecol* **26**, 1010–1024 (2022).

6. Schafer, P. & Schmidt, M. Discrete-Point Analysis of the Energy Demand of Primary versus Secondary Metal Production. *Environ Sci Technol* **54**, 507–516 (2020).

7. Torrubia, J., Parvez, A. M., Sajjad, M., García Paz, F. A. & van den Boogaart, K. G. Recovery of copper from electronic waste: An energy transition approach to decarbonise the industry. *J Clean Prod* **485**, 144349 (2024).

8. Yakoumis, I., Panou, M., Moschovi, A. M. & Panias, D. Recovery of platinum group metals from spent automotive catalysts: A review. *Cleaner Engineering and Technology* vol. 3 Preprint at https://doi.org/10.1016/j.clet.2021.100112 (2021).

9. Fatema, K., Hassan, M. N., Hasan, S. & Roy, H. E-waste recycling in an optimized way for copper recovery by leaching and a case study on E-waste generation and management in Dhaka city. *Heliyon* **11**, (2025).

10. Liang, G. & Qu, Z. Insight into Pyrometallurgical Recovery of Platinum Group Metals from Spent Industrial Catalyst: Co-disposal of Industrial Wastes. *ACS ES and T Engineering* **3**, 1532–1546 (2023).

11. Golmohammadzadeh, R., Rashchi, F. & Vahidi, E. Recovery of lithium and cobalt from spent lithium-ion batteries using organic acids: Process optimization and kinetic aspects. *Waste Management* **64**, 244–254 (2017).

12. Gao, W. *et al.* Comprehensive evaluation on effective leaching of critical metals from spent lithium-ion batteries. *Waste Management* **75**, 477–485 (2018).

13. Jadhav, U. U. & Hocheng, H. *A Review of Recovery of Metals from Industrial Waste Industrial Management and Organisation*.

14. Gerold, E., Schinnerl, C. & Antrekowitsch, H. Critical Evaluation of the Potential of Organic Acids for the Environmentally Friendly Recycling of Spent Lithium-Ion Batteries. *Recycling* **7**, (2022).

15. Song, D. *et al.* Characteristic comparison of leaching valuable metals from spent power Li-ion batteries for vehicles using the inorganic and organic acid system. *J Environ Chem Eng* **10**, (2022).

16. Gao, J., Lu, W., Li, Y. & Wu, T. Organic acid-mediated leaching kinetics study and selective extraction of Mo, V, and Ni from spent catalysts. *Waste Management* **187**, 198–206 (2024).

17. Moccia Paradisi, A., Hernández Pardo, D., Ardila Santamaria, N. & Delvasto, P. Hydrometallurgical valorization of spent Ni-Cd batteries using organic acids as selective leaching agents. *Ingeniería y Desarrollo* **41**, 117–136 (2023).

18. Okonkwo, E. G., Wheatley, G. & He, Y. The role of organic compounds in the recovery of valuable metals from primary and secondary sources: a mini-review. *Resources, Conservation and Recycling* vol. 174 Preprint at https://doi.org/10.1016/j.resconrec.2021.105813 (2021).

19. Abashina, T. N., Yachkula, A. A. & Vainshtein, M. B. Prevention of sulfuric acid pollution: Intensification of metal leaching with organic acids. in *IOP Conference Series: Earth and Environmental Science* vol. 981 (IOP Publishing Ltd, 2022).

20. Leardi, R. Experimental design in chemistry: A tutorial. *Anal Chim Acta* **652**, 161–172 (2009).

21. Brown, S., Tauler, R. & Walczak, B. *COMPREHENSIVE CHEMOMETRICS: CHEMICAL AND BIOCHEMICAL DATA ANALYSIS SECOND EDITION*. vol. 1.

22. Farinini, E. Use of Experimental Design and Multivariate Analysis for solving industrial problems. (2024).

23. Altomare, A., Cuocci, C., Giacovazzo, C., Moliterni, A. & Rizzi, R. QUALX: A computer program for qualitative analysis using powder diffraction data. *Journal of Applied Crystallography* vol. 41 815–817 Preprint at https://doi.org/10.1107/S0021889808016956 (2008).

24. Altomare, A. *et al.* QUALX2.0: A qualitative phase analysis software using the freely available database POW-COD. *J Appl Crystallogr* **48**, 598–603 (2015).

25. Kerr, B. V. *et al.* Characterization of Energy Materials with X-ray Absorption Spectroscopy─Advantages, Challenges, and Opportunities. *Energy and Fuels* vol. 36 2369–2389 Preprint at https://doi.org/10.1021/acs.energyfuels.1c04072 (2022).

26. D'Acapito, F. *et al.* The LISA beamline at ESRF. *J Synchrotron Radiat* **26**, 551–558 (2019).

27. Muchuweni, E., Mombeshora, E. T., Muiva, C. M. & Sathiaraj, T. S. Lithium-ion batteries: Recent progress in improving the cycling and rate performances of transition metal oxide

anodes by incorporating graphene-based materials. *Journal of Energy Storage* vol. 73 Preprint at https://doi.org/10.1016/j.est.2023.109013 (2023).

28. Li, L. *et al.* A facile recovery process of cathodes from spent lithium iron phosphate batteries by using oxalic acid. *Journal of power and energy systems* 219–225 (2018) doi:10.17775/CSEEJPES.2016.01880.

29. Li, H. *et al.* Recovery of Lithium, Iron, and Phosphorus from Spent LiFePO4 Batteries Using Stoichiometric Sulfuric Acid Leaching System. *ACS Sustain Chem Eng* **5**, 8017–8024 (2017).

30. Mahandra, H. & Ghahreman, A. A sustainable process for selective recovery of lithium as lithium phosphate from spent LiFePO4 batteries. *Resour Conserv Recycl* **175**, (2021).

31. Kumar, J., Shen, X., Li, B., Liu, H. & Zhao, J. Selective recovery of Li and FePO4 from spent LiFePO4 cathode scraps by organic acids and the properties of the regenerated LiFePO4. *Waste Management* **113**, 32–40 (2020).

32. Rautela, R., Yadav, B. R. & Kumar, S. A review on technologies for recovery of metals from waste lithium-ion batteries. *J Power Sources* **580**, (2023).

33. Liu, A., Hu, G., Wu, Y. & Guo, F. Life cycle environmental impacts of pyrometallurgical and hydrometallurgical recovery processes for spent lithium-ion batteries: present and future perspectives. *Clean Technol Environ Policy* **26**, 381–400 (2024).

34. Golmohammadzadeh, R., Faraji, F. & Rashchi, F. Recovery of lithium and cobalt from spent lithium ion batteries (LIBs) using organic acids as leaching reagents: A review. *Resources, Conservation and Recycling* vol. 136 418–435 Preprint at https://doi.org/10.1016/j.resconrec.2018.04.024 (2018).

35. Xiao, X. *et al.* Ultrasound-assisted extraction of metals from Lithium-ion batteries using natural organic acids. *Green Chemistry* **23**, 8519–8532 (2021).

36. He, L. P., Sun, S. Y., Mu, Y. Y., Song, X. F. & Yu, J. G. Recovery of Lithium, Nickel, Cobalt, and Manganese from Spent Lithium-Ion Batteries Using l -Tartaric Acid as a Leachant. *ACS Sustain Chem Eng* **5**, 714–721 (2017).

37. Kontogiannopoulos, K. N., Patsios, S. I. & Karabelas, A. J. Tartaric acid recovery from winery lees using cation exchange resin: Optimization by Response Surface Methodology. *Sep Purif Technol* **165**, 32–41 (2016).

38. Devesa-Rey, R. *et al.* Valorization of winery waste vs. the costs of not recycling. *Waste Management* **31**, 2327–2335 (2011).

39. Ebrahimi-Najafabadi, H., Leardi, R. & Jalali-Heravi, M. Experimental design in analytical chemistry -Part I: Theory. *Journal of AOAC International* vol. 97 3–11 Preprint at https://doi.org/10.5740/jaoacint.SGEEbrahimi1 (2014).

40. Li, L. *et al.* Sustainable Recovery of Cathode Materials from Spent Lithium-Ion Batteries Using Lactic Acid Leaching System. *ACS Sustain Chem Eng* **5**, 5224–5233 (2017).

41. Shin, D. J., Joo, S. H., Lee, D. & Shin, S. M. Precipitation of lithium phosphate from lithium solution by using sodium phosphate. *Canadian Journal of Chemical Engineering* **100**, 3760–3767 (2022).

42. Annunzi, F., Nicolella, C., Stella, R. S., Lenzi, M. & Signorini, F. Recovery of Lithium from Brine by Phosphate Precipitation. *Chem Eng Trans* **98**, 207–212 (2023).

43. Xiao, C. & Zeng, L. Thermodynamic study on recovery of lithium using phosphate precipitation method. *Hydrometallurgy* **178**, 283–286 (2018).

44. Li, H. *et al.* Recovery of Lithium, Iron, and Phosphorus from Spent LiFePO4 Batteries Using Stoichiometric Sulfuric Acid Leaching System. *ACS Sustain Chem Eng* **5**, 8017–8024 (2017).

45. Yang, Y. *et al.* Selective recovery of lithium from spent lithium iron phosphate batteries: A sustainable process. *Green Chemistry* **20**, 3121–3133 (2018).

46. Levenspiel, O. *Chemical Reaction Engineering*. (1998).

47. Habbache, N., Alane, N., Djerad, S. & Tifouti, L. Leaching of copper oxide with different acid solutions. *Chemical Engineering Journal* **152**, 503–508 (2009).

48. Moretti, A. *et al.* Structural and Electrochemical Characterization of Vanadium-Doped LiFePO 4 Cathodes for Lithium-Ion Batteries . *J Electrochem Soc* **160**, A940–A949 (2013).

49. https://chemaxon.com.

50. Chen, X. *et al.* Separation and recovery of valuable metals from spent lithium ion batteries: Simultaneous recovery of Li and Co in a single step. *Sep Purif Technol* **210**, 690–697 (2019).

51. Musariri, B., Akdogan, G., Dorfling, C. & Bradshaw, S. Evaluating organic acids as alternative leaching reagents for metal recovery from lithium ion batteries. *Miner Eng* **137**, 108–117 (2019).

52. Kostromina, N. A., Trunova, E. K. & Tananaeva, N. N. Complex formation of Fe(III) with tartaric acid by the method of nuclear magnetic relaxation. *Theoretical and Experimental Chemistry* **23**, 462–466 (1998).

53. Yokoi, H., Mitani, T., Mori, Y. & Kawata, S. Complex formation between iron (III) and tartaric and citric acids in a wide pH range 1 to 13 as studied by magnetic susceptibility measurements. *Chem Lett* **23**, 281–284 (1994).

54. European Commission. https://eur-lex.europa.eu/legal-content/EN/ALL/?uri=CELEX%3A32012R0231. (2012).

55. David R. Lide. *'Solubility Product Constants' in CRC Handbook of Chemistry and Physics*. (2007).

56. Vyas, P., Jethva, H., John Joshi, S. & Janakrai Joshi, M. *The Roles of Gel Medium and Gelling Solution in the Growth of the Crystals: A Case Study of Calcium Levo-Tartrate*. https://www.researchgate.net/publication/259675669.

57. Sahaya Shajan, X. & Mahadevan, C. *On the Growth of Calcium Tartrate Tetrahydrate Single Crystals*. *Bull. Mater. Sci* vol. 27 (2004).

58. Ben Bechir, M. & Ben Rhaiem, A. The lithium-ion battery: Study of alternative current conduction mechanisms on the Li3PO4 - based solid electrolyte. *Physica E Low Dimens Syst Nanostruct* **130**, (2021).

59. Benoy, S. M., Singh, S., Pandey, M. & Manoj, B. Characterization of nanocarbon based electrode material derived from anthracite coal. *Mater Res Express* **6**, (2019).

60. Aarabi-Karasgani, M., Rashchi, F., Mostoufi, N. & Vahidi, E. Leaching of vanadium from LD converter slag using sulfuric acid. *Hydrometallurgy* **102**, 14–21 (2010).

61. Prakash, S., G.D. Tuli, S.K. Basu & R.D. Madan. *Advanced Inorganic Chemistry*. vol. 2 (2006).

62. Grohol, M. & Veeh, C. *Study on the Critical Raw Materials for the EU*. http://www.europa.eu (2023) doi:10.2873/725585.

63. Kar, B. B., Datta, P. & Misra, V. N. Spent catalyst: Secondary source for molybdenum recovery. *Hydrometallurgy* **72**, 87–92 (2004).

64. IMOA. Mining & processing. https://www.imoa.info/molybdenum/molybdenum-mining.php.

65. Vemic, M., Bordas, F., Guibaud, G., Lens, P. N. L. & van Hullebusch, E. D. Leaching and Recovery of Molybdenum from Spent Catalysts. in *Sustainable Heavy Metal Remediation* 207–239 (2017). doi:10.1007/978-3-319-61146-4_7.

66. Brookes, C., Bowker, M. & Wells, P. P. Catalysts for the selective oxidation of methanol. *Catalysts* vol. 6 Preprint at https://doi.org/10.3390/catal6070092 (2016).

67. Malik, M. I., Abatzoglou, N. & Achouri, I. E. Methanol to formaldehyde: An overview of surface studies and performance of an iron molybdate catalyst. *Catalysts* vol. 11 Preprint at https://doi.org/10.3390/catal11080893 (2021).

68. *Global Formaldehyde Industry*. (2022).

69. Kar, B. B., Datta, P. & Misra, V. N. Spent catalyst: Secondary source for molybdenum recovery. *Hydrometallurgy* **72**, 87–92 (2004).

70. Gao, B. *et al.* High-efficiency recycling method for Mo and Ni from spent catalyst via soda roasting and solvent extraction. *J Clean Prod* **367**, (2022).

71. Zhang, M. *et al.* Highly efficient recovery of molybdenum from spent catalyst by optimized process. *J Air Waste Manage Assoc* 971–979 (2020) doi:10.1080/10962247.2020.1792377.

72. Akcil, A., Vegliò, F., Ferella, F., Okudan, M. D. & Tuncuk, A. A review of metal recovery from spent petroleum catalysts and ash. *Waste Management* vol. 45 420–433 Preprint at https://doi.org/10.1016/j.wasman.2015.07.007 (2015).

73. Monjezi, M., Shahriar, K., Dehghani, H. & Samimi Namin, F. Environmental impact assessment of open pit mining in Iran. *Environmental Geology* **58**, 205–216 (2009).

74. Yao, Z. *et al.* Solidification of municipal solid waste incineration fly ash through co-mechanical treatment with circulation fluidized bed combustion fly ash. *Materials* **13**, (2020).

75. IMOA. Molybdenum market information. https://www.imoa.info/molybdenum/molybdenum-global-production-use.php.

76. Rezki, A. S., Sumardi, S., Astuti, W., Made Bendiyasa, I. & Petrus, H. T. B. M. Molybdenum Extraction from Spent Catalyst Using Citric Acid: Characteristic and Kinetics Study. in *IOP Conference Series: Earth and Environmental Science* vol. 830 (IOP Publishing Ltd, 2021).

77. Cucciniello, R. & Intiso, A. *La Valorizzazione Dei Sottoprodotti Della Filiera Vitivinicola*. http://www.oiv.int/oiv/ (2021).

78. Kersen, Ü. & Keiski, R. L. Preliminary study on the selective oxidation of H2S over LaVO4 and Fe2(MoO4)3 oxides, produced by a solvothermal method. *Catal Commun* **10**, 1039–1042 (2009).

79. Soares, A. P. V, Farinha Portela, M., Kiennemann, A., Hilaire, L. & Millet, J. M. M. *Iron Molybdate Catalysts for Methanol to Formaldehyde Oxidation: Effects of Mo Excess on Catalytic Behaviour*. *Applied Catalysis A: General* vol. 206 (2001).

80. Medvedev, A. S. & Malochkina, N. V. Sublimation of molybdenum trioxide from exhausted catalysts employed for the purification of oil products. *Russian Journal of Non-Ferrous Metals* **48**, 114–117 (2007).

81. Mahandra, H. & Ghahreman, A. A sustainable process for selective recovery of lithium as lithium phosphate from spent LiFePO4 batteries. *Resour Conserv Recycl* **175**, (2021).

82. Zollfrank, C., Gutbrod, K., Wechsler, P. & Guggenbichler, J. P. Antimicrobial activity of transition metal acid MoO3 prevents microbial growth on material surfaces. *Materials Science and Engineering C* **32**, 47–54 (2012).

83. Rohwer, E. A. & J.J. Cruywagen. *A Comparative Study of the Complex Formation of Molybdenum(Vl) and Tungsten(Vl) with Ligands Derived from Carboxylic Acids*. http://scholar.sun.ac.za (2000).

84. Ana M. V. S. V. Cavaleiro, Victor M. S. Gil, Julio D. Pedrosa de Jesus, Robert D. Gillard & Peter A. Williams. N.m.r. Studies of Complexes of Molybdenum(VI) with Tartaric Acid in Aqueous Solution. *Transitions Metal chemistry* **9**, 62–67 (1984).

85. Cuin, A. & Massabni, A. C. Synthesis and characterization of solid molybdenum(VI) complexes with glycolic, mandelic and tartaric acids. Photochemistry behaviour of the glycolate molybdenum complex. *J Coord Chem* **60**, 1933–1940 (2007).

86. Jha, M. K. *et al.* Recovery of lithium and cobalt from waste lithium ion batteries of mobile phone. *Waste Management* **33**, 1890–1897 (2013).

87. Ye, R., Zhao, Z., Gao, R., Wan, J. & Cao, X. Conversion of Calcium Citrate to Citric Acid with Compressed CO2. *ACS Omega* **7**, 683–687 (2022).

88. Faraji, F., Alizadeh, A., Rashchi, F. & Mostoufi, N. Kinetics of leaching: A review. *Reviews in Chemical Engineering* vol. 38 113–148 (2022).

89. Leardi, R. D-Optimal Designs. in *Encyclopedia of Analytical Chemistry* 1–11 (Wiley, 2018). doi:10.1002/9780470027318.a9646.

90. Chernousova, S. & Epple, M. Silver as antibacterial agent: Ion, nanoparticle, and metal. *Angewandte Chemie - International Edition* vol. 52 1636–1653 Preprint at https://doi.org/10.1002/anie.201205923 (2013).

91. Cho, S. Y., Kim, T. Y. & Sun, P. P. Recovery of silver from leachate of silicon solar cells by solvent extraction with TOPO. *Sep Purif Technol* **215**, 516–520 (2019).

92. Grohol, M. & Veeh, C. *Study on the Critical Raw Materials for the EU 2023*. (2023) doi:10.2873/725585.

93. Sah, D., Chitra & Kumar, S. Recovery and analysis of valuable materials from a discarded crystalline silicon solar module. *Solar Energy Materials and Solar Cells* **246**, (2022).

94. Chen, P.-H., Chen, W.-S., Lee, C.-H. & Wu, J.-Y. Comprehensive Review of Crystalline Silicon Solar Panel Recycling: From Historical Context to Advanced Techniques. *Sustainability* **16**, 60 (2023).

95. Tao, M. *et al.* Major challenges and opportunities in silicon solar module recycling. *Progress in Photovoltaics: Research and Applications* **28**, 1077–1088 (2020).

96. Sabia, G., Tammaro, M., Cerchier, P., Salluzzo, A. & Brunelli, K. Treatment and management of the effluents generated by hydrometallurgical processes applied to End-of-Life Photovoltaic Panels. *Journal of Water Process Engineering* **47**, (2022).

97. Gervais, E., Kleijn, R., Nold, S. & van der Voet, E. Risk-based due diligence in supply chains: The case of silver for photovoltaics. *Resour Conserv Recycl* **198**, (2023).

98. Russo, R. E. *et al.* Hydrometallurgical Molybdenum Recovery from Spent Catalyst Using Tartaric Acid Derived from Agrifood Waste. *ACS Sustain Chem Eng* **11**, 15644–15650 (2023).

99. Masson, G., De l'Epine, M. & Kaizuka, I. *Trends in Photovoltaic Applications 2023 by IEA*. www.iea-pvps.org (2023).

100. Chen, P. H., Chen, W. S., Lee, C. H. & Wu, J. Y. Comprehensive Review of Crystalline Silicon Solar Panel Recycling: From Historical Context to Advanced Techniques. *Sustainability (Switzerland)* vol. 16 Preprint at https://doi.org/10.3390/su16010060 (2024).

101. Zhang, C. *et al.* Recovery of silver from crystal silicon solar panels in Self-Synthesized choline Chloride-Urea solvents system. *Waste Management* **150**, 280–289 (2022).

102. Yue, Y., Zhuo, Y., Li, Q. & Shen, Y. Experimental and numerical study of extracting silver from end-of-life c-Si photovoltaic solar cells in rotating systems. *Resour Conserv Recycl* **186**, (2022).

103. C.Weast, R., J.Astle, M. & H.Beyer, W. *Handbook of Chemistry and Physics*. vol. 64 (1984).

104. Hyk, W. & Kitka, K. Highly efficient and selective leaching of silver from electronic scrap in the base-activated persulfate – ammonia system. *Waste Management* **60**, 601–608 (2017).

105. Bell, S. Experimental Design. *International Encyclopedia of Human Geography* 672–675 (2009) doi:10.1016/B978-008044910-4.00431-4.

106. Shaltry, M. R., Yoo, T.-S. & Fredrickson, G. L. *Experimental Study of Codeposition Electrochemistry Using Mixtures of ScCl3 and YCl3 in LiCl-KCl Eutectic Salt at 500°C*. (2017) doi:10.2172/1392964.

107. Elomaa, H., Halli, P., Sirviö, T., Yliniemi, K. & Lundström, M. A future application of pulse plating–silver recovery from hydrometallurgical bottom ash leachant. *Transactions of the Institute of Metal Finishing* **96**, 253–257 (2018).

108. Yliniemi, K. *et al.* Effect of Impurities in Precious Metal Recovery by Electrodeposition-Redox Replacement Method from Industrial Side-Streams and Process Streams. *ECS Trans* **85**, 59–67 (2018).

109. Cui, L., Yliniemi, K., Vapaavuori, J. & Lundström, M. Recent developments of electrodeposition-redox replacement in metal recovery and functional materials: A review. *Chemical Engineering Journal* vol. 465 Preprint at https://doi.org/10.1016/j.cej.2023.142737 (2023).

110. Tsai, J. T. & Lin, S. T. Silver powder effectiveness and mechanism of silver paste on silicon solar cells. *J Alloys Compd* **548**, 105–109 (2013).

111. Fields, J. D. *et al.* The formation mechanism for printed silver-contacts for silicon solar cells. *Nat Commun* **7**, (2016).

112. House, D. A. *Kinetics and Mechanism of Oxidations by Peroxydisulfate*. https://pubs.acs.org/sharingguidelines (1961).

113. Furman, O. S., Teel, A. L. & Watts, R. J. Mechanism of base activation of persulfate. *Environ Sci Technol* **44**, 6423–6428 (2010).

114. Jiju, A. *Design of Experiments for Engineers and Scientists*. vol. Third Edition (2023).

115. Johnston, R. Linear Regression Model. In: Michalos, A.C. (eds) Encyclopedia of Quality of Life and Well-Being Research. *Springer, Dordrecht* 3621–3627 (2014) doi:https://doi.org/10.1007/978-94-007-0753-5_1659.

116. Wang, D. *et al.* Highly selective recovery of gold and silver from E-waste via stepwise electrodeposition directly from the pregnant leaching solution enabled by the MoS2 cathode. *J Hazard Mater* **465**, (2024).

117. Halli, P., Elomaa, H., Wilson, B. P., Yliniemi, K. & Lundström, M. Improved Metal Circular Economy-Selective Recovery of Minor Ag Concentrations from Zn Process Solutions. *ACS Sustain Chem Eng* **5**, 10996–11004 (2017).

118. Korolev, I. *et al.* Electrochemical recovery of minor concentrations of gold from cyanide-free cupric chloride leaching solutions. *J Clean Prod* **186**, 840–850 (2018).

119. Kowalska, S., Lukomska, A., Los, P., Chmielewski, T. & Wozniak, B. *Potential-Controlled Electrolysis as an Effective Method of Selective Silver Electrowinning from Complex Matrix Leaching Solutions of Copper Concentrate. Int. J. Electrochem. Sci* vol. 10 www.electrochemsci.org (2015).

120. Jung, B., Park, J., Seo, D. & Park, N. Sustainable System for Raw-Metal Recovery from Crystalline Silicon Solar Panels: From Noble-Metal Extraction to Lead Removal. *ACS Sustain Chem Eng* **4**, 4079–4083 (2016).

121. Ajermoun, N. *et al.* Electrodeposition of silver onto carbon graphite and their catalysis properties toward thiamethoxam reduction: application in food and beverage samples. *Heliyon* **6**, (2020).

122. Wang, Z., Yliniemi, K., Wilson, B. P. & Lundstöm, M. Targeted surface modification of Cu/Zn/Ag coatings and Ag/Cu particles based on sacrificial element selection by electrodeposition and redox replacement. *Surf Coat Technol* **441**, (2022).

123. Kanellos, G., Tremouli, A., Tsakiridis, P. & Remoundaki, E. Silver recovery from chemical extract originating from End-of-Life photovoltaic panels using a Microbial Fuel Cell. (2023) doi:10.21203/rs.3.rs-2337564/v1.

124. Hannula, P. M. *et al.* Controlling the deposition of silver and bimetallic silver/copper particles onto a carbon nanotube film by electrodeposition-redox replacement. *Surf Coat Technol* **374**, 305–316 (2019).